AD NUMBER

AD480100

NEW LIMITATION CHANGE

TO

Approved for public release, distribution unlimited

FROM

Distribution authorized to U.S. Gov't. agencies and their contractors; Critical Technology; NOV 1965. Other requests shall be referred to Air Force Aero Propulsion Laboratory, Wright-Patterson AFB, OH 45433.

AUTHORITY

AFAPL ltr dtd 12 Apr 1972

[redacted]

Vol. I
Part III

AFAPL-TR-65-53
Part IV
Vol. I

ENCL . TO LMSC A811667

480100

PROGRAM ASTEC
(ADVANCED SOLAR TURBO ELECTRIC CONCEPT)

Part IV. Solar Collector Development Support Tasks

Vol. I. Optical Parameters Affecting Petal-Type Solar Energy Concentrators

H. P. Greinel
R. C. Redden

Lockheed Missiles & Space Company

TECHNICAL REPORT AFAPL-TR-65-53, PART IV, VOL. I

November 1965

Air Force Aero Propulsion Laboratory
Research and Technology Division
Air Force Systems Command
Wright-Patterson Air Force Base, Ohio

NOTICES

When Governmental drawings, specifications, or other data are used for any purpose other than in connection with a definitely related Government procurement operation, the United States Government thereby incurs no responsibility nor any obligation whatsoever; and the fact that the Government may have formulated, furnished, or in any way supplied the said drawings, specifications or other data, is not to be regarded by implication or otherwise as in any manner licensing the holder or any other person or corporation, or conveying any rights or permission to manufacture, use, or sell any patented invention that may in any way be related thereto.

Foreign announcement and distribution of this report is not authorized. Release to the Clearinghouse for Federal Scientific and Technical Information, CFSTI, (formerly OTS) is not authorized.

The distribution of this report is limited because it contains technology identifiable with items on the Strategic Embargo Lists excluded from export or re-export under U.S. Export Control Act of 1949 (63 STAT .7), as amended (50 USC APP 2020.2031), as implemented by AFR 400-10.

Copies of this report should not be returned to the Research and Technology Division unless return is required by security considerations, contractual obligations, or notice on a specific document.

PROGRAM ASTEC
(ADVANCED SOLAR TURBO ELECTRIC CONCEPT)

Part IV. Solar Collector Development Support Tasks

Vol. I. Optical Parameters Affecting Petal-Type Solar Energy Concentrators

H. P. Greinel
R. C. Redden

FOREWORD

This document is one of a series pertaining to the Advanced Solar Turbo Electric Concept (ASTEC) Program conducted for the Air Force Aero Propulsion Laboratory by the Lockheed Missiles & Space Company (LMSC), Sunnyvale, California, under Air Force Project 678A, Contract AF 33(615)-1577.

The Air Force Program Manager is Mr. Buryl L. McFadden, Jr. The Project Engineer is Lt. P. W. Lauderback, who directs the program for Mr. G. E. Thompson, Technical Manager, Dynamic Energy Conversion (APIP-1), Flight Vehicle Power Branch, Aerospace Power Division.

At LMSC, responsibility is assigned to the ASTEC Program Office of the Booster Programs Organization. Mr. W. W. Hurtt is Program Manager.

This report (Part IV, Volume I) covers work performed by LMSC from August 1964 through December 1964. The report was submitted by the authors in May 1965. The Lockheed number for this report (Part IV, Volume I) is D-03-65-1.

This series of documents comprises the following:

Part I Candidate Materials Laboratory Tests
Part II High-Temperature Materials Laboratory Tests
Part III Candidate Materials Orbital Evaluation
Part IV Solar Collector Development Support Tasks

This technical report has been reviewed and is approved.

Glenn M. Kevern, Chief
Energy Conversion Branch
Aerospace Power Division

ABSTRACT

A preliminary study has been performed of the optical qualities and the behavior of large solar concentrators in terrestrial and space environments. The reflector is characterized by relatively large surface inaccuracies that cause unusual optical problems. The meaning of solar concentrator efficiency is discussed. The effects of geometric-optical aberrations and of surface reflectance upon efficiency are investigated. Concepts and implementations of methods for testing the geometric-optical surface quality are described, and a short commentary is devoted to surface reflectance tests. The mathematical bases for analyzing paraboloidal reflectors are developed and, to some extent, evaluated in appendixes. From the work completed, in general, it is concluded that geometric-optical analysis is needed to determine the effects of vignetting in the focal region by the heat-receiver aperture. Digital computer programs are to be developed for this analysis, employing good criteria for data acceptance/rejection or grouping. The important mathematical functions that describe primary geometrical contour errors and that have been derived as part of this study can serve as the basis for a number of criteria in subsequent studies. The geometric-optical and geometrical contour descriptions permit the correlation of environmental effects and specific concentrator and heat-receiver designs, in terms of achievable input temperatures.

CONTENTS

ILLUSTRATIONS

TABLES

Section I
INTRODUCTION

A series of studies is being conducted at the Lockheed Missiles and Space Company on optical, thermal, and structural properties of materials and on flight-test system requirements for large optical concentrators in earth-orbiting solar turboelectric power systems. The studies will be used to evaluate the results of fabrication and testing programs by several manufacturers of large unfurlable metal, petal-type, solar reflectors. The studies are part of the Advanced Solar Turbo Electric Concept (ASTEC) Program directed by the Air Force Aero Propulsion Laboratory, Research and Technology Division, Air Force System Command, Wright-Patterson Air Force Base, Ohio.

This report is a preliminary study of the optical qualities and behavior of the solar concentrator in both ground and space environments. The large solar reflector has unusual optical problems because of its relatively large, allowable surface inaccuracies. Also, the very large diameters, small focal ratios, and ultra-lightweight materials, as compared with conventional mirrors used for image formation or projection, produce uncommon problems in testing. These problems are usually considered geometrical optical topics. In particular, the geometrical optical properties, alignments, and deformations are analyzed and discussed from a general viewpoint. The specific designs of solar concentrators are not treated, since these are quite variable. Also, those factors unique to specific designs relative to a specific environmental parameter (such as temperature) were not analyzed at this time, but deserve attention and should be considered for analysis at a later date.

Performance of a solar concentrator is the resultant of overall geometrical optical accuracy, average surface reflectivity, optical-mechanical alignment relative to the sun position, and location (and orientation) of the heat-receiver aperture with respect to the paraxial focal point and the optical axis. These parameters have been evaluated qualitatively, using approaches conventional to geometrical optics. The evaluation shows the need for detailed studies to develop design criteria for system optimization, and also to develop specifications for the manufacturing process control, and qualification and acceptance test procedures.

The efficiency of solar concentrators is discussed in Section II. The generalized factors of geometrical optical aberrations and reflectance are discussed in terms of their effect on the image-intensity distribution function in Sections III and V. Section IV is concerned with concepts and implementations of methods for testing the geometrical optical surface quality. Section VI is a short commentary on surface reflectance tests. Section VII concerns conclusions and recommendations derived, to date, from the studies.

In the Appendixes, the mathematical bases for analyzing paraboloidal reflectors composed of segmental areas or petals are developed, and, to a certain extent, the derived results are numerically evaluated.

NOTE

The terms "collector," "reflector," and "concentrator" are, in general, interchangeable; they are used throughout this report to describe the same optical device, i.e., a paraboloidal mirror that collects, reflects, and concentrates incident radiation to a focus. To be sure, none of these three terms describes the mirror completely. Preference has been given to the term "reflector" when reflectance and reflectivity are discussed, or when some comparison is made between a reflector and a refractor.

Section II

EFFICIENCY OF SOLAR CONCENTRATORS

The optical efficiency of a solar concentrator is an important index to evaluating both material and fabrication techniques. The usual definition of optical efficiency (sometimes called either optical gain or concentration ratio) is ratio of flux density in the image to the flux density at the entrance pupil of the concentrator. Although the definition is simple, the measurement of optical efficiency can be quite complicated. The flux density in the image may vary over the extent of the image. Furthermore, the "extent" of real images is itself describable only in terms of some arbitrary threshold flux density. Nevertheless, optical efficiency is extremely useful in evaluating the image-forming capability of a solar concentrator. The effects of geometrical aberrations, reflectivity, and diffuse reflectance are contained in the single index – optical efficiency.

There is, however, another factor involved with solar concentrators which tends to diminish the importance of optical efficiency. This is the aperture of the device used in the image region to transform radiant energy into stored heat in some substance. Usually this device is a type of "black body" cavity with a circular aperture nominally located in the focal plane and perpendicular to the optical axis. The physical area of the heat-receiving cavity may be much larger than the image. Hence, the flux density in the image is no more significant than a possible flux density averaged over the aperture area, assuming total power to be the same for the real image as for a hypothetical beam passing through the heat-receiver aperture. Geometrical optical aberrations must be related to the heat-receiver aperture to determine permissible tolerances; the usual result is to lower the optical efficiency (as defined in the previous paragraph).

A short digression into the reasons for selecting a heat-receiver aperture larger than the image is necessary here. It is easy to show on theoretical bases that the heat-receiver aperture should match the image size and shape. This condition produces the maximum attainable temperature for the heat-storage substance, which is the source of heat for some engine producing work. The work output is a function of the maximum realizable temperature difference in the thermodynamic cycle. However, the heat-receiver aperture cannot usually be designed to match the minimum possible size. The limiting factors are summarized as follows:

- The safe temperature limits of both the structure and the heat-transfer medium of the heat receiver must not be exceeded (as measured by some significant parameter such as creep, melting point, pressure, etc.); hence the size of the heat receiver tends to increase to maintain a safety factor.
- The pointing errors of the solar concentrator relative to the sun, and the effect of this on image blur size, tend to increase the size of the heat-receiver aperture to permit realization of practical tolerances.

- The mechanical alignment of the heat receiver is a function of the assembly tolerances and expansion/bending of the supporting structures (due to environmental effects of temperature, temperature cycling, and accelerations); hence, the size of the receiver aperture also tends to increase to compensate for these effects, as well as for the effects noted above.

The mathematical definition for the optical efficiency of a solar concentrator must be sufficiently general to enforce recognition of the relationship between the image blur size and shape and the independent parameters of heat-receiver aperture size and location. The following definition approximates this relationship for a heat receiver with a circular aperture in the plane of the optical image:

$$E = P_a/P_i$$

where

E = optical efficiency (dimensionless unit)[1]

P_a = total flux through (displaced) heat-receiver aperture (watts)

P_i = total flux incident upon the reflector (watts)

The total flux incident upon the reflector is

$$P_i = H_s A_m$$

$$= H_s \eta \pi \left(R_m^2 - R_h^2\right) \quad \text{(watts)}$$

where

H_s = incident solar flux density (solar constant = 0.135 watts/cm^2)

A_m = effective reflector area (cm^2)

η = obscuration factor = ratio of projected illuminated portion of reflector area to total projected area (dimensionless units)

R_m = mirror rim radius (cm)

R_h = mirror hub radius (cm)

1. This definition of the efficiency provides good, unique results if applied to actual measurements in well-aligned systems. However, it can only be considered as providing approximate results if applied to misaligned systems, since the amount of misalignment may be different at different times of system operation. If the efficiency is to be generalized on the basis of theoretical considerations, a more elaborate definition is necessary to account for the statistical variation of intensity distributions and heat-receiver locations.

To find an appropriate expression for the total flux through the (somewhat displaced) heat-receiver aperture, two Cartesian coordinate systems, (X, Y) and (X', Y'), can be used to describe the situation encountered (Fig. 1). The (X, Y)-system has its origin O_c, defined by the center of the (ideal) receiver aperture at the optical axis of the concentrator. The radius r_a, in centimeters, is such that

$$-r_a \leq X \leq r_a \; ; \; -r_a \leq Y \leq r_a \; ; \; X^2 + Y^2 \leq r_a^2$$

The (X', Y')-system has its origin O_d at the center of the actual aperture, the area of which constitutes the usable portion of the image plane; i.e., the flux falling outside this usable portion does not contribute to P_a. Here, radius r_a is such that

$$-r_a \leq X' \leq r_a \; ; \; -r_a \leq Y' \leq r_a \; ; \; X'^2 + Y'^2 \leq r_a^2$$

The displacement (misalignment) of the actual aperture's center from O_c is denoted by X_d and Y_d, respectively. Consequently, measurements of the intensity distribution in the plane of the optical image blur (irradiance distribution) can be referred only to the (X, Y)-system. Therefore, the local distribution to the total flux, by usual definition, is to be expressed by

$$dP_a = H_i(X, Y)\, dXdY$$

where

$H_i(X,Y)$ = intensity distribution function in the optical image blur (watts/cm^2)

The image-intensity distribution function is a complicated resultant of incident solar flux, effective area of concentrator, effective reflectance, ordinary geometric-optical aberrations, aberrations due to nonuniform reflecting contours of the concentrator, and masking or obscuration by mechanical structures.

The expression for the total flux through the actual aperture is

$$P_a = \int\int_{A'_a} H_i(X, Y)\, dXdY \quad \text{(watts)}$$

where

A'_a = area of actual (displaced) aperture (cm^2); i.e., $|X_d| \geq 0$, $|Y_d| \geq 0$

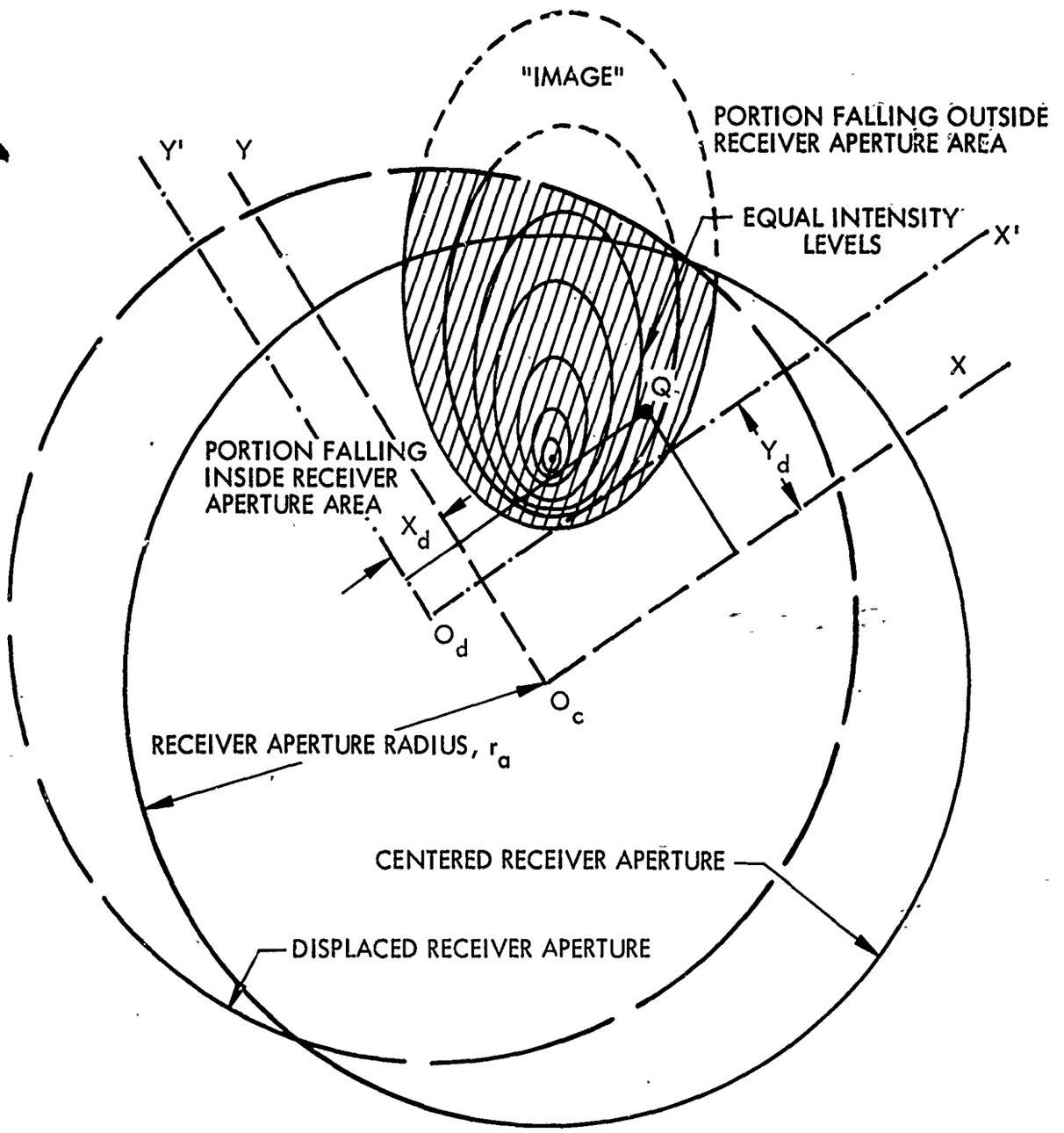

Figure 1 Typical Image Blur; Geometrical Relation to Heat-Receiver Aperture

The image-intensity distribution does not have a unique value except when all component effects and locations are defined. Since these in themselves may be dynamical quantities, or at least may be variable in different environments, the intensity distribution could be further generalized by introducing a time parameter, and thereby defining an average optical efficiency. This generalization, however, would not be especially helpful in early or preliminary analyses.

Also, the heat-receiver aperture is not necessarily a mechanical part in a plane; it may have conical walls which act as an auxiliary optical device, to be considered in conjunction with the concentrator. This arrangement has not been included in the previous definition of optical efficiency, because the image-intensity distribution would be too complicated for simple evaluations.

Some idea of the dynamics of the image-intensity distribution is conveyed by Table I, which shows some relationships between environment and optical parameters. The list of parameters has been compiled assuming a petal type of solar concentrator and both ground-test and space-operation environments.

The generalized parameters of geometrical optical aberrations and reflectivity, as well as their effect on the image-intensity distribution function, are discussed in more detail in Sections III and V.

Table I

IMAGE-INTENSITY-DISTRIBUTION PARAMETERS
AS A FUNCTION OF ENVIRONMENT

Optical Parameter	Environmental Factors: Static — Gravitational	Static — Thermal	Dynamic — Accelerations	Dynamic — Thermal	Dynamic — Vacuum	Dynamic — Ultraviolet
Optical Axis Pointing	x	x	x	x		
Heat-Receiver Aperture Location	x	x	x	x		
Petal Axis Pointing	x	x	x	x		
Petal Displacement	x	x	x	x		
Average Petal Contour	x	x	x	x		
Petal Contour Waviness		x		x	x	
Reflectivity, Specular, Effective					x	x
Reflectivity, Diffuse, Effective				x	x	
Petal Interface Obscurations				x		

NOTE: The x denotes a physical cause that could perturb the design value of the optical parameter.

Section III

GEOMETRICAL OPTICAL ABERRATIONS

1. REQUIREMENT FOR IMAGE-INTENSITY DISTRIBUTIONS

The objective in describing the optical quality of a solar reflector is to provide useful formulations for component and system optimization. Analytical expressions that may be directly related to controllable variables but that do not indicate the magnitude of effects on overall performance are not completely useful. This condition arises commonly in radiometry, in which accurate predictions of the energy transfer efficiency are desired for specific optical systems. The usual ray trace results show the geometrical optical behavior, but they are independent of the system's transmissivity (or reflectivity). Also, to derive an intensity distribution for an extended source image is a difficult task, even for a computer, because many integrations are required. Normally, an intensity distribution is not used in computing the radiant energy transfer of optical systems. The radiometric formulas commonly used for total flux transfer are approximations, based on an average loss per transmission element and on simplifying assumptions as to aperture distances and the integrated effect of aberrations.

To complicate matters for solar concentrators, two features require somewhat unusual treatment, relative to conventional optical practices: (1) the allowable macroscopic optical surface errors and large aberrations, due to ultralight structures; and (2) a relatively large exit pupil. The second feature compensates somewhat for the first, although it is not clear whether this compensation is a major criterion in the design of a heat receiver. The large exit pupil is identical to the entrance aperture of the heat receiver, and, when the aperture is about two or three times the largest on-axis theoretical optical blur circle, there is little need for niceties in specifying optical quality. On the other hand, there are considerations which might reverse this opinion, such as off-axis blurs and multiple images from misaligned petals.

The requirement for describing an image-intensity distribution is illustrated by Fig. 1. The amount of energy lost to the heat receiver because of spill-over of the image at the edge of the receiver must be computed. This condition arises when the image location deviates because of pointing errors in the solar concentrator system. Also, the effect is combined with displacement of the heat-receiver aperture. Pointing errors and displacements both are real possibilities, and practical tolerances must be assigned to each.

The illustration shows only a simple type of image aberration. A discussion of the classification of types of images is presented in succeeding paragraphs.

2. TYPES OF IMAGE BLURS

As stated previously, the petal type of parabolic reflectors, used for concentrating solar energy within a cavity, can exhibit a number of geometrical optical faults and errors which affect its efficiency as compared to that of a theoretically perfect concentrator. Any flux that falls outside the heat-receiver aperture of the cavity is to be considered a loss to the heat engine system. The simplest way to approach an understanding of the loss due to geometrical faults and errors is to consider it as a resultant of two types of solar images combined with the geometrical size and location of the heat-receiver aperture.

a. Type I Image

The Type I image is an asymmetrical blur produced by a combination of off-axis image position and the optical aberrations arising from the form of the reflecting surface. The image is relatively small, since it is produced by nearly continuous reflecting elements which closely approximate the design form selected as the optimum surface of revolution for the reflector. The usual faults causing the departure from the ideal form are as follows:

- Misalignment errors, such as
  1. Optical axis pointing error, i.e., angular deviations of the mirror's optical axis from the line-of-sight to the apparent sun disk's center
  2. Receiver aperture misalignment, i.e., its dislocation from, and inclination relative to, the theoretical paraxial focal plane
  3. Misalignment of individual petals, i.e., their displacements and inclinations with respect to the theoretical paraboloid (and to each other)
- Mechanical deformation errors, such as
  1. Improper surface shape due to manufacturing
  2. Bending under gravitational load, as in terrestrial conditions
  3. Time-varying, thermally induced strains and deformations

Whereas misalignment errors do not change the form of the paraboloid of revolution or that of its particular segments, mechanically deformed surfaces are to be described by analytic equations with higher-order terms than those used for the description of the parabolic reflector. The image blur is basically due to conventional optical aberrations and may be determined by applying the analytical ray-tracing method described in Appendix I. However, the apparent blur associated with Type I images may also be due to multiple images formed by individual elements (such as petals) which mechanically form the reflector (see Appendix II in this view). Since the location of each image is due to the coordinates of such elements, and since these elements may be

somewhat independent relative to each other, the apparent image size may be an enlargement of the image produced by a single element.

b. Type II Image

The Type II image is a relatively large symmetrical blur produced by a nonuniform reflecting surface which must be described by equations with even more higher-order terms than those used for the description of deformed (but uniform) surfaces. The actual surface will probably have to be treated in the frequency domain by Fourier analysis. The Type II image category includes the following:

- Wavy surfaces
- Surfaces with sharp inflections
- All surfaces which scatter radiation in random directions

The Type II image is relatively large, because it is produced either by extreme departures in contour from the geometrical design form or by scattering from elements not identified with the reflecting surface. The reflecting elements which cause this effect are generally small and may even tend toward the microscopic. Waviness may be due to the manufacturing process and the lightweight structure, as well as to degeneration of the reflecting thin films. With respect to the faults of waviness, an approximation of the effect on the image can be achieved by treating the individual "wavelets" as unique optical elements, with focal lengths and apertures, producing out-of-focus and displaced images. As the geometrical period of the wave decreases with constant amplitude, the magnitude of the out-of-focus condition increases. As a result, the solar energy is spread more widely relative to the heat-receiver aperture. Other faults which may produce large image blurs of this type are the edges and mechanical elements in the intersections of petals, although these faults are not expected to be classified as major.

c. Estimation of the Effects of Type I Images

The image of an off-axis point source formed by a paraboloidal surface of revolution appears, in the paraxial focal plane, as a radial line. This effect is characteristic of optical reflectors with astigmatism. Additionally, the paraboloid is characterized by coma, which is an aberration arising from the lack of constancy in focal length for each annular zone of the entrance aperture. The effects of coma and astigmatism appear to combine to produce a line image with fairly uniform flux density gradient, with the peak intensity nearest the center of the image field.

The image of an extended source, such as the sun, also shows a much higher flux density nearer the optical axis than for image regions farther from the axis. The shape of the image of the sun appears as "comatic"; i.e., it appears as a comet with a bright head near the axis and a less bright tail farther from the axis.

If the sun is considered nearly a uniform square area in shape, and the edge of the solar heat-receiver aperture is considered approximately a straight edge, the loss of energy as a function of angular deviation of the centroid can be approximated in a

fairly simple manner. Even though these convenient conditions do not exist, the approximations serve a useful purpose. Using as the dimensions of a parabolic reflector a 26-ft outer radius, 10-ft inner radius, 60-deg rim angle, and 20-in. heat-receiver diameter, the estimated effect of geometrical aberrations on efficiency has been computed as approximately 3 percent loss in energy for 2 min of arc deviation outward from the axis. The image is assumed to be tangent to the heat-receiver edge as an initial condition. This estimation has not been computed with the desired precision for the ASTEC system analysis; however, the results are useful for comparison with the effect of the Type II image, as presented next, computed to the same degree of precision. In any complete analysis, the macroscopic deformation of the surface contour and the large errors in bending expected from real solar concentrators (of this size and construction) will probably override the conventional aberrations of the parabolic mirror.

d. Estimation of the Effect of Type II Images

The effect of waviness on the surface of paraboloidal collectors can be evaluated by considering a wavelet as an image-forming reflector with properties independent of the primary surface. A wavelet is defined here as a half-period element, either convex or concave. It has a radius of curvature, and hence an effective focal length, in the Gaussian sense.

The wavelet forms a severely aberrated image, either as an approximate line or as an approximate circular disk. These aberrations will complicate the analysis of the effect of waviness. However, some idea of the minimum effect on efficiency can be obtained by considering the wavelet as spherically convex or concave, and the image as symmetrical to the wavelet's optical axis. The reference condition for evaluating a wavelet is to assume that the source is on-axis (no pointing error) and that the wavelet image that just fills the heat-receiver aperture will define the maximum acceptable wavelet. The convex wavelet produces the worse effect.

A convex wavelet with a half-period of 12 in. and an amplitude of 0.005 in. will form an image that will project to fill a 20-in. -diameter heat receiver, at the focal plane of a 52-ft-diameter concentrator with a 60-deg rim angle. The location on the paraboloidal surface is assumed to be at the average zonal focal length, i.e., near the middle zone of the collector. To estimate the effect on efficiency, it is estimated that 50 percent of the energy from the wavelet would be lost if the line-of-sight to the sun was at 0 deg, 48 min, and if the wavelet image aberrations are included. For example, if 3 percent of the total energy from the concentrator were an allowable limit for the fault of waviness, approximately four such waves per petal could be permitted in a 50-petal assembly.

Evaluation of smaller wavelets, concave wavelet shapes, and distributions have been conducted on an estimated basis; however, the numerical results would not be helpful here. With smaller wavelets, a greater number of waves can be tolerated per collector surface. The effect of concave shapes is not so severe as that from the convex shapes. The effect of waviness as a function of radial distribution is greater severity at the outer zones.

e. Combinations of Types of Images

The types of geometrical faults are evidently different and independently related; hence, criteria for combinations of faults will have to be established on a statistical basis and used in acceptance of solar concentrators. This method will require a computer program to determine overall efficiency. The program should include both digital and analog computers, with the latter developed specifically for the ASTEC concentrator. The scope of the present study and report does not permit more elaboration at this time.

3. DISCUSSION OF METHODS FOR ANALYZING SOLAR CONCENTRATOR IMAGES

The methods and the problems of describing the images of solar concentrators are partly the same as found in radiometric (and photometric) optics, and partly unique because of the nature of the solar concentrator reflecting surfaces and contours. The first step in conventional optics is to obtain the equation of the ideal surface of revolution of the reflector (and/or refractor). The second step is to trace a number of rays reflected (or refracted) from the surface. The result of this second step is a geometrical plot of rays intercepting some reference plane perpendicular to the axis of revolution (optical axis). This tracing is commonly called a spot diagram, and the reason for producing it is generalized as "diagnosis."

Since this report deals only with solar concentrators, the body of knowledge and techniques of synthesis or manipulation of surface contours is not pertinent. The major problem for solar concentrators is to obtain an intensity contour for the image, preferably in the form of a continuous function of two variables with the absolute flux value normalized to unity at the peak value. The spot diagram is purely geometrical and does not normally contain sufficient intensity information, but if a large number of rays are used, the spot density can be considered an approximation of the flux density. This approach is questionable if the reflectivity of the concentrator is variable over the reflecting surface.

Theoretically, the computer program can be developed to handle all variables and to generate sufficient data for deriving the required intensity distribution. In practice, however, this method results in an enormous amount of data and very lengthy computer runs. Large memories are required, and extensive computer time is used to interpolate and extrapolate from the spot-diagram data. A better approach for solar concentrators appears to be a combination of digital-computer ray tracing and real three-dimensional models.

Several methods for implementing this idea are possible, based on contemporary techniques. The method recommended here is to trace rays of equal-area annuli of the reflector (or annuli with known area relationships) and form the usual spot diagram. The spots in the diagram could probably be given equal weight as intensity elements, since preliminary analysis indicates only a slight edge gradient to the intensity contour of the image from an annulus with uniform surface. The outline of the spot diagram could be used as a template, and the thickness of the template would have the dimensions of intensity. The use of such templates, as well as stacking them to form three-dimensional displays, is common. Only a few representative displays would be needed for a complete analysis. Further analysis is required to relate this approach to higher-order reflecting contours.

This method has been used in study and analysis of other physical phenomena, such as plotting the thermal gradients over honeycomb sections. Once the three-dimensional model is achieved, analyzing the effects of image spill-over relative to the heat receiver of a solar concentrator could potentially be predicted with good accuracy.

Section IV

QUALIFICATION TEST OF GEOMETRICAL OPTICAL SURFACES

1. GENERAL INFORMATION

The problems of performing geometrical optical tests on large solar concentrators are uncommon in the field of optics. Special problems arise because of the large diameters and the small focal ratios (large rim angles). The distances involved in positioning test apparatus are large, and they complicate the problem of providing stable and accurate reference surfaces. The usual equipment employed for optical testing does not have the light intensity needed for the long distances involved. The imperfections of solar concentrator reflecting surfaces are gross as compared with those of conventional optical collectors.

Conventional optical test methods that are most promising have been reviewed in the light of these problems. Although the Hartman test appears useful, the necessity of moving a projection collimator to provide the equivalent of the conventional apertured plate appears difficult to accomplish. The Foucault test method (including the Platzeck and Gaviola versions) has been reviewed, but it is not especially useful for off-axis aberration analysis. Furthermore, the test results would be difficult to use for reasonably accurate computations of either reflector contours or image size and shape. The wire grid tests of Ronchi and Jentsch do not appear to be useful since they usually depend on a star source for producing the characteristic shadow-fringe pattern. Such a source is difficult to achieve for a large collector.

In addition to the aforementioned problems involving both the basic reflector and the conventional optical test methods, there is a serious problem in positioning a large and relatively flimsy optical reflecting surface in a manner suitable for testing. The geometrical axes of the basic reflector may never coincide with the optical test equipment structures, and the effects of gravity and the orientation may both combine to produce contours other than surfaces of revolution.

To solve these problems, a new optical test system concept has been developed by the Lockheed Missiles & Space Company. This concept is described in sufficient detail to convey an understanding of its major features. The detailed analysis of this concept will be presented in later reports.

2. CONVENTIONAL OPTICAL TEST METHODS

Optical test methods are grouped in two general categories: (1) ray-path tests, and (2) wavefront interference tests. The wavefront interference tests are performed for ultra-sensitive measurements on either optical images or polished contours, and they have no utility for testing solar concentrators. The ray-path methods are, in principle, satisfactory for measuring the properties of this type of optical reflector.

The ray-path tests can be made in the image focal plane region or in the vicinity of the origin of the radii of curvature of the surface. When the tests are in the image region, the intercept location of rays in one or more planes of reference indicate the degree of symmetry and convergence achieved by the reflector. Two well-known and different test methods can be employed for this type of testing, the Foucault knife-edge test and the Hartman test. Of these two, the Hartman test is more informative for both on-axis and off-axis image testing (the Foucault test is usually employed only for on-axis testing).

The Hartman test concept is illustrated by Fig. 2. In one method, individual ray paths are defined by apertures in a plate with light from a distant source. Alternatively, an individual projector (with a small exit pupil) may be moved in a plane perpendicular to the optical axis. The spots of light on a reference plane in the image region can be qualitatively used to evaluate the image. A quantitative measurement of the image shape can be made if two or more reference planes are used, and the ray-path equations are then derived. Also, the geometrical contour of the surface can be derived from the intersection points of the incident and reflected rays and the angles of the reflected rays.

The Hartman test has two major drawbacks: (1) a large number of ray paths must be used to obtain accurate measurements; and (2) the spots of light in the reference planes must be identified with corresponding apertures or positions of the projection collimator. These difficulties are not too troublesome if the optical surface under test is relatively small, but, for surfaces as large as used for solar concentrators, the Hartman test can be a laborious procedure. Nevertheless, it is the most useful method for direct measurements of image size and shape.

An alternative to optical tests in the image region is to test in the region of the origin of the radii of curvature, as illustrated by Fig. 3. The sketch shows a variation of the Foucault test—one which uses an aperture plate to define annular zones. The knife edge is used to locate the intersection of the reflected rays by moving along, and perpendicular to, the optical axis. When the positions of the light source, the annular apertures, and the image are known, the geometrical contour can be computed.

This type of Foucault test has several drawbacks: (1) the annular apertures cause a spreading of the reflected beams, and in addition the center of the aperture is difficult to define relative to the true optical surface; (2) the knife edge must be moved in two directions to seek the exact intersection point of the reflected rays; and (3) the light source is rarely in the same plane as the knife edge, and additional mathematical corrections must be employed. Nevertheless, even with these defects, the Foucault test has one great advantage, namely, that a single light source can be used with one annular zone, full or partial segment.

Because of the great diameter of the ASTEC solar concentrator and the large rim angle, both the Hartman and the modified Foucault tests are difficult to apply. A new type of optical testing which alleviates many problems of conventional tests is observed next.

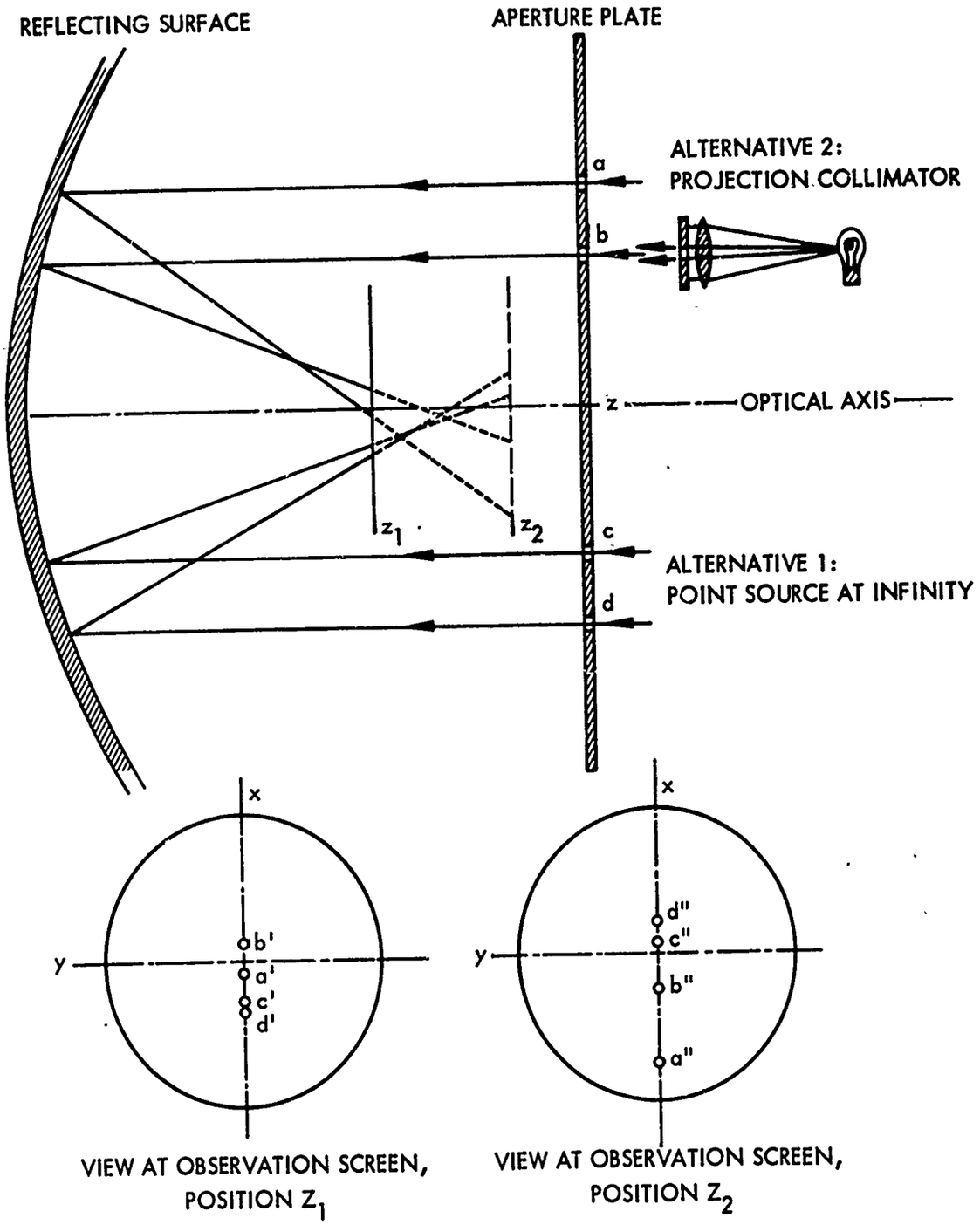

NOTE: THIS IS A SIMPLIFIED REPRESENTATION OF PRINCIPLE, SINCE NO DEVIATIONS OF LIGHT SPOTS IN Y-DIRECTION ARE ASSUMED.

Figure 2 The Hartman Test

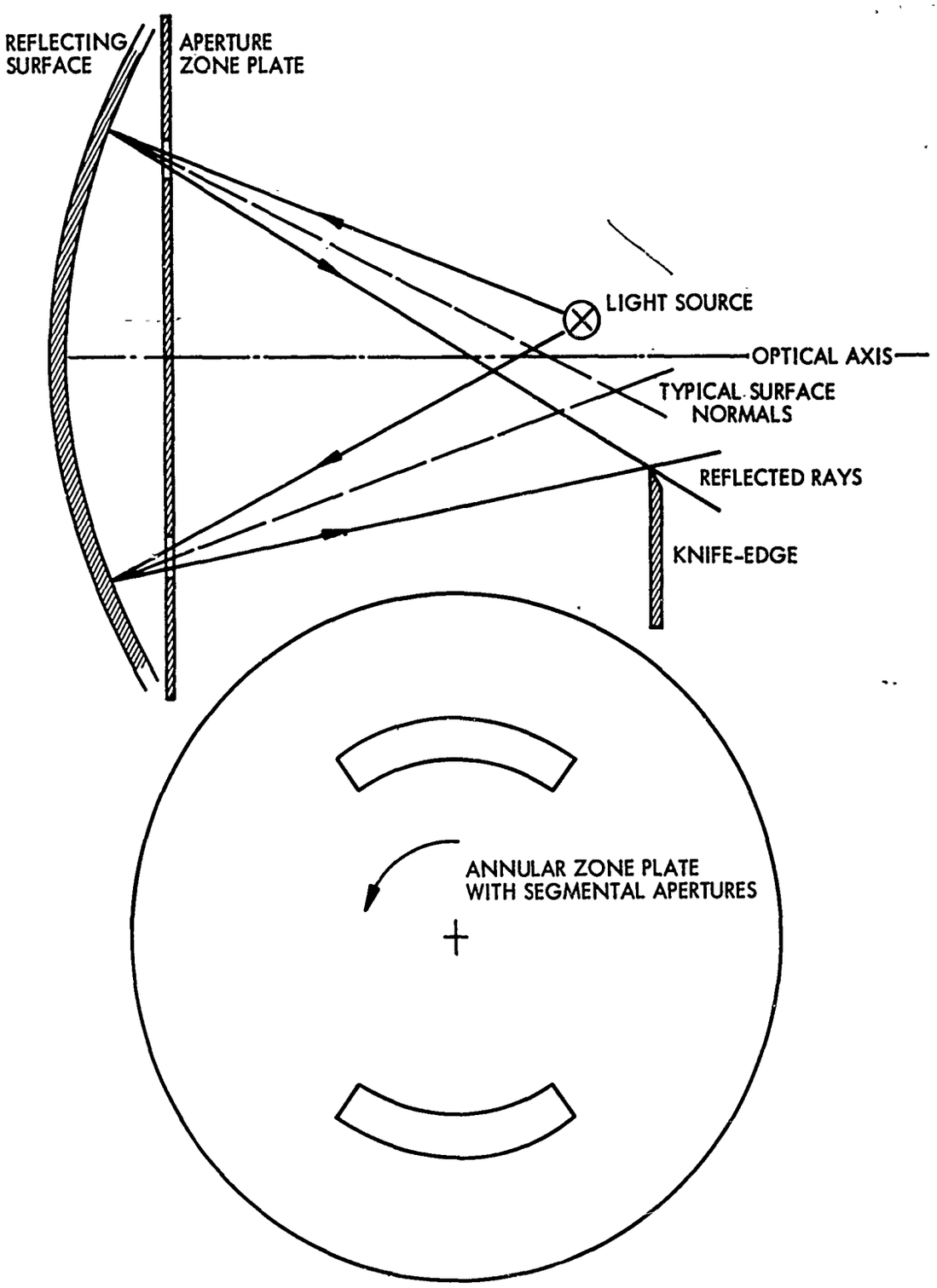

Figure 3 The Foucault Test (One Variation)

3. OPTICAL TEST METHOD RECOMMENDED FOR THE ASTEC COLLECTOR

The concept of an optical test method suitable for large solar concentrators is shown by Fig. 4. A light beam is directed along the nominal position of the optical axis outward from the apex region of the concentrator. The beam is intercepted by a small mirror situated in the region where the reflector surface normals tend to intersect the optical axis. The small mirror is tilted and translated in two directions, along and perpendicular to the optical axis. This procedure permits "seeking" one normal to the reflector surface, which is identified by a return of the light beam along its path of propagation. This normal also identifies an annular zone. An exact determination of a normal is not necessary, as explained later. Once a surface is determined, as shown by Fig. 4A, the small mirror is rotated about the ray path of the light beam. Any lack of symmetry of the normals to the annular zone is detected by the beam reflected off the concentrator and deviated from the reference normal. The reflected beam is intercepted by a diffused reflecting (projection) screen, which surrounds the small mirror, as shown by point a in Fig. 4B.

The contour of the concentrator can be determined from the set of data points produced by measuring two positions (along and lateral to the light beam "axis") and two angles (small mirror tilt and rotation). Also, the data can be used to directly determine the size and shape of the image without first deriving the geometrical contour.

The disadvantages of the Lockheed test described above are several. The small mirror must be moved in two directions to closely determine a suitable reference normal, and thus to guarantee that all beams reflected off the concentrator will be intercepted by the projection screen. However, it is sufficient to obtain a trace of the intersections of the beam with the screen, as the small mirror rotates, since any anomalies show as unsymmetrical departures from an ideal circular pattern. Given a complete trace, its centroid can be determined without driving the small mirror to "null" along one normal.

The accuracy of the derived contour or the image shape and size is dependent upon the accuracy of the measurements of the position of the spots (or continuous trace) on the projection screen. The screen is relatively inaccessible because of the large dimensions of the concentrator; hence, highly accurate measurements are difficult.

Lastly, small imperfections in the reflecting surface of the concentrator will tend either to scatter the reflected light beams or to blur the spots (because of geometrical aberrations).

The major advantages of the Lockheed test method are: (1) the reflecting contour tangent plane angles can be measured directly; (2) both random and periodic variations in the contour can be identified and measured; (3) the base curve and the translation/rotation of geometrical axes can be determined; (4) the aberrations and scattering from small surface elements can be detected; and (5) compound curvatures of the reflecting surface can be measured as easily as surfaces of revolution.

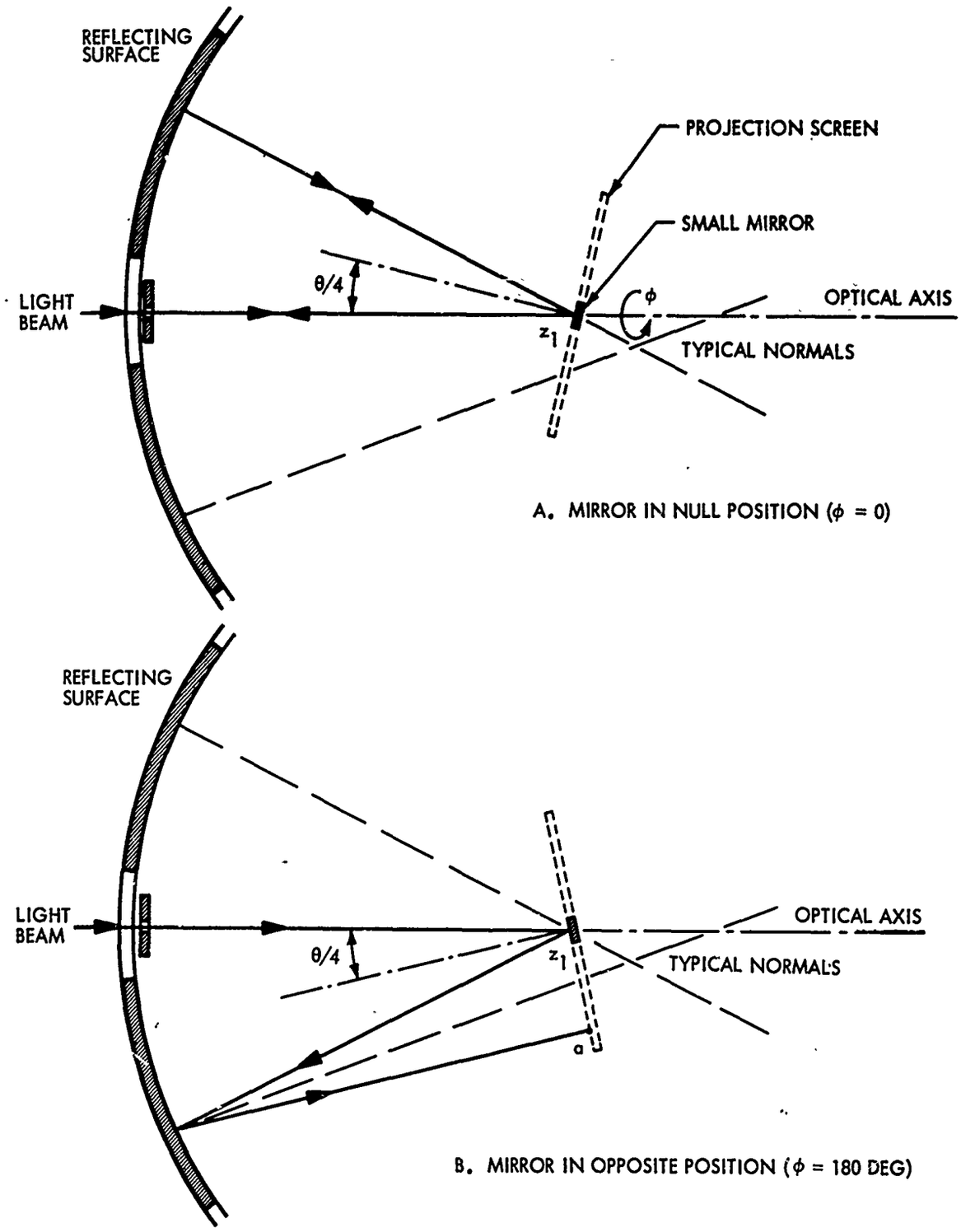

Figure 4 The Lockheed Test

Section V

SURFACE REFLECTANCE

1. GENERAL INFORMATION

The effect of surface reflectance on the efficiency of a solar concentrator can be both simple and complicated. When the reflectance is considered only as a measure of the absorptance (or filtering of energy potentially available to the heat receiver), the maximum efficiency of the concentrator is equal to the reflectance. Absorption of energy (and hence a rise in temperature) by the reflecting surface, however, affects the geometrical contour and positional properties of the concentrator; this effect may, in turn, affect the overall efficiency in the same manner as "normal" optical and alignment errors. Also, it is theoretically possible to reflect energy without absorption, but the reflections may be specular or diffuse.

The "effect" of specular reflectance is identical to the effect of geometrical and alignment aberrations; hence "specularity" is not a useful concept here. The effect of diffuse reflectance, however, must be handled differently, since it does not have any necessary connection with geometrical properties. In one sense, the amount of diffuse reflectance is a measure of the specular reflectance, but the two are usually separated because their physical causes and methods of measurement are different.

An outline of problem areas and indication of the effects of reflectance on solar concentrator efficiency is presented here. Both diffuse/ specular and total-energy/spectral reflectance are discussed.

2. DEFINITION OF TERMS

There is a conspicuous lack of precision in the meaning of terms used to express the reflection of energy per unit time (flux) from surfaces. This difficulty has developed over a long period of time and it probably will never be fully resolved in a practical way. It is important, however, to present specific definitions here, primarily to permit discussions of the reflection from isolated material samples and from large optical solar concentrators. The definitions are presented after a brief review of contemporary and past authoritative sources on the meaning of the terms reflectivity and reflectance.

Various definitions and discussions of reflectivity and reflectance are available from important reference sources.

Robert I. Sarbacher (Encyclopedic Dictionary of Electronics and Nuclear Engineering, Prentice-Hall, 1959, page 1103) provides the following definitions:

- Reflectivity. "The ratio of the light reflected from a surface to the total incident light. The coefficient (of reflectivity) may refer to diffuse or to specular reflection. In general it varies with the angle of incidence and with the wavelength of the light. Syn. Reflectance; Reflection Factor."

- Reflection Factor. "In physical optics, the ratio of the total luminous flux reflected by a given surface to the incident flux; also known as reflectance or reflectivity, q.v."

The American Institute of Physics Handbook (McGraw-Hill, 1957, page 6-7) defines reflection coefficient, or reflectivity as "the ratio of the light reflected from a surface to the total incident light. The coefficient may refer to diffuse or to specular reflection. In general it varies with the angle of incidence and with the wavelength of the light."

The IES Lighting Handbook (published by the Illuminating Engineering Society, 3rd edition, 1959, page 3-10) defines reflectance as "the ratio of the flux reflected by a surface or medium to the incidence flux. The quantity reported may be total reflectance, regular (specular) reflectance, diffuse reflectance, or spectral reflectance, depending on the component measured."

Max Born and Emil Wolf (Principles of Optics, Pergamon Press, 1959, pages 40-41) remark:

"The ratios

$$\mathcal{R} = \frac{J^{(r)}}{J^{(i)}} = \frac{|R|^2}{|A|^2} \text{ and } \mathcal{T} = \frac{J^{(t)}}{J^{(i)}} = \frac{n_2 \cos\theta_t \, |T|^2}{n_1 \cos\theta_i \, |A|^2}$$

are called the reflectivity and transmissivity respectively ..."

"The amount of energy in the primary wave which is incident on a unit area of the boundary per second is

$$J^{(i)} = S^{(i)} \cos\theta_i = \frac{cn_1}{4\pi} |A|^2 \cos\theta_i$$

and the energies of the reflected and transmitted wave leaving a unit area of the boundary per second are given by similar expressions:

$$J^{(r)} = S^{(r)} \cos\theta_i = \frac{cn_1}{4\pi} |R|^2 \cos\theta_i$$

$$J^{(t)} = S^{(t)} \cos\theta_t = \frac{cn_2}{4\pi} |T|^2 \cos\theta_t \text{ "}$$

Arthur C. Hardy and Fred H. Perrin (The Principles of Optics, McGraw-Hill, 1st edition, 1932, page 143) comment: "Before the laws of radiation can be discussed, it will be necessary to define certain properties of radiating surfaces. The emissive power of a surface at a given temperature will be defined as the amount of energy

radiated per unit time per unit area. This quantity will be designated by E . Conversely, the amount of incident radiant energy falling per unit time on a unit area of a surface will be designated by I . Now, in general, the radiation falling on a body is partly reflected, partly transmitted, and partly absorbed. Let it be supposed that a fraction R of the incident radiation is reflected and a fraction A is absorbed. The quantities R and A are known as the reflectivity and the absorptivity of the surface respectively."

At another point (page 277), they observe that "in general, when light falls on a substance, part of it is transmitted, part is reflected, and the remainder is absorbed. Most substances of ordinary thickness are so opaque that the proportion of the light transmitted can be neglected. The proportion absorbed cannot be measured directly, but it can be inferred from measurements of the proportion reflected. The ratio of the luminous flux that is reflected to the flux that is incident is known as reflectance of the substance, but the term is meaningless unless conditions of illumination and observation are specified." A footnote remarks, further: "In lieu of any general agreement on the use of the terms 'reflectivity' and 'reflectance' the former is used ... in connection with the total amount of energy reflected by a surface, and the latter ... to indicate the amount of visible light that is reflected."

As can be discerned from the above, reflectivity tends to be associated with a known flux per unit area, and reflectance tends to be concerned only with flux per se. This distinction is in consonance with other terminology and quantities in physics. For example, emissivity is the ratio of flux emitted per unit area of a body to the flux emitted per unit area of a theoretical black body (perfect emitter). But emittance can be simply the flux from a body; i.e., emissivity is dimensionless, and emittance has at least the units of power. (Neither of these latter terms is accepted universally as presented here, so they are not presented as a complete justification for defining reflectivity and reflectance.) The practicalities of solar concentrators, and imperfect optical systems in general, combined with these semantic distinctions, demand a recognition of the following observations:

- Reflectance. Reflectance can be measured from any combination of surfaces within an area, which can be irradiated or illuminated with any pattern of flux filling the area. All that is required is a measure of the total fluxes, incident and reflected. This condition is sufficient for measurement of the performance of an optical collector or concentrator.
- Reflectivity. When the physical properties of reflecting surfaces must be analyzed, then constraints on angles of incidence, angles of reflection, sizes of surface areas, uniformity of surface area, source radiance, source size, source uniformity, instrument aperture, etc., are imposed by both instrumentation and mathematical simplicity. All of these constraints should be included explicitly or implicitly in the results of the analysis; hence, "normalized" quantities will be used. Reflectivity is an appropriate term to indicate the control of independent variables in reflection measurements and the ratio of normalized quantities.

The following definitions will be useful for the problems discussed in this report:

- Reflectance: the ratio of total flux on a surface to the total flux reflected from the surface
- Reflectivity: the ratio of uniform flux per unit area incident on plane area to the flux per unit area reflected from the irradiated area

3. DIFFUSE AND SPECULAR REFLECTANCE

The energy per unit time or flux incident on a solar concentrator is partitioned into several forms and modes. The most important of these is the specular reflectance mode, in which the flux follows a path of propagation predictable by geometrical optics. Furthermore, this mode can be described only by assuming relatively large areas that are operating as uniform reflectors. Small areas must be treated under diffuse reflectance.

Diffuse reflection cannot be predicted by geometrical contour and ray-path analysis. It arises from small imperfections in surface smoothness. The size of these imperfections tends to be about a wavelength of the incident flux; hence, diffraction optical effects are as important as "ray" optics. The theoretical bases for describing diffuse reflection incorporate the same quantities and relationships used in treatment of scattering. The diffuse reflection generally has a strong dependence on wavelength, size of the imperfections, and number of imperfections per unit area (or volume).

The primary phenomena of diffuse reflection are angular distributions around the nominal direction of propagation and magnitude of the relative amount of flux totally scattered from the incident beam. (Polarization of the scattered flux is also present, but this is not significant to solar concentrators.) The measurement of diffuse reflectance from large concentrators would be difficult to separate from the geometrical optical effects of poor contours. Some idea of the magnitude of diffuse reflectance can be obtained from data on small replica mirrors (Refs. 1 and 2). These mirrors are made by a process very similar to that used for the reflecting surface of large rigid petals for solar concentrators.

The data referenced in the previous paragraph (Refs. 1 and 2) indicate that 2 to 3 percent of the available flux is scattered into a "lobe" around the primary reflected bundle. The width of the lobe is unknown, but the half-power, half-width is estimated at 1 deg or smaller.

On the basis of these estimates, a concentrator with a 60-deg rim angle and a heat receiver subtending 4.245 deg at the paraxial focal plane would not suffer from diffuse reflectance if all other conditions (contour, pointing, and alignment) were perfect.

There is also a possibility that the magnitude of diffuse reflectance may increase with relatively high temperature for epoxy substrate mirrors. This effect has not been reported for solar concentrators up to now.

4. TOTAL ENERGY AND SPECTRAL REFLECTANCE

The reflecting ability of thin films of metal deposited under high-vacuum conditions is well known. Various metals—primarily aluminum, gold, copper, silver, and rhodium—are being used, but aluminum has the best performance when averaged over all spectral regions. Pure aluminum films show a reflectivity of approximately 91 percent averaged over the 0.2- to 0.7-μ wavelength interval, and 95 percent in the 1- to 2-μ region (Ref. 3).

The aluminum films without any protective coating are easily scratched and difficult to clean. Aging in a moderate environment produces no serious loss of reflectivity, but in severe environments the film could be eroded. For these reasons, most thin-film aluminum (Al) mirrors are overcoated with a protective material, usually silicon monoxide (SiO). This overcoating reduces reflectivity, particularly in the ultraviolet region (0.2- to 0.3-μ wavelength).

The data on Al + SiO mirrors show an average perpendicular reflectivity of 88 percent for the solar spectrum (Ref. 4). This reflectivity is for thick SiO overcoatings at thicknesses greater than 0.25 μ.

The use of Al + SiO reflecting surfaces for solar concentrators would be a routine matter in fabrication, but the large size of useful concentrators presents special problems. The vacuum chamber for depositing the films must also be large, and the usual techniques such as glow-discharge cleaning, high rate of evaporation of aluminum, control of film thickness, and control of angle of evaporation are difficult to apply. It is known (Ref. 3) that Al films thicker than 0.06- to 0.07-μ develop coarse surface irregularities which scatter light and decrease spectral reflectivity.

Because of the problems of fabricating large solar concentrators, it is best to consider measuring reflectance from full-scale structures as the only way to evaluate absorption accurately. Since the reflectance could easily drop to about 75 percent, the values of 88 percent stated above should be considered the upper limit for a perfect mirror.

In addition to the loss of energy to the heat receiver caused by low reflectance (high absorptance), the absorbed energy potentially can affect the contour accuracy of the reflector. A thermal gradient from the reflecting surface to the back face of the solar concentrator will produce bending or warpage. This effect has been noted for many years by astronomers using telescopes that have large glass mirrors with reflective coatings. The effect is expressed as a change in focal length (Ref. 5) by the following:

$$\Delta f = -2f^2 \alpha \frac{\Delta T}{W}$$

where:

f = focal length
α = linear coefficient of expansion
ΔT = temperature difference
W = thickness

The equation is probably useful only for reflectors with homogeneous and uniform cross sections. Any application of the equation to solar concentrators might be misleading. It would be possible to show conditions that would produce large changes in focal length; but useful concentrators will probably employ various controls over the effective temperature gradient, and these are outside the scope of this study.

5. SUMMARY

The surface spectral reflectance of solar concentrators will decrease the optical efficiency by at least 12 percent for aluminum reflecting films overcoated with silicon monoxide. Further losses will be experienced directly by diffuse reflectance, although the lack of data makes it impossible to determine a basis for estimating this loss. Indirectly, absorption of energy at the reflecting face will cause a loss of energy to the heat receiver if the concentrator changes its contour because of thermal gradients induced across its thickness.

Section VI

SURFACE REFLECTANCE TESTING

The several types of reflectance have been discussed in Section V. The different types indicate the problems, methods, and instrumentation for testing full-scale solar concentrators. Only the most preliminary ideas, problems, and solutions are presented here.

Diffuse reflectance can probably be tested with either wide-spectrum or monochromatic sources, since it is closely related to geometrical optical errors. The direction of propagation of test beams must be accurately determined for geometrical tests, and diffuse reflectance is measurable around this direction. A major problem arises if the diffuse "component" has a large angular extent, thereby requiring a hemispherical field-of-view sensor. This condition does not seem to be a logical possibility for solar concentrator surfaces. The measurement data on diffuse-reflectance spread for individual surface elements can be used to predict the diffuse reflectance of the concentrator as a whole.

The problems are much more complicated for spectral and/or total energy reflectance. This type of reflectance must be measured as a function of the absorption of flux in the incident beam. Both the absolute magnitudes of the incident flux and the reflected flux are required. The only safe way to make a test is to employ sensors adjacent to the surface element under test. This method will be difficult with full-scale concentrators. It may not be too difficult, however, on tests of individual petals of certain types of solar concentrators, using a large version of a reflectometer. If the tests are to be used to evaluate accurately reflectance as a whole, the angle of incidence of the irradiating beam should be adjusted to conform to the solar angle of incidence for the surface area being measured. The surface element test is recommended over the full-area tests because it is difficult to obtain a valid absolute measure of the total flux in a large and aberrated image of a reference source such as the sun or high-power gas-discharge arc. The working distances are so large, for solar concentrators, that the flux can be significantly attenuated (by scattering and absorption) by the intervening atmosphere; and geometrical aberrations plus diffuse reflectance would complicate matters. To compensate for this complication would be difficult.

Performing the spectral reflectance test on large surface areas in a vacuum would lessen the problems, although the geometrical aberrations would still be present.

The tests of the indirect effects of absorption on collector efficiency—namely, the bending or warpage due to thermal gradients—will require full-area tests. Preferably, the test should be performed on the collector as a whole to take advantage of mechanical constraints and thermal distortion compensators. Since the test results will be

primarily geometrical data, the radiometric characteristics of the heaters and coolers (used to produce a thermal gradient) are not very important. The importance of these characteristics for the test results has to be evaluated more fully, however, because the principal absorption of energy by the reflective surface is in the ultraviolet region. If the radiant source emitted sufficient power in the ultraviolet region, thermal gradients could be established more quickly than would be possible with infrared emitters.

In summary, surface reflectance testing will be difficult to achieve. First of all, tests in vacuum are mandatory. Also, tests of small elements (petals) are practical only if care is taken to simulate the mechanical linkages of the full-scale concentrator. If the simulation is performed with sufficient accuracy, then tests of small areas of reflectance within the elements are satisfactory for both diffuse and spectral reflectance. Nevertheless, tests of the effects of both cross-sectional and circumferential thermal gradients will be meaningful only if the entire surface of an element is used.

Section VII
CONCLUSIONS

1. GENERAL CONCLUSIONS

The primary objective of this study was to assess the relationship of geometrical optical characteristics to solar concentrator performance and component specifications. The most general conclusion derived as a result of the work completed was that geometrical optical analysis is needed to determine the effects of vignetting in the focal region by the heat-receiver aperture. The geometrical extent of the solar flux in the focal region is relatively large, and spillage outside the heat-receiver aperture may be a significant cause for a loss of overall system efficiency. The derivation of numerical estimates of the energy lost to the heat receiver due to geometrical contour errors was outside the scope of the study. That problem has to be analyzed using the typical errors of real solar concentrator contours.

The nature, magnitude, and statistics of the typical errors have yet to be determined, especially for the new designs of solar concentrators being considered for the ASTEC Program. Digital computer programs are needed for the analysis, and these will probably have to be developed after achieving a good understanding of the contour errors. It is expected, on the basis of past experience, that the capacity of large computers will become overloaded by the large amount of data involved, if simple curve-fitting routines are used: hence, good criteria for data acceptance/rejection or grouping will have to be employed. The important mathematical functions for describing primary geometrical contour errors have been derived as part of this study. These can serve as the basis for a number of criteria in subsequent studies.

2. FURTHER CONCLUSIONS

a. Optical Aberrations

Conventional geometrical optical aberrations of a solar concentrator are very important in analyzing the relationships of pointing and misalignment errors to contour errors. Typical values used in the study were: a 52-ft-diam. paraboloidal reflector with a 60-deg rim angle, a 20-in.-diam. heat receiver, a 12-min-of-arc pointing error, and a 5-min-of-arc misalignment of the center of the heat-receiver aperture. On the basis of these conditions, approximately an 8-min-of-arc average deviation in the surface normals from the ideal can be allowed. This is considered to be a very tight tolerance.

b. Deformation Errors

Geometrical optical errors due to contour imperfections are both static and dynamic. The static (or systematic) errors arise from limitations in manufacturing tooling and

in process control. The dynamic errors are due to effects of the environment encountered in earth orbits. Also, the environmental differences between terrestrial and orbital locations can produce apparent errors of contour, and these can be called dynamic in a limited sense. The major problem is the mechanical distortion and warpage induced by thermal gradients. The magnitude of this effect on the ASTEC concentrators has not been evaluated in this study.

c. Optical Qualities

The description of geometrical optical qualities cannot be divorced from the property of diffuse reflectance. The only meaningful way to characterize the geometrical optical performance is by intensity distributions in the focal region. If the diffuse reflectance of local areas in the reflector, such as defined by annular zones, varies from other areas, the intensity distribution in the focal region may be significantly different from that of the ideal. It is expected that the diffuse reflectance will have a strong dependence on angle (i.e., be non-Lambertian), and this dependence will affect the allowable tolerances on the combined pointing-angle and contour errors. The magnitude of this effect has not been evaluated since it appears to depend on specific surface degradation caused by temperature and duration of exposure. Also, variations in spectral reflectance will affect the intensity distribution, but probably only to a small degree.

d. Testing Optical Qualities

The best method for testing geometrical optical qualities appears to be the measurement of deviations in the angle of the normals to the reflecting surface. The measurements should be made for large numbers of zones and of elemental areas within these zones.

e. Design Concept

A design concept for a geometrical optical test system was evolved for the ASTEC solar concentrator. The system employs a laser beam reflecting off a servo-driven, gimballed mirror, with the mirror in the region of the axial intercept of the surface normals. The test system instrumentation is feasible, as demonstrated by past developments. The design concept offers the advantage of providing the data required for derivation by digital computer of the geometrical contours of the concentrator.

f. Utility of Descriptions

The utility of geometrical optical and geometrical contour descriptions is that they permit correlation of environmental effects and specific designs of concentrators and heat receivers, in terms of achievable input temperatures. (The possibility arises that an oblate spheroid may be a better contour than a perfect paraboloid for the thermal cycling conditions encountered in orbit.)

In summary, the solar concentrator is an optical-mechanical device; and testing and evaluation, to determine upper limits of performance, must necessarily include geometrical optical characterizations.

Appendix I

IMAGE FORMATION BY A PARABOLOIDAL REFLECTOR

1. INTRODUCTION

A paraboloid of revolution is very well defined mathematically. Its basic properties are characterized by the symmetry axis and its paraxial focal point. If a paraboloid is used as an image-forming, reflective optical system, the image quality is dependent on the size and the location of the object with respect to the optical axis (axis of rotational symmetry), and on the paraxial focal length as a function of the mirror's diameter and rim angle. Even though the paraboloid may be perfect, the image of an object subtending a large angle is poorer in quality at the edges of the paraboloid than at the regions nearer the optical axis.

Analyzing the aberrations of the image of an off-axis point object is generally considered the best way to characterize the image quality in the sense of geometrical optics. The methods of describing the aberrations may vary with different mathematical treatments, but they are, in principle, based on or related to three-dimensional analytical geometry formulations. For this reason, the derivation of the common algebraic equations expressing the relationship of optical parameters to useful coordinate systems is presented in this appendix.

2. GENERAL REPRESENTATION

a. The Paraboloid of Revolution

The image formation by a paraboloidal reflector for off-axis objects at infinity (point sources) is treated by an analytical ray-tracing method.

The equation of the paraboloid of revolution, basically, may be written in the form

$$X^2 + Y^2 = 4f(Z + f) \tag{1}$$

where f denotes the paraxial focal length and the Cartesian coordinates (X, Y, Z) refer to a system with origin at the paraxial focal point. The Z-axis coincides with the optical axis; its positive branch points from the focal point in direction to the object plane at infinity. The vertex is defined by $Z_V = -f$, $X_V = Y_V = 0$. Usual polar coordinates may be introduced by

$$X = R\cos\phi \quad ; \quad Y = R\sin\phi$$

$$R = r\sin\theta \quad ; \quad Z = -r\cos\theta$$

where

r = distance between the paraxial focal point and a specific annular zone of light-ray incidence at the paraboloidal surface
R = radius of the zone
θ = zone angle between r and the optical axis (Fig. 5)

Solving Eq. (1) in terms of θ produces

$$r = \frac{2f}{1 + \cos\theta} = \frac{f}{\cos^2 \theta/2} \tag{2}$$

For the solar energy reflector under consideration. the mirror is assumed to be characterized by a fixed diameter, D_m, whereas its rim angle, θ_m, may be changeable. Thus, the paraxial focal length becomes a function of these two parameters; i.e., one has

$$f = \frac{D_m}{4} \operatorname{cotan} \theta_m/2 = \frac{D_m}{4} \frac{1 + \cos\theta_m}{\sin\theta_m} \tag{3}$$

Sometimes it may be more advantageous to describe the paraboloidal surface in another coordinate system. For example, a Cartesian coordinate system (x,y,z) with origin at the apex may be used, yielding

$$x^2 + y^2 = 4fz^{(2)} \tag{4}$$

The tangential plane at a specific point $P_i (X_i, Y_i, Z_i)$ on the paraboloidal surface is known to be described by

$$X_i(X - X_i) + Y_i(Y - Y_i) - 2f(Z - Z_i) = 0 \tag{5}$$

resulting in the direction cosines

$$\cos\alpha_n = \frac{X_i}{\sqrt{X_i^2 + Y_i^2 + 4f^2}}; \cos\beta_n = \frac{Y_i}{\sqrt{X_i^2 + Y_i^2 + 4f^2}}; \cos\gamma_n = -\frac{2f}{\sqrt{X_i^2 + Y_i^2 + 4f^2}} \tag{6}$$

---

2. For greater generality, it may also be convenient to use nondimensional representations by referring the Cartesian coordinates and length units either to the rim radius, $R_m = D_m/2$, or to the rim diameter of the mirror, and to express the dimensionless focal length by the rim angle θ_m.

where

r = distance between the paraxial focal point and a specific annular zone of light-ray incidence at the paraboloidal surface
R = radius of the zone
θ = zone angle between r and the optical axis (Fig. 5)

Solving Eq. (1) in terms of θ produces

$$r = \frac{2f}{1 + \cos\theta} = \frac{f}{\cos^2 \theta/2} \tag{2}$$

For the solar energy reflector under consideration. the mirror is assumed to be characterized by a fixed diameter, D_m, whereas its rim angle, θ_m, may be changeable. Thus. the paraxial focal length becomes a function of these two parameters; i.e., one has

$$f = \frac{D_m}{4} \operatorname{cotan} \theta_m/2 = \frac{D_m}{4} \frac{1 + \cos\theta_m}{\sin\theta_m} \tag{3}$$

Sometimes it may be more advantageous to describe the paraboloidal surface in another coordinate system. For example, a Cartesian coordinate system (x,y,z) with origin at the apex may be used, yielding

$$x^2 + y^2 = 4fz^{(2)} \tag{4}$$

The tangential plane at a specific point $P_i (X_i, Y_i, Z_i)$ on the paraboloidal surface is known to be described by

$$X_i(X - X_i) + Y_i(Y - Y_i) - 2f(Z - Z_i) = 0 \tag{5}$$

resulting in the direction cosines

$$\cos\alpha_n = \frac{X_i}{\sqrt{X_i^2 + Y_i^2 + 4f^2}}; \cos\beta_n = \frac{Y_i}{\sqrt{X_i^2 + Y_i^2 + 4f^2}}; \cos\gamma_n = -\frac{2f}{\sqrt{X_i^2 + Y_i^2 + 4f^2}} \tag{6}$$

---

2. For greater generality, it may also be convenient to use nondimensional representations by referring the Cartesian coordinates and length units either to the rim radius, $R_m = D_m/2$, or to the rim diameter of the mirror, and to express the dimensionless focal length by the rim angle θ_m.

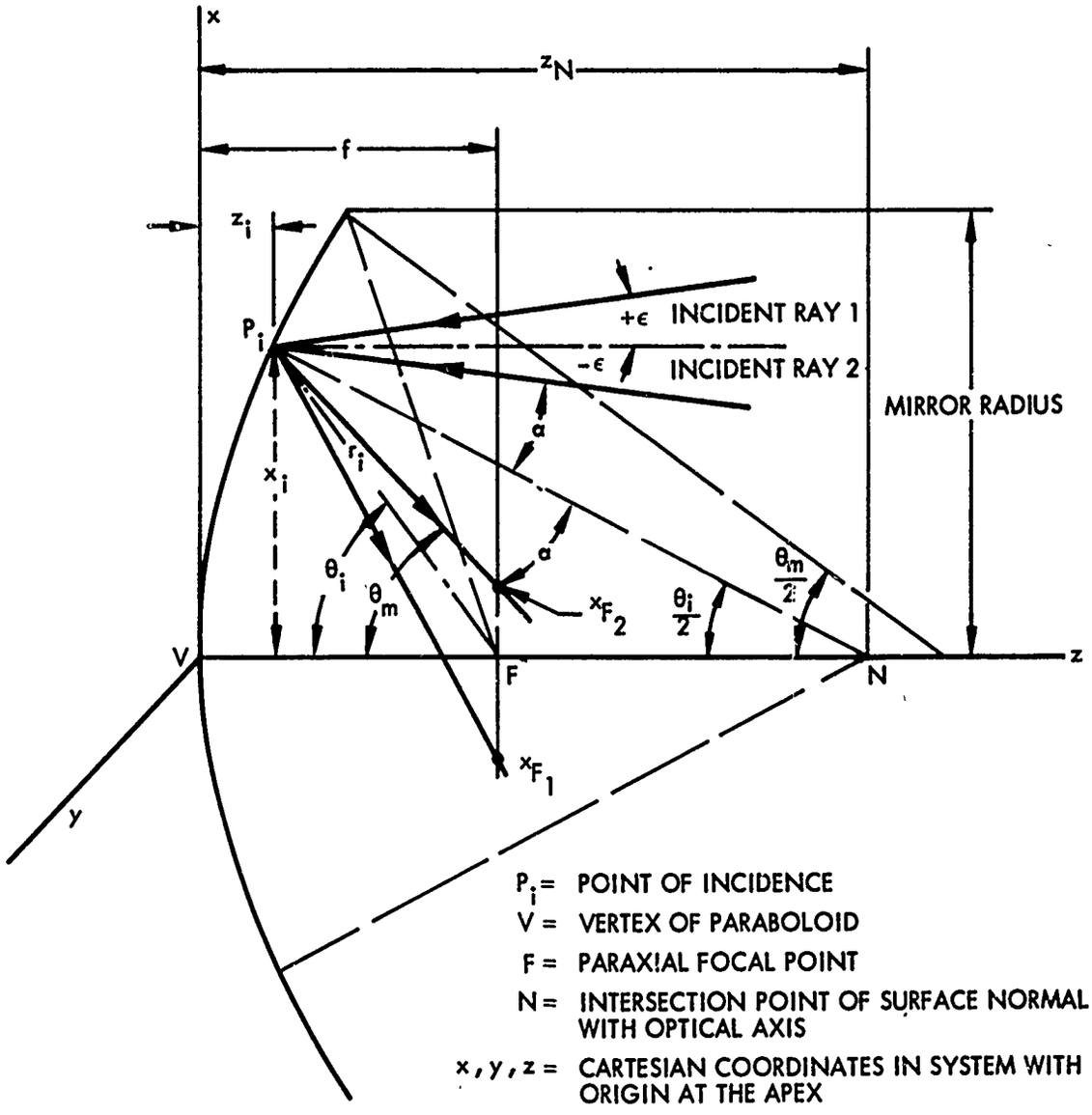

Figure 5 Image Formation by a Paraboloid of Revolution, Tangential Plane Representation of Geometrical Configuration Encountered

Thus, the normal at P_i is given by

$$\frac{X - X_i}{\cos \alpha_n} = \frac{Y - Y_i}{\cos \beta_n} = \frac{Z - Z_i}{\cos \gamma_n} \tag{7}$$

i.e. as intersection of the two planes

$$\left.\begin{aligned} (X - X_i) \cos \gamma_n - (Z - Z_i) \cos \alpha_n &= 0 \\ (Y - Y_i) \cos \gamma_n - (Z - Z_i) \cos \beta_n &= 0 \end{aligned}\right\} \tag{8}$$

For later applications, the intersection point N of the normal with the optical axis, $X = Y = 0$, is of special interest. It is determined by

$$X_N = Y_N = 0 \; ; Z_N = Z_i - X_i \frac{\cos \gamma_n}{\cos \alpha_n} = Z_i + 2f = \frac{2f}{1 + \cos \theta_i} = r_i$$

(see Fig. 6). The length of the normal between the two points P_i and N may also be of interest (see Fig. 7):

$$r_N = \frac{Z_N - Z_i}{\cos \theta_i/2} = \frac{2f}{\cos \theta_i/2}$$

The paraxial focal point F is only one specific point characterizing the properties of a paraboloidal reflector. A deeper insight is obtained by determining the Gaussian focal surface, a surface of revolution defined by the principles of geometrical optics as locus of all points at half the distances between the points P_i on the paraboloid and their correlated centers of curvature. One easily obtains the coordinates of the centers of curvature:

$$R_C = 3 R_i + 4f \; ; \; Z_C = -\frac{Z_i^3}{4f^2}$$

as well as those of the corresponding points on the Gaussian focal surface:

$$R_G = 2(R_i + f) \; ; \; Z_G = \frac{Z_i}{8f^2}(4f^2 - Z_i^2)$$

The cross-sections through the two surfaces (Figure 8) show that the Gaussian focal surface, especially for larger zone angles, deviates significantly from the paraxial focal piane.

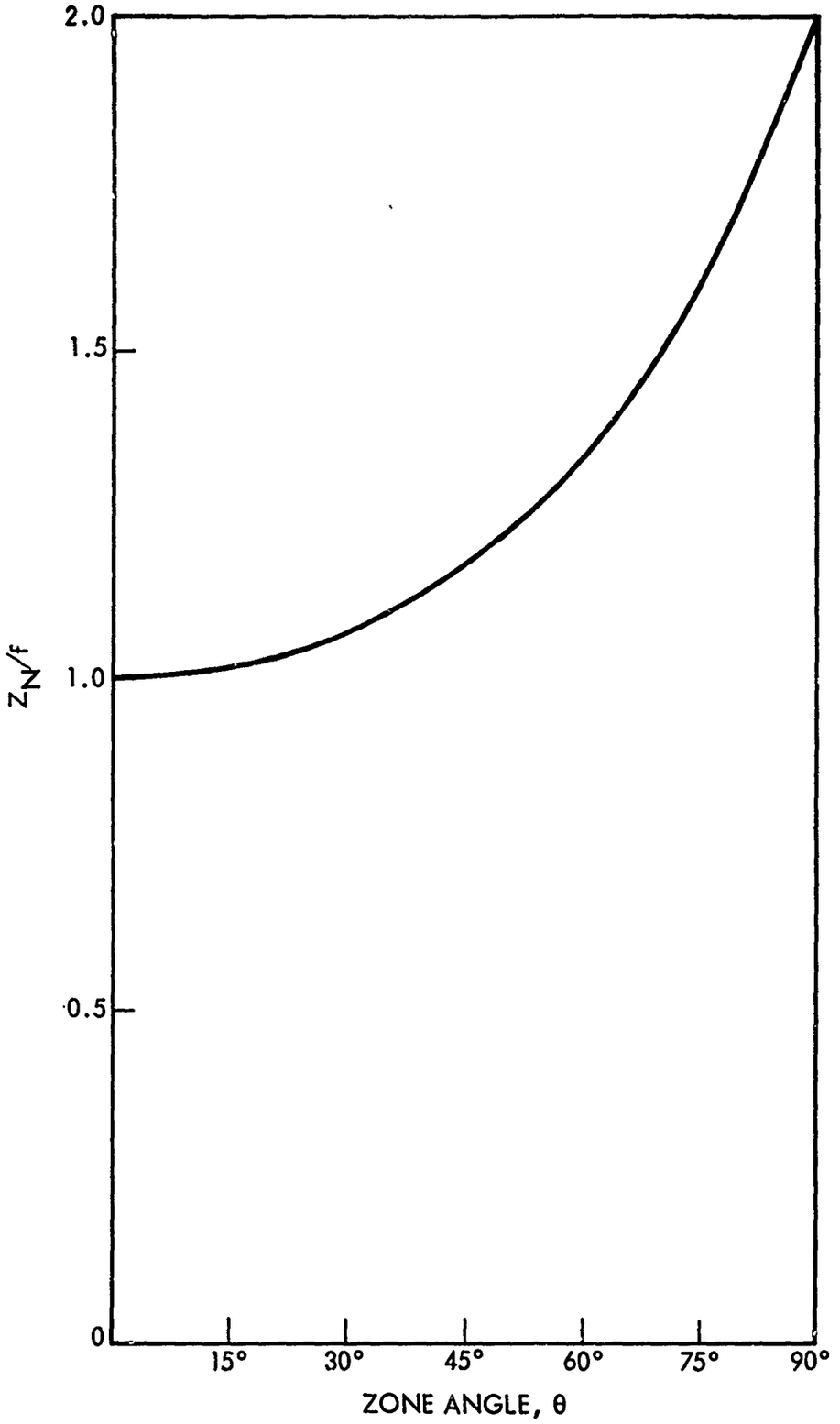

Figure 6 Distance of Paraboloidal Surface
Normal Intersect with Optical Axis from Focus, $Z_N = 2f/(1 + \cos\theta)$

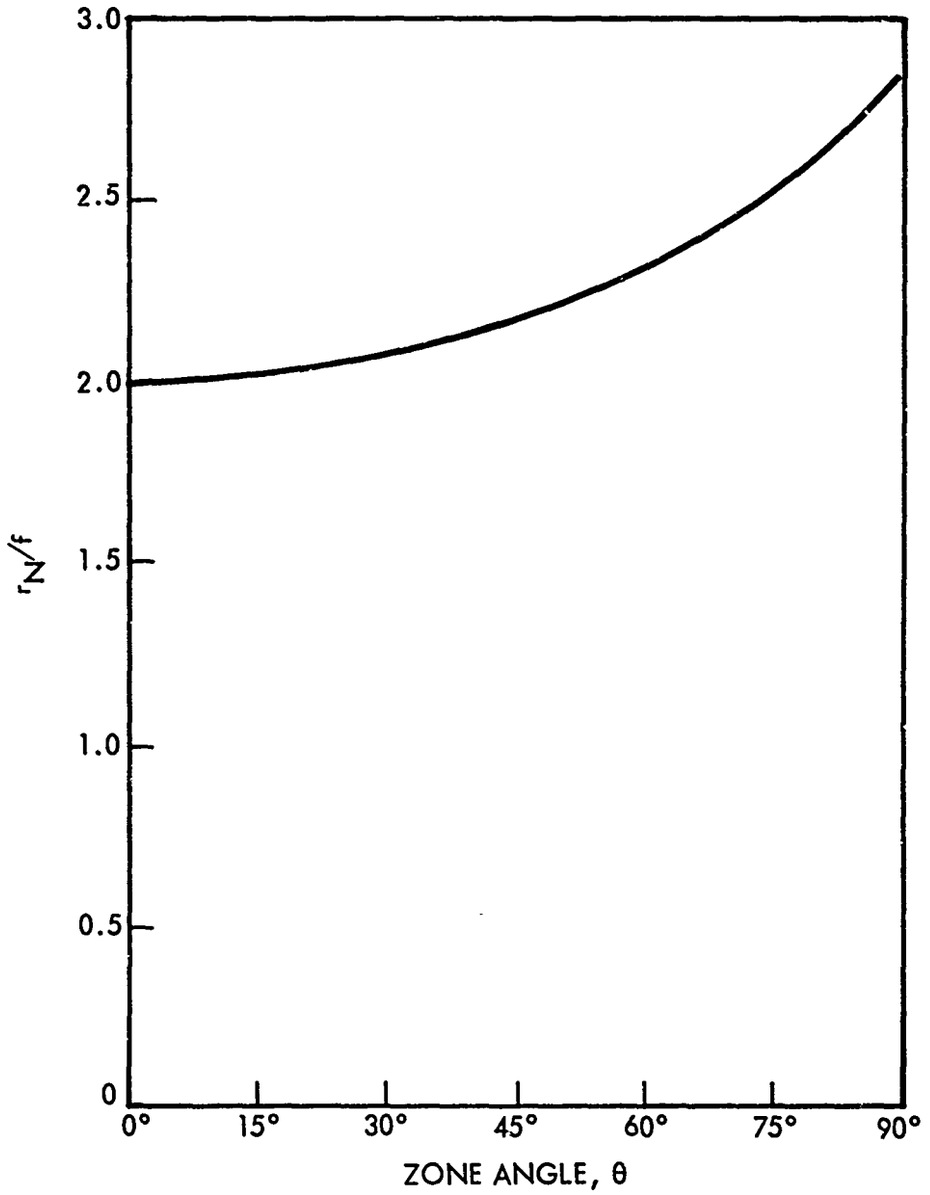

Figure 7 Length of Paraboloidal Surface
Normal Between Surface and Intersect with Optical Axis, $r_N = 2f/\cos(\theta/2)$

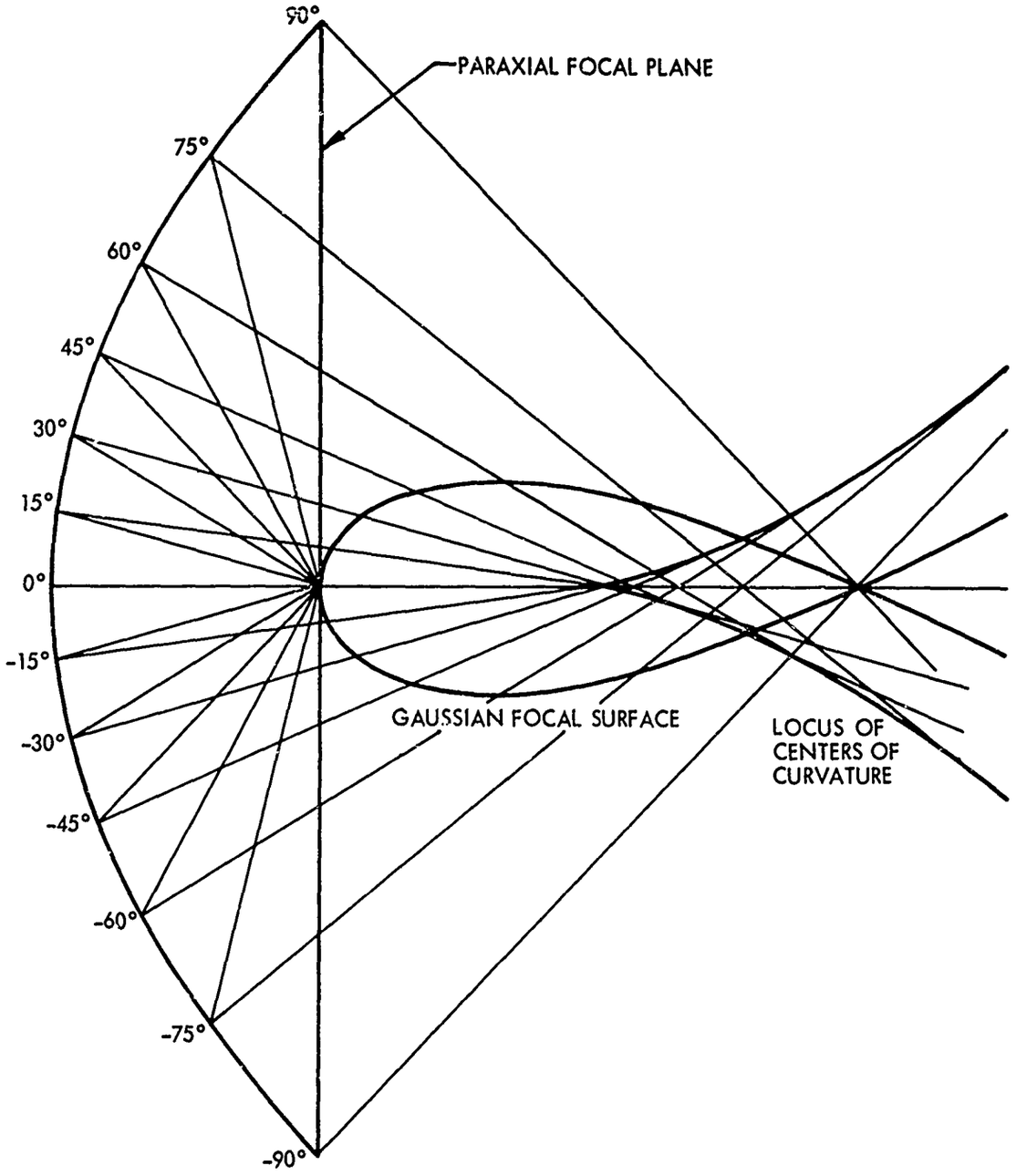

Figure 8 Evolute and Gaussian Focal Surface of a Paraboloid of Revolution

This fact may be considered an indication of the unusual problems encountered in the image formation by large rim-angle paraboloidal mirrors. If referred to origins at the peak C of the evolute and the branch intersect G of the Gaussian focal surface, the two surfaces of revolution are described, in polar coordinates, by

$$\rho_C = f\frac{27}{4}\frac{\sin^2\theta_C}{\cos^3\theta_C} \; ; \; -\pi/2 \leqq \theta_C \leqq \pi/2$$

and

$$\rho_G = 2f\frac{\cos^2\theta_G - 4\sin^2\theta_G}{\cos^3\theta_G} \; ; \; -\pi/2 \leqq \theta_G \leqq \pi/2$$

respectively, where θ_C is the angle between ρ_C and the positiveZ-axis, and θ_G is the angle between ρ_G and the negative Z-axis. In the original system, the points C and G have the coordinates $X_C = Y_C = 0, Z_C = 2f$ and $X_G = Y_G = 0$, $Z_G = 3f$. respectively.

b. Principles of Ray Tracing

The principal ray in a parallel beam of incident light (corresponding to a point source at infinity) may be assumed, without restricting the generality, to be located in the specific meridional plane defined by the X- and Z-axes, and to be inclined by an angle ϵ with respect to the optical axis. To characterize a particular ray of the bundle, the parameters R_i and ϕ_i as well as θ_i may be introduced, where R_i is the radial distance of the zone considered from the optical axis, ϕ_i is the angle made by the radius vector R_i with the X-axis, and θ_i is the zone angle.

Then, the incident ray is defined as the intersection line of the two planes:

$$\left.\begin{aligned}(X - X_i)\cos\epsilon - (Z - Z_i)\sin\epsilon &= 0\\ Y - Y_i &= 0\end{aligned}\right\} \qquad (11)$$

Both the incident and the reflected rays make the angle α with the normal to the reflecting surface at the incidence point P_i; the angle between them is 2α. To determine the angle α, the following relations may be used:

$$X_i = R_i\cos\phi_i \; , \; Y_i = R_i\sin\phi_i \; , \; 2f = Z_N - Z_i = R_i\,\mathrm{cotan}\,\theta_i/2$$

This results in the direction cosines of the normal

$$\cos\alpha_n = \cos\phi_i \sin\theta_i/2 \ , \ \cos\beta_n = \sin\phi_i \sin\theta_i/2 \ , \ \cos\gamma_n = -\cos\theta_i/2$$

On the other hand, the direction cosines of the incident ray are

$$\cos\alpha_i = \sin\epsilon \ , \ \cos\beta_i = 0 \ , \ \cos\gamma_i = \cos\epsilon$$

Hence, the angle α is determined by

$$\cos\alpha = \cos\alpha_n \cos\alpha_i + \cos\gamma_n \cos\gamma_i = \cos\phi_i\left(\sin\theta_i/2\right)\sin\epsilon - \left(\cos\theta_i/2\right)\cos\epsilon$$

With the reflected ray now denoted by the subscript 0, its direction cosines ($\cos\alpha_o$, $\cos\beta_o$, $\cos\gamma_o$) are to be found by solving the triple equation

$$\begin{aligned}
&\cos\alpha_n \cos\alpha_o + \cos\beta_n \cos\beta_o + \cos\gamma_n \cos\gamma_o = \cos\alpha \\
&\cos\alpha_i \cos\alpha_o \qquad\qquad\qquad\quad \cos\gamma_i \cos\gamma_o = \cos 2\alpha \\
&\cos^2\alpha_o \qquad + \cos^2\beta_o \qquad + \cos^2\gamma_o \qquad = 1
\end{aligned}$$

The solution is obtained in the form

$$\begin{bmatrix}\cos\alpha_o \\ \cos\gamma_o\end{bmatrix} = \frac{1}{C_o}\begin{bmatrix}-C_1\cos\beta_o + C_2 \\ C_3\cos\beta_o - C_4\end{bmatrix}$$

where

$$\begin{aligned}
C_0 &= \cos\alpha_n\cos\gamma_i - \cos\gamma_n\cos\alpha_i = \cos\phi_i\left(\sin\theta_i/2\right)\cos\epsilon + \left(\cos\theta_i/2\right)\sin\epsilon \\
C_1 &= \cos\beta_n\cos\gamma_i = \sin\phi_i\left(\sin\theta_i/2\right)\cos\epsilon \\
C_2 &= \cos\gamma_i\cos\alpha - \cos\gamma_n\cos 2\alpha = -\cos\epsilon\cos\alpha + \left(\cos\theta_i/2\right)\cos 2\alpha \\
C_3 &= \cos\beta_n\cos\alpha_i = \sin\phi_i\left(\sin\theta_i/2\right)\sin\epsilon = C_1\tan\epsilon \\
C_4 &= \cos\alpha_i\cos\alpha - \cos\alpha_n\cos 2\alpha = \sin\epsilon\cos\alpha - \cos\phi_i\left(\sin\theta_i/2\right)\cos 2\alpha
\end{aligned}$$

$$\cos\beta_o = \frac{C_1 C_2 + C_3 C_4}{C_1^2 + C_3^2 + C_0^2}\left[1 \pm \sqrt{1 - \frac{\left(C_1^2 + C_3^2 + C_0^2\right)\left(C_2^2 + C_4^2 - C_0^2\right)}{\left(C_1 C_2 + C_3 C_4\right)^2}}\right] \quad (3)$$

3. For uniqueness of the solution, one has to ask for
$\left(C_1^2 + C_3^2 + C_0^2\right)\left(C_2^2 + C_4^2 - C_0^2\right) = \left(C_1 C_2 + C_3 C_4\right)^2$

The reflected ray, then, is determined by the two planes

$$\left.\begin{aligned}(X - X_i)\cos\gamma_o - (Z - Z_i)\cos\alpha_o &= 0\\ (Y - Y_i)\cos\gamma_o - (Z - Z_i)\cos\beta_o &= 0\end{aligned}\right\} \quad (12)$$

and its intersection point with the paraxial focal plane is given by

$$\left.\begin{aligned}X_F &= X_i - Z_i\frac{\cos\alpha_o}{\cos\gamma_o} = R_i\left(\cos\phi_i + \operatorname{cotan}\theta_i\frac{\cos\alpha_o}{\cos\gamma_o}\right)\\ Y_F &= Y_i - Z_i\frac{\cos\beta_o}{\cos\gamma_o} - R_i\left(\sin\phi_i + \operatorname{cotan}\theta_i\frac{\cos\beta_o}{\cos\gamma_o}\right)\\ Z_F &= 0\end{aligned}\right\} \quad (13)$$

3. PARTICULAR CASES OF INTEREST

a. Point Source at Infinity

Of particular interest are those pairs of parallel rays whose incidence points on the paraboloidal mirror are diametrically located relative to the optical axis. The most significant pairs, obviously, are the following:

Case 1. Tangential rays, defined by $\phi_i = 0$ and $\phi_i = \pi$
Case 2. Sagittal rays, defined by $\phi_i = \pi/2$ and $\phi_i = 3\pi/2$

In the case of tangential ray pairs, the coordinate Y vanishes, and the incident ray, the surface normal, and the reflected ray all lie in the meridional plane defined above as the (X, Z)-plane. This means that

$$X = \pm X_i = \pm R_i$$

$$Y - Y_i = 0$$

and

$$\cos\beta_i - \cos\beta_n = \cos\beta_o = 0$$

The case is most simply treated by purely geometrical considerations derived from Fig. I-5. One obtains very easily

	$\phi_i = 0$	$\phi_i = \pi$ (4)
$\cos \alpha_o$	$\sin (\theta_i + \epsilon)$	$\sin (\theta_i - \epsilon)$
$\cos \gamma_o$	$-\cos (\theta_i + \epsilon)$	$\cos (\theta_i - \epsilon)$

resulting in

$$\left.\begin{aligned} X_F &= -\frac{R_i \sin \epsilon}{\sin \theta_i \cos (\theta_i + \epsilon)} \quad \text{for} \quad \phi_i = 0 \\ X_F &= -\frac{R_i \sin \epsilon}{\sin \theta_i \cos (\theta_i - \epsilon)} \quad \text{for} \quad \phi_i = \pi \\ Y_F &= 0 \\ Z_F &= 0 \end{aligned}\right\} \quad (14)$$

In the case of sagittal ray pairs, the coordinate X is vanishing. Although one has again

$$\cos \beta_i = 0$$

one obtains

$$\cos \beta_n \neq \cos \beta_o \neq 0$$

This results in

	$\phi_i = \pi/2$	$\phi_i = 3\pi/2$ (5)
$\cos \alpha_o$	$-\sin \epsilon$	$-\sin \epsilon$
$\cos \beta_o$	$-\sin \theta_i \cos \epsilon$	$+\sin \theta_i \cos \epsilon$
$\cos \gamma_o$	$\cos \theta_i \cos \epsilon$	$\cos \theta_i \cos \epsilon$

4. Note that, always by definition, $\theta_i \geqq 0$.
5. It can be shown that, in this special case, $\left(C_1^2 + C_3^2 + C_0^2\right)\left(C_2^2 + C_4^2 - C_0^2\right) = (C_1 C_2 + C_3 C_4)^2$

It follows that

$$\left.\begin{aligned} X_F &= -\frac{R_i}{\sin\theta_i}\tan\epsilon \quad \text{for both } \phi_i = \pi/2 \text{ and } \phi_i = 3\pi/2 \\ Y_F &= 0 \\ Z_F &= 0 \end{aligned}\right\} \qquad (15)$$

From the fact that, for both tangential and sagittal ray pairs, the image points lie on a straight line, it can be concluded that the image of a point source at infinity in off-axis position is represented by a straight line in the paraxial focal plane.[6] This is primarily characteristic of optical reflectors with astigmatism. On the other hand, the image formation by a paraboloid of revolution is additionally characterized by coma, an aberration arising from the inconstancy of the actual focal length (in the sense of Gaussian optics) for every annular zone of the entrance pupil, as shown in Figure 8. The effects of astigmatism and coma, apparently, combine to produce the straight-line image in the paraxial focal plane. Thus, diametrically located rays emerging from a point source at infinity can be considered to define the performance of a paraboloidal reflector in terms of the overall geometrical-optical aberration effects encountered (coma, astigmatism,, curvature of field).

Pairs of diametrically located, parallel rays, of course, can very well be used to determine actual focal points and actual focal surfaces. For tangential ray pairs, as defined above for $\phi_i = 0$ and $\phi_i = \pi$, one obtains a specific cross-section through the actual focal surface for positive and negative values of the inclination angle, ϵ. The curved line, shown in Figure 9, is determined by

$$\left.\begin{aligned} X_f &= -R_i\frac{\sin 2\epsilon}{\sin 2\theta_i} = -2f\tan\theta_i/2\,\frac{\sin 2\epsilon}{\sin 2\theta_i} \\ Y_f &= 0 \\ Z_f &= -R_i\frac{(1-\cos 2\epsilon)}{\sin 2\theta_i} = -2f\tan\theta_i/2\,\frac{1-\cos 2\epsilon}{\sin 2\theta_i} \end{aligned}\right\} \qquad (16)$$

It may be seen seen that this cross-sectional line does not deviate appreciably from a straight line through the focus, defined by an angular deviation ϵ from the paraxial focal plane. Hence, if ϵ is a small quantity, the deviation of the meridional cross-section through the actual focal surface from the paraxial focal plane is not essential.

---

6. To prove this statement, it may be sufficient to treat intermediate cases of symmetrically located rays, like those defined by $\phi_i = \pm\pi/4$ and $\phi_i = \pm 3\pi/4$.

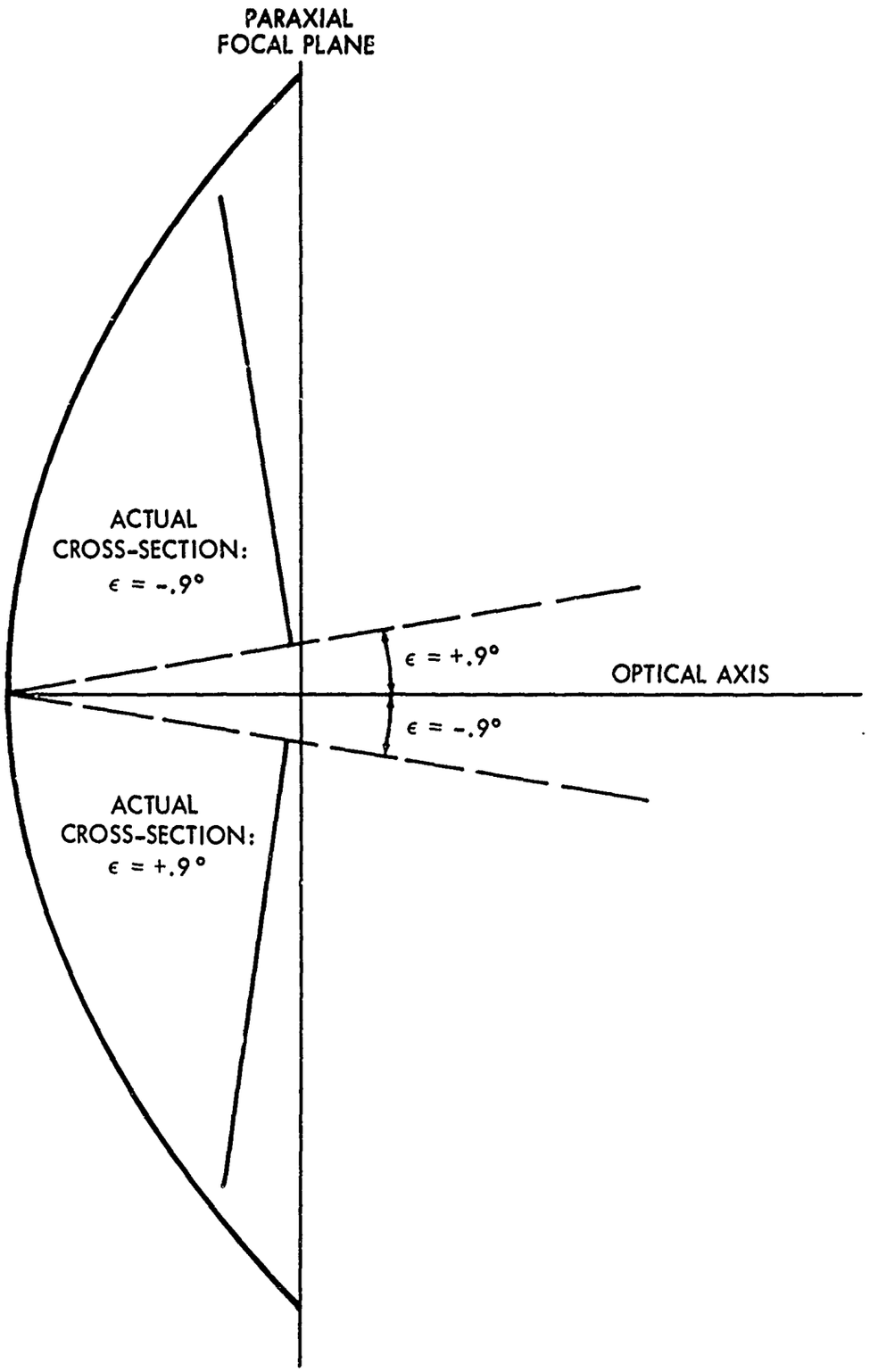

Figure 9 Meridional Cross-Section Through Actual Focal Surface, as Defined by Pairs of Parallel Tangential Rays

For relatively small inclination angles ϵ of the incident ray with respect to the optical axis, Figs. 10 and 11 show the dependence of the dimensionless quantities X_f/f and Z_f/f, respectively, from ϵ for a few zone angles θ as parameters.

From the particular rays obtained by reflection of the corresponding rays within a parallel bundle of light, incident at an angle ϵ relative to the optical axis, the meridional cross-section through the paraboloidal catacaustic can also be found, as shown partially in Fig. 12.

b. Light Cone From a Circular Source

It is assumed that a conical pencil of light rays with circular cross-section relative to its symmetry axis is incident upon a paraboloid of revolution in such a manner that the cone axis is parallel to the optical axis of the mirror. The angular subtense may be denoted by 2ϵ. The incidence point (cone vertex) may be chosen as $(X_i, 0, Z_i)$.

Then, from Eq. (14), one obtains immediately the intersection points of the reflected cone-mantle rays of the meridional plane with the paraxial focal plane:

$$\left.\begin{aligned} X_{F1,2} &= -\frac{R_i \sin\epsilon}{\sin\theta_i \cos(\theta_i + \epsilon)} \; ; \; R_i = X_i \; ; \; \epsilon \gtrless 0 \quad (7) \\ Y_{F1,2} &= 0 \\ Z_{F1,2} &= 0 \end{aligned}\right\} \quad (17)$$

For the reflected cone-mantle rays of the plane perpendicular to the meridional plane, one has, after appropriate modification, from Eq. (15).

$$\left.\begin{aligned} X_{F3,4} &= 0 \\ Y_{F3,4} &= -\frac{R_i}{\sin\theta_i}\tan\epsilon \; ; \; R_i = X_i \; . \; \epsilon \gtrless 0 \\ Z_{F3,4} &= 0 \end{aligned}\right\} \quad (18)$$

As the reflected light cone also has a circular cross-section (and angular subtense 2ϵ), its intersection with the paraxial focal plane, being inclined relative to the cone's symmetry axis, is an ellipse; i.e., the image of a circular source produced, in any plane perpendicular to the optical axis, by a small element of the reflecting paraboloidal

7. Note that $R_i/\sin\theta_i = r_i = 2f/(1 + \cos\theta_i)$

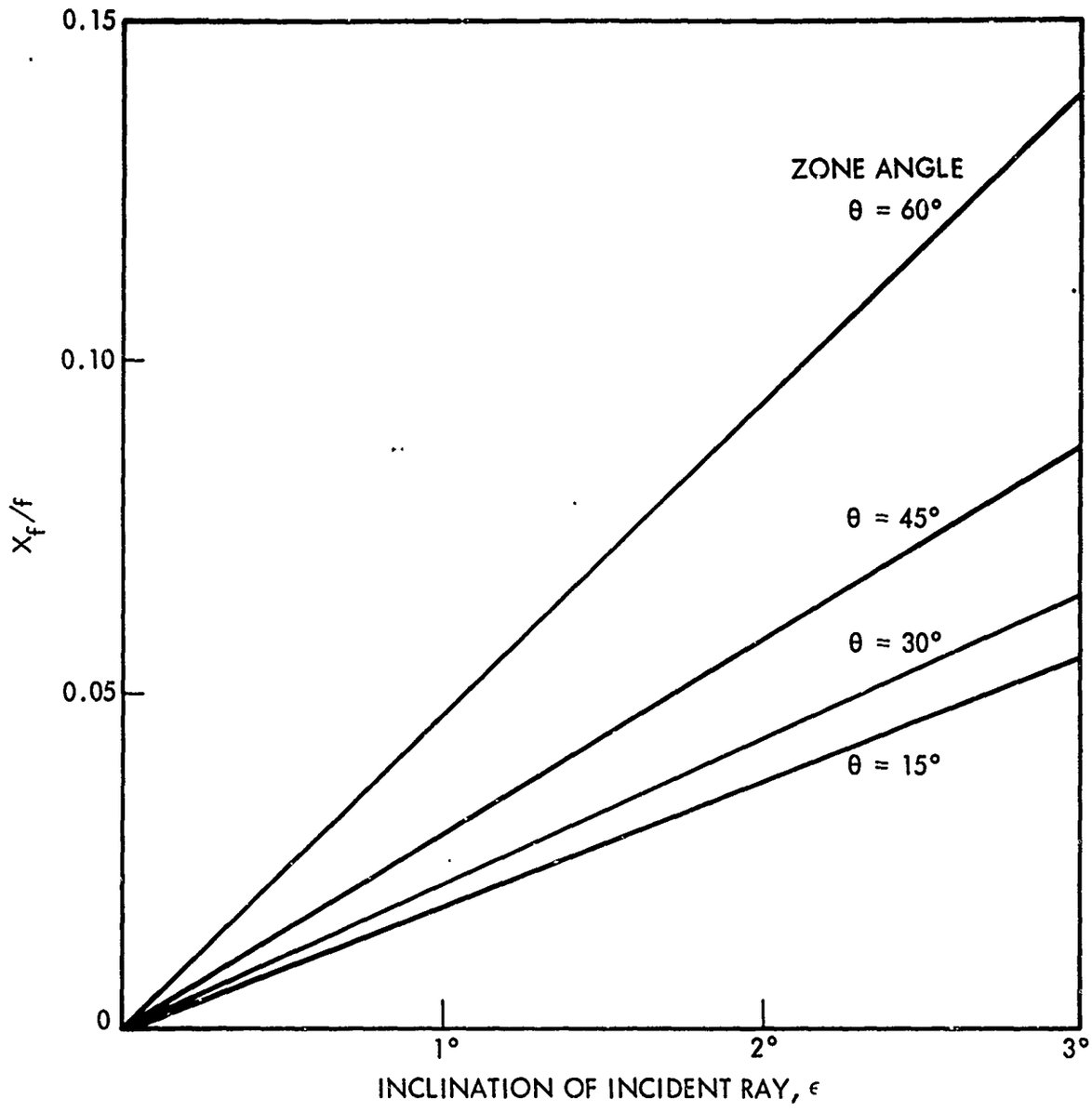

Figure 10 Actual Focal Point Location,
as Defined by Pairs of Parallel Tangential Rays, x-Direction

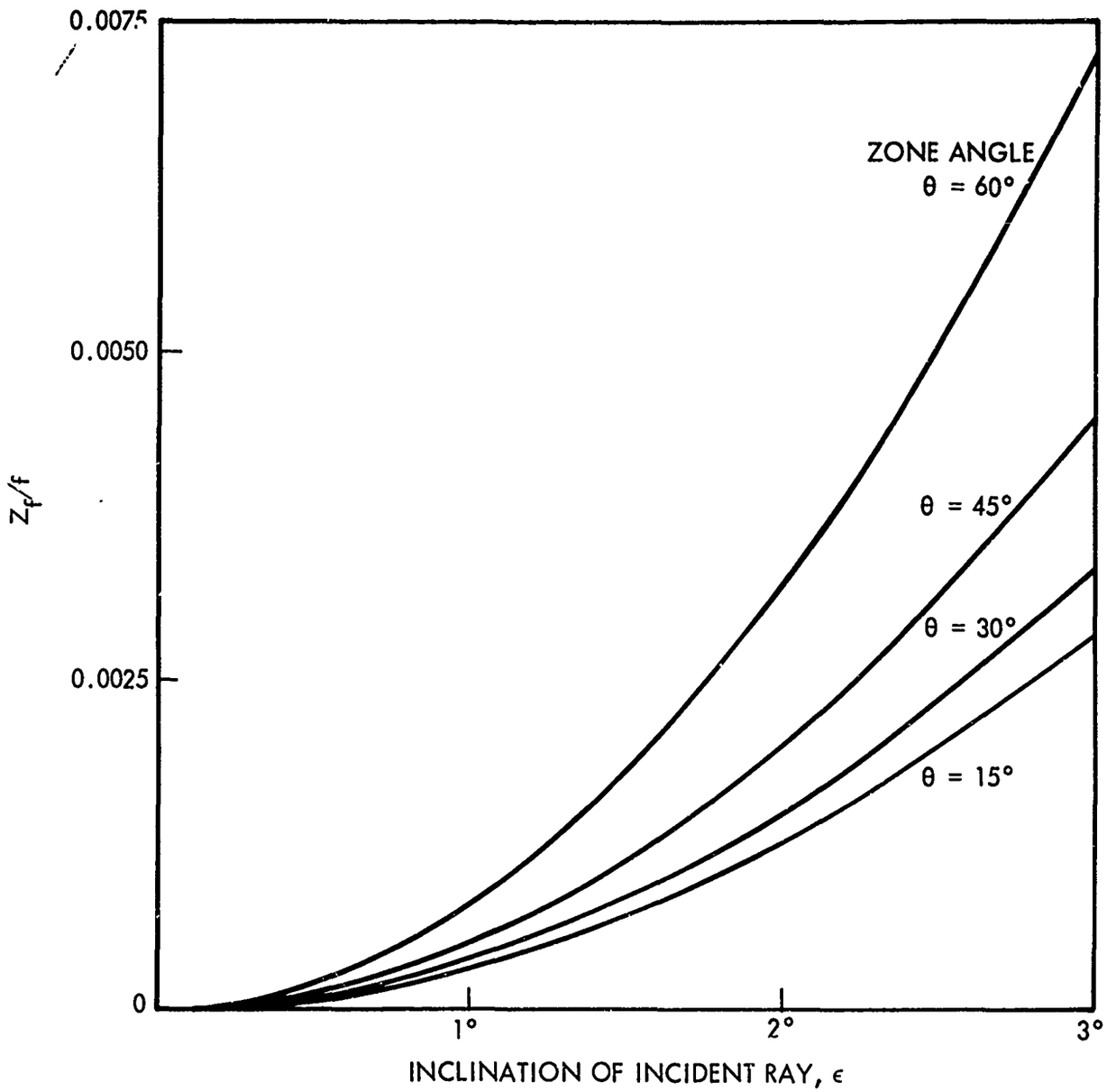

Figure 11 Actual Focal Point Location,
as Defined by Pairs of Parallel Tangential Rays, z-Direction

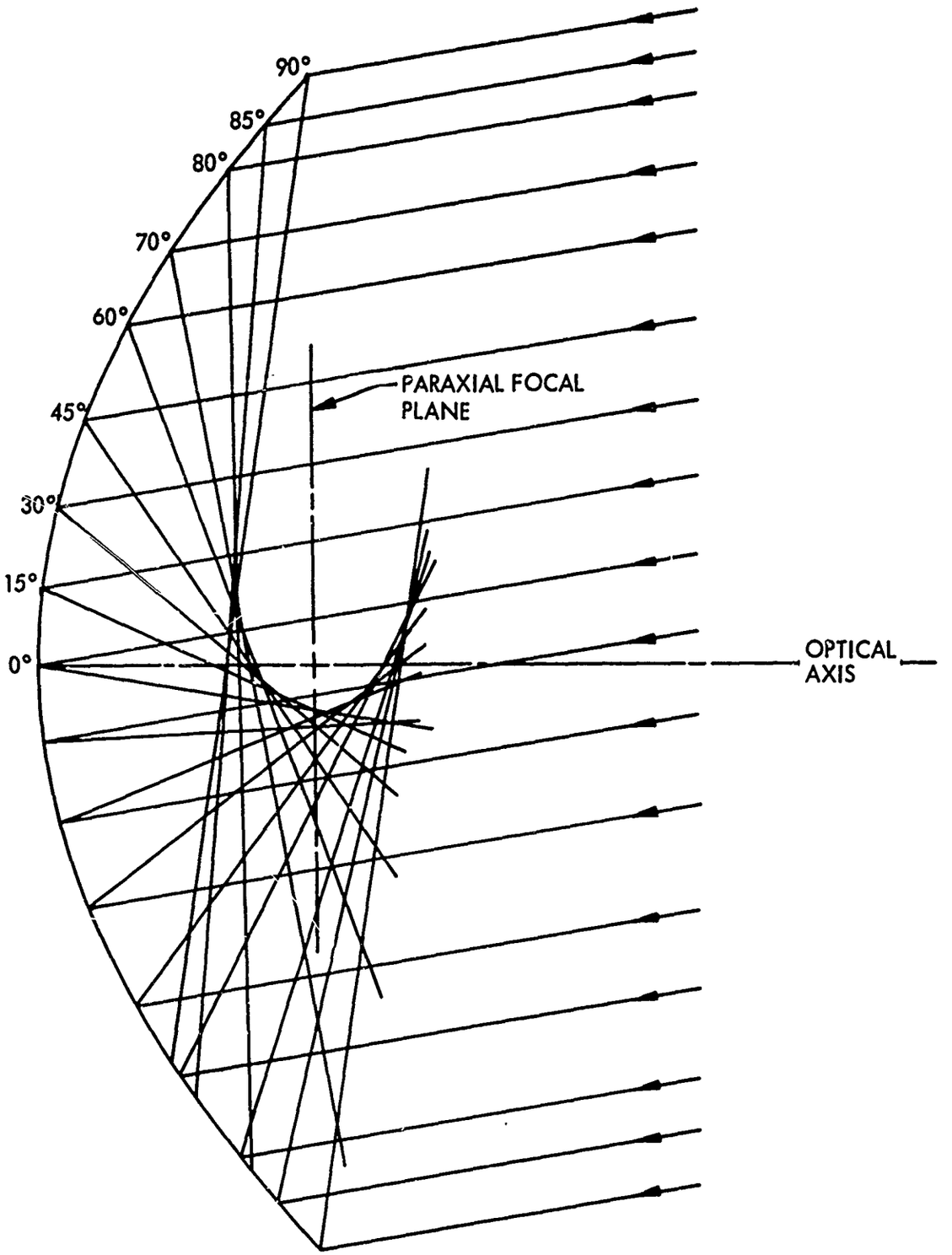

Figure 12 Catacaustic from Parallel Inclined Rays Incident Upon a Paraboloid of Revolution

surface has, in general, an elliptical boundary. Only the image formed by the mirror's central portion ($X_V = Y_V = 0$; $Z_V = -f$) is a circle of diameter $D_S = 2f\tan\epsilon$, provided that the incident light cone's symmetry axis is parallel to the optical axis.

Taking the four points $(X_{F1}, 0, 0)$, $(X_{F2}, 0, 0)$, $(0, Y_{F3}, 0)$, $(0, Y_{F4}, 0)$ one can determine the major half-axes, as well as the center of the image ellipse from

$$b^2 (X - X_e)^2 + a^2 (Y - Y_e)^2 - a^2 b^2 = 0$$

This results in

$$\left.\begin{aligned} X_e &= \frac{1}{2}(X_{F1} + X_{F2}) = -2f \frac{\sin\theta_i}{1 + \cos\theta_i} \frac{\sin^2\epsilon}{\cos 2\theta_i + \cos 2\epsilon} \\ &= -2f \frac{\tan\theta_i}{\cos\theta_i (1 + \cos\theta_i)} \frac{\tan^2\epsilon}{1 - \tan^2\theta_i \tan^2\epsilon} \\ Y_e &= \frac{1}{2}(Y_{F3} + Y_{F4}) = 0 \\ Z_e &\equiv 0 \end{aligned}\right\} \quad (19)$$

$$\left.\begin{aligned} a &= \frac{1}{2}|X_{F1} - X_{F2}| = 2f \frac{\cos\theta_i}{1 + \cos\theta_i} \frac{|\sin\epsilon|\cos\epsilon}{\cos 2\theta_i + \cos 2\epsilon} \\ &= 2f \frac{1}{\cos\theta_i (1 + \cos\theta_i)} \frac{|\tan\epsilon|}{1 - \tan^2\theta_i \tan^2\epsilon} \end{aligned}\right\} \quad (20)$$

$$\left.\begin{aligned} b &= \frac{|Y_{F3}|}{\sqrt{1 - \tan^2\theta_i \tan^2\epsilon}} = 2f \frac{\cos\theta_i}{1 + \cos\theta_i} \frac{|\sin\epsilon|}{\sqrt{\cos 2\theta_i + \cos 2\epsilon}} \\ &= 2f \frac{1}{1 + \cos\theta_i} \frac{|\tan\epsilon|}{\sqrt{1 - \tan^2\theta_i \tan^2\epsilon}} \end{aligned}\right\} \quad (21)$$

showing that

$$X_e = -a \tan \theta_i \, |\tan \epsilon|$$

$$b = a \cos \theta_i \sqrt{1 - \tan^2 \theta_i \tan^2 \epsilon}$$

(The deviation X_e of the ellipse center from the paraxial focal point is a very small quantity, if referred to the solar disk as radiation source, i.e., to $\epsilon = \epsilon_S \approx 0.00465$ rad. The quantity $(1 - \tan^2 \theta_i \tan^2 \epsilon_S)$ is approximately equal to unity even if θ_i becomes large within the range $0 \leqq \theta_i \leqq \theta_m$; therefore, this quantity is usually neglected. The large half-axis a , of course, is the most sensitive quantity if regarded as a function of θ_i .)

Neglecting the dislocation of the ellipse centers from the paraxial focal point, and assuming the incident light cone's symmetry axis to be parallel to the optical axis, Fig. 13 shows image ellipses of the apparent sun disk for some values of the zone angle θ . It is seen that the boundary of every individual image ellipse surrounds the image of the solar disk for $\theta = 0$; i.e., the circle of diameter $D_S = 2f \tan \epsilon_S$.

Even if the specific intensity of the source is uniformly distributed over its circular area, it results, for the elliptical image in the paraxial focal plane, in a nonuniform irradiance distribution along the X-axis whereas the distribution along the Y-axis may be approximately uniform. Since the flux in an elementary cone is constant, the average value of the irradiance distribution decreases as the area of the ellipse increases with increasing θ .

If, instead of a single point of incidence, a zone of incidence with radial distance R_i from the optical axis is considered, the image produced by the infinity of individual light cones is obtained by superimposing the corresponding image ellipses. It results in an image of circular shape around the paraxial focal point, the radius of which is determined by $|X_{F1}|$.

The image produced by all possible zones located infinitely close on the paraboloidal reflector, of course, has also a circular shape. The diameter of this image is defined by the rim angle θ_m of the mirror and by the half-cone angle. The intensity distribution in the image is to be obtained by superimposing the distributions in the images of the individual conical rings. Since the image size is determined by aberration effects, it is usually defined as a circle of confusion.

These statements are important insofar as they provide the fundamental means for optimizing the solar energy concentrator. If the radius of the apparent sun disk's image produced by all possible angular zones on the perfectly aligned paraboloidal reflector is determined by application of geometrical optics, the radius of the radiation-receiving aperture in the paraxial focal plane should not be smaller than the ideal image radius in order to avoid energy losses.

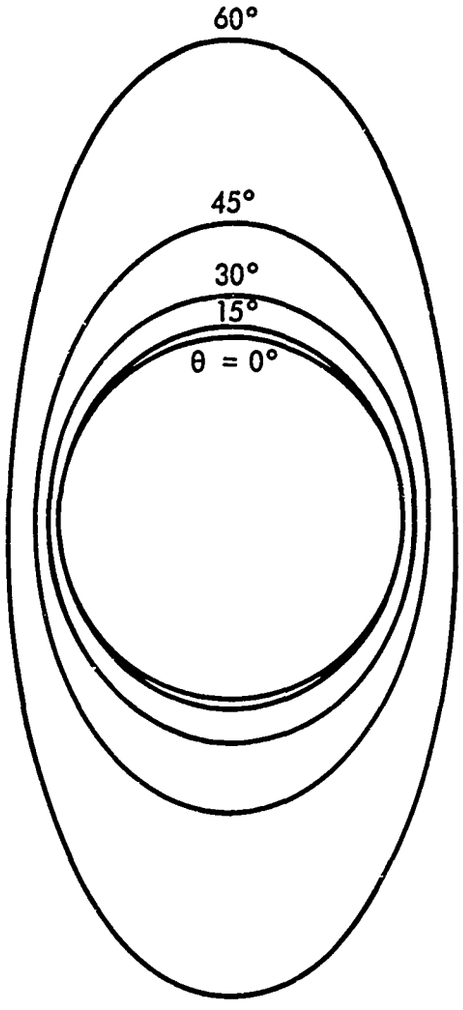

Figure 13 Image Ellipses of Apparent Solar Disk, Dislocations of Ellipse Centers Neglected

Of course, misalignment errors of the mirror-receiver system have to be taken into account, such as either or both of the following:

- Inclination of the mirror's optical axis with respect to the line-of-sight to the sun disk's center
- Dislocation and inclination of the receiver aperture plane relative to the paraxial focal plane

The inclination error of the reflector's optical axis, in principle, has already been treated in subsection 3a. The treatment resulted in the statement that the image of the sun disk's center, considered as a point source, appears as a straight line in the paraxial focal plane. However, denoting the inclination error by ϵ_i , and the half-angular subtense of the sun by ϵ_S , the effect of the finite extension of the solar disk must additionally be incorporated in order to determine the shape of the apparent sun disk's image in the paraxial focal plane. This may be done in the following way:

a. Consider first the vertex of the paraboloid as incidence point; i.e., take $X_i = Y_i = 0$, $Z_i = -f$. and define four characteristic cone-mantle rays of incidence (Fig. 14) as follows:

Ray 1. $X \cos(\epsilon_i + \epsilon_S) - (Z + f) \sin(\epsilon_i + \epsilon_S) = 0$ [8]

$$Y = 0$$

$$\cos \alpha_{i1} = \sin(\epsilon_i + \epsilon_S) \; ; \cos \beta_{i1} = 0 \; ; \cos \gamma_{i1} = \cos(\epsilon_i + \epsilon_S)$$

Ray 2. $X \cos(\epsilon_i - \epsilon_S) - (Z + f) \sin(\epsilon_i - \epsilon_S) = 0$

$$Y = 0$$

$$\cos \alpha_{i2} = \sin(\epsilon_i - \epsilon_S) \; ; \cos \beta_{i2} = 0 \; ; \cos \gamma_{i2} = \cos(\epsilon_i - \epsilon_S)$$

Ray 3. $X \cos \epsilon_i - (Z + f) \sin \epsilon_i = 0$

$$Y \cos \epsilon_S - (Z \; 2 \; f) \sin \epsilon_S = 0$$

$$\cos \alpha_{i3} = \frac{\sin \epsilon_i \cos \epsilon_S}{\sqrt{1 - \sin^2 \epsilon_i \sin^2 \epsilon_S}} \; ; \cos \beta_{i3} = \frac{-\cos \epsilon_i \sin \epsilon_S}{\sqrt{1 - \sin^2 \epsilon_i \sin^2 \epsilon_S}} \; ;$$

$$\cos \gamma_{i3} = \frac{\cos \epsilon_i \cos \epsilon_S}{\sqrt{1 - \sin^2 \epsilon_i \sin^2 \epsilon_S}}$$

---

8. Note that, in this denotation, one has always: $\epsilon_i > 0$; $\epsilon_S > 0$.

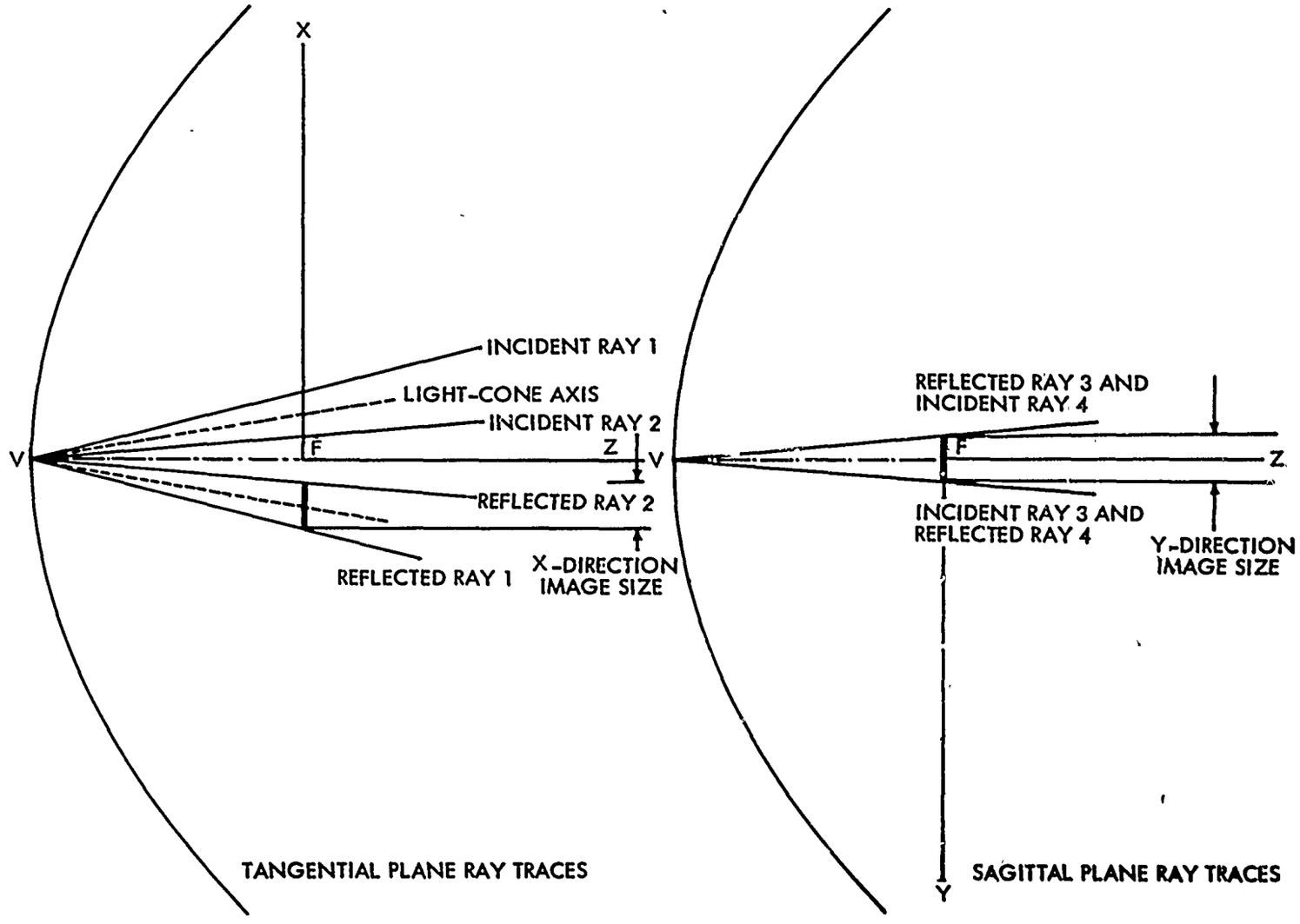

Figure 14 Central Light-Cone Image from Tangential and Sagittal Cone-Mantle Rays

Ray 4. $X \cos \epsilon_i - (Z + f) \sin \epsilon_i = 0$

$-Y \cos \epsilon_S - (Z + f) \sin \epsilon_S = 0$

$$\cos \alpha_{i4} = - \frac{\sin \epsilon_i \cos \epsilon_S}{\sqrt{1 - \sin^2 \epsilon_i \sin^2 \epsilon_S}} : \cos \beta_{i4} = + \frac{\cos \epsilon_i \sin \epsilon_S}{\sqrt{1 - \sin^2 \epsilon_i \sin^2 \epsilon_S}} :$$

$$\cos \gamma_{i4} - \frac{\cos \epsilon_i \cos \epsilon_S}{\sqrt{1 - \sin^2 \epsilon_i \sin^2 \epsilon_S}}$$

Since for all these incident rays, the normal is defined by the direction cosines

$$\cos \alpha_n = \cos \beta_n = 0 \quad \text{and} \quad \cos \gamma_n = 1$$

the equations of the specifically corresponding reflected rays and their intersection points with the paraxial focal plane may be obtained in the usual manner. The result can very well be stated a priori: Since the reflected light cone has a circular cross-section but its symmetry axis is inclined by the angle ($\epsilon = -\epsilon_i$) relative to the optical axis, one obtains an elliptical image of the solar disk as the central portion of the total image.

b. In order to determine the shape of the image produced by a particular zone, or the boundary of the total image, four characteristic cone-mantle rays and their correlated surface normals may be defined also. The situation encountered is illustrated in Figs. 15 and 16, showing cross-sections through the tangential and sagittal planes.

Ray 1. $(X - R_i) \cos (\epsilon_i + \epsilon_S) - (Z + R_i \operatorname{cotan} \theta_i) \sin (\epsilon_i + \epsilon_S) = 0$

$Y = 0$

$$\cos \alpha_{i1} = \sin (\epsilon_i + \epsilon_S) ; \cos \beta_{i1} = 0 : \cos \gamma_{i1} = \cos (\epsilon_i + \epsilon_S)$$

$$\cos \alpha_{n1} = \sin \frac{\theta_i}{2} ; \cos \beta_{n1} = 0 ; \cos \gamma_{n1} = - \frac{1}{2 \cos \theta_i / 2}$$

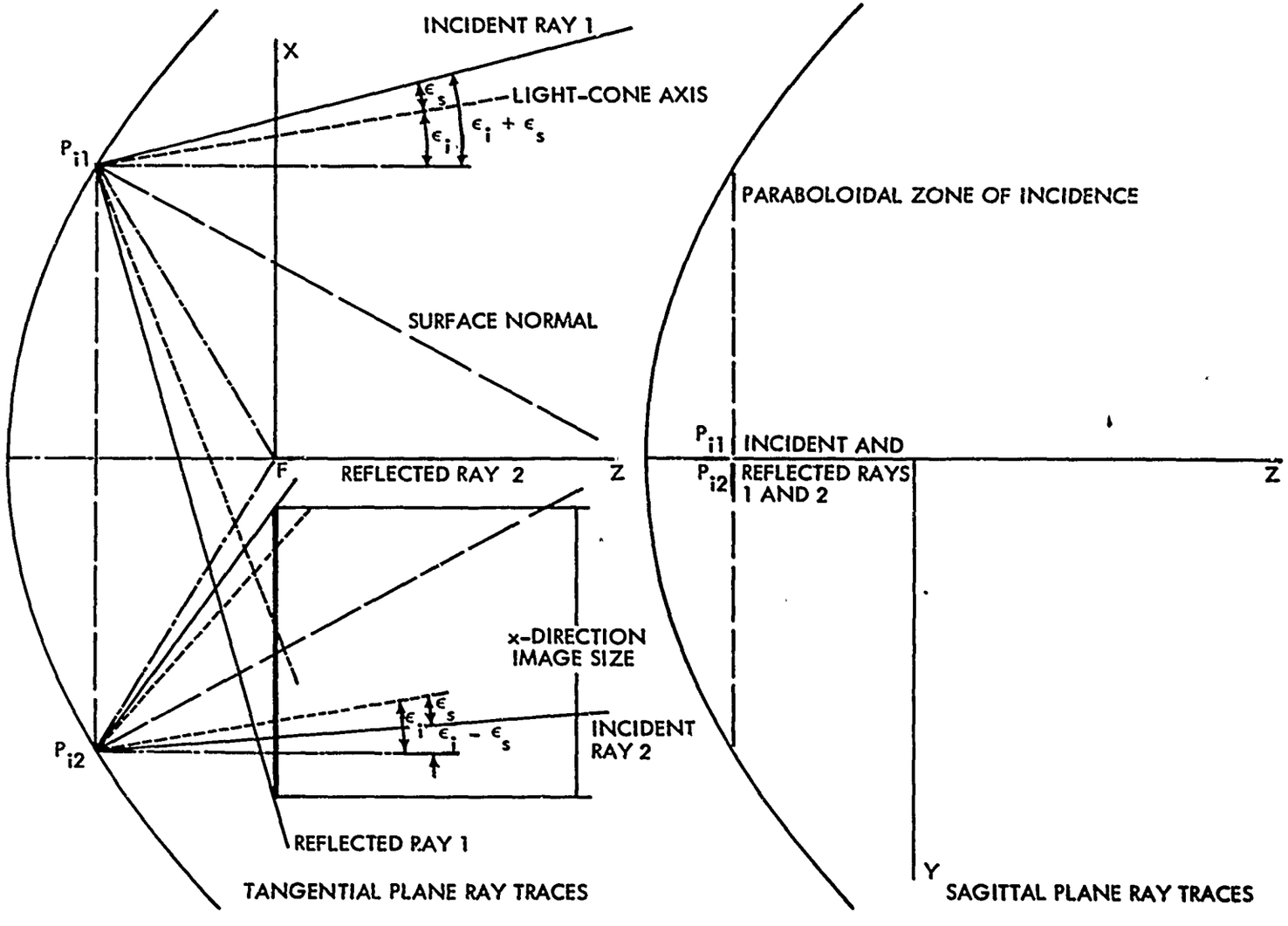

Figure 15 Zonal Light-Cone Image from Tangential Cone-Mantle Rays

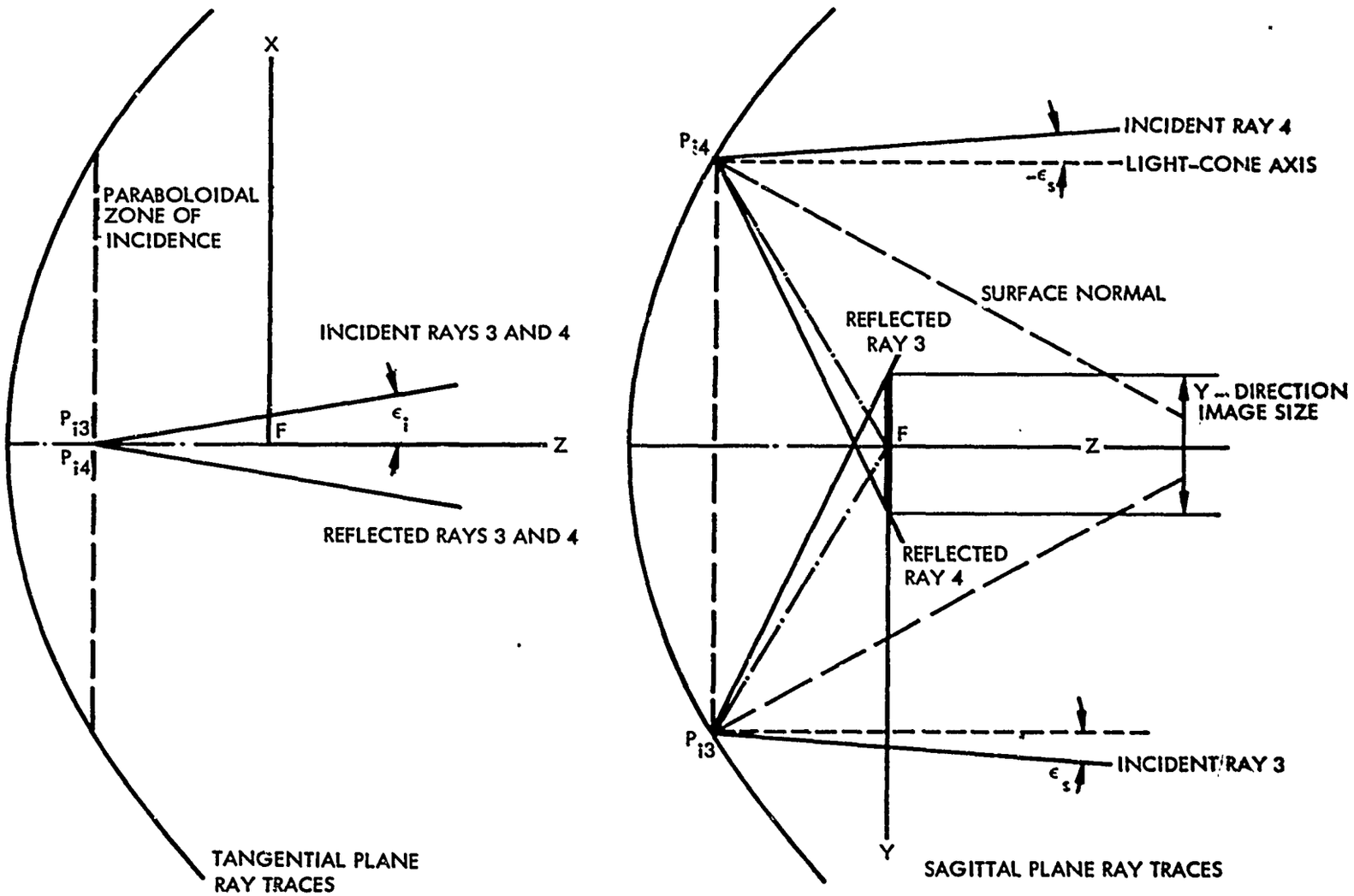

Figure 16 Zonal Light-Cone Image From Sagittal Cone-Mantle Rays

Ray 2. $-(X + R_i)\cos(\epsilon_i - \epsilon_S) + (Z + R_i \operatorname{cotan}\theta_i)\sin(\epsilon_i - \epsilon_S) = 0$

$$Y = 0$$

$$\cos\alpha_{i2} = -(\epsilon_i - \epsilon_S)\ ;\ \cos\beta_{i2} = 0\ ;\ \cos\gamma_{i2} = -\cos(\epsilon_i - \epsilon_S)$$

$$\cos\alpha_{n2} = -\sin\theta_i/2\ ;\ \cos\beta_{n2} = 0\ ;\ \cos\gamma_{n2} = -\frac{1}{2\cos\theta_i/2}$$

Ray 3. $X\cos\epsilon_i - (Z + R_i \operatorname{cotan}\theta_i)\sin\epsilon_i = 0$

$$(Y - R_i)\cos\epsilon_S - (Z + R_i \operatorname{cotan}\theta_i)\sin\epsilon_S = 0$$

$$\cos\alpha_{i3} = \frac{\sin\epsilon_i\cos\epsilon_S}{\sqrt{1 - \sin^2\epsilon_i \sin^2\epsilon_S}}\ ;\ \cos\beta_{i3} = -\frac{\cos\epsilon_i \sin\epsilon_S}{\sqrt{1 - \sin^2\epsilon_i \sin^2\epsilon_S}}\ ;$$

$$\cos\gamma_{i3} = \frac{\cos\epsilon_i\cos\epsilon_S}{\sqrt{1 - \sin^2\epsilon_i \sin^2\epsilon_S}}$$

$$\cos\alpha_{n3} = 0\ ;\ \cos\beta_{n3} = \sin\theta_i/2\ ;\ \cos\gamma_{n3} = -\frac{1}{2\cos\theta_i/2}$$

Ray 4. $X\cos\epsilon_i - (Z + R_i \operatorname{cotan}\theta_i)\sin\epsilon_i = 0$

$$-(Y + R_i)\cos\epsilon_S - (Z + R_i \operatorname{cotan}\theta_i)\sin\epsilon_S = 0$$

$$\cos\alpha_{i4} = -\frac{\sin\epsilon_i\cos\epsilon_S}{\sqrt{1 - \sin^2\epsilon_i \sin^2\epsilon_S}}\ ;\ \cos\beta_{i4} = \frac{\cos\epsilon_i \sin\epsilon_S}{\sqrt{1 - \sin^2\epsilon_i \sin^2\epsilon_S}}\ ;$$

$$\cos\gamma_{i4} = -\frac{\cos\epsilon_i\cos\epsilon_S}{\sqrt{1 - \sin^2\epsilon_i \sin^2\epsilon_S}}$$

$$\cos\alpha_{n4} = 0\ ;\ \cos\beta_{n4} = -\sin\theta_i/2\ ;\ \cos\gamma_{n4} = \frac{1}{2\cos\theta_i/2}$$

The appropriate mantle rays corresponding to the reflected cones (of circular cross-section) and their intersection points with the paraxial focal plane may now be found in the general way outlined earlier. The images of the apparent sun disk produced by particular paraboloidal zones can be anticipated to have elliptical boundaries. The solar disk's total image, then, is obtained by superimposition of the images of the particular zones, and will show the characteristic properties of coma and astigmatism.

If the mirror-receiver system is to be optimized in the sense that the total radiation reflected from the mirror is to be collected by the receiver aperture in the paraxial focal plane, then, of course, the effect of the misalignment has to be taken into account. This can certainly be done by enlarging the diameter of the receiver aperture appropriately. On the other hand, the shape of the aperture may be changed; most probably it will be characterized by an ellipse-type or even an elliptical boundary. In this case, however, one has to provide means to place the larger aperture symmetry axis into the meridional plane. If a compromise solution is adequate – i.e., if a certain percentage loss of the total radiation reflected can be tolerated – either the size (and shape) of the aperture actually to be used can be determined or the maximum admissible inclination error – in this case, $\epsilon = \epsilon_i + \epsilon_S$ – can be defined for a given aperture size. The latter case has been treated numerically by assuming a mirror rim diameter of 52 ft, a rim angle of 60 deg, and a receiver aperture diameter of 20 in. The result is shown in Figs. 17 and 18. One concludes that, for this special situation, an error of $\epsilon = 0.785$ deg can be tolerated at the rim; of course, the admissible error is larger for smaller zone angles.

Receiver aperture dislocation errors may be classified as displacements of the aperture center along, and perpendicular to, the optical axis. It can easily be shown that a displacement of the aperture plane along the optical axis either reduces or enlarges the size of the actually received solar disk image. If Δz_a is the displacement error one obtains.

$$X_A = X_F - \Delta z_a \tan(\theta_i + \epsilon)^{(9)} \qquad (22)$$

where X_F is the intersect of the reflected ray from a point source at infinity (angular deviation ϵ relative to the optical axis) with the paraxial focal plane. Since, in this specific case, one has $X_F < 0$, the displacement effect is equivalent to an image size enlargement for $\Delta z_a > 0$, i.e., equivalent to a larger inclination error $\bar{\epsilon} = \epsilon_i + \epsilon_S + \epsilon_a$. For a rim angle of 60 deg, a numerical evaluation of Eq. (22) is shown in Fig. 19; for more generality, a dimensionless representation has been used. It is seen that small aperture displacements in the order of $\Delta z_a = \pm 0.001\,f$ correspond to equivalent inclination errors of approximately $\epsilon_a = \pm 0.05$ deg, respectively. Dislocating the aperture center perpendicularly to the optical axis, of course, results in efficiency losses, if efficiency is defined as ratio of the actually received to the theoretically receivable radiation. This effect, therefore, may also be considered equivalent to an

9. The quantity X_F is defined by Eq. (14); ϵ is given by $\epsilon = \epsilon_i + \epsilon_S$.

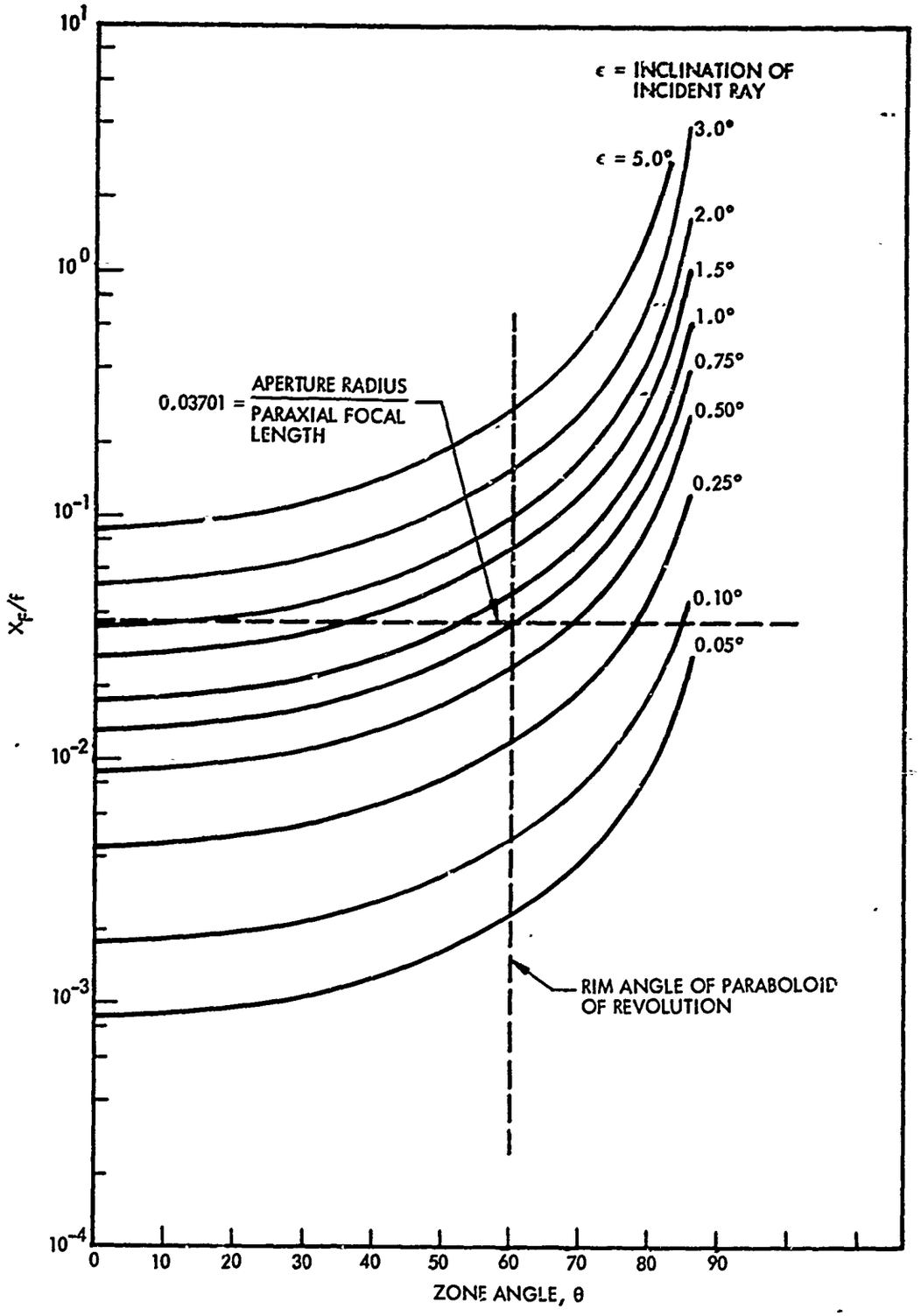

Figure 17 Point-Source Image Deviation From Optical Axis in Paraxial Focal Plane; Dependence on Zone Angle, θ

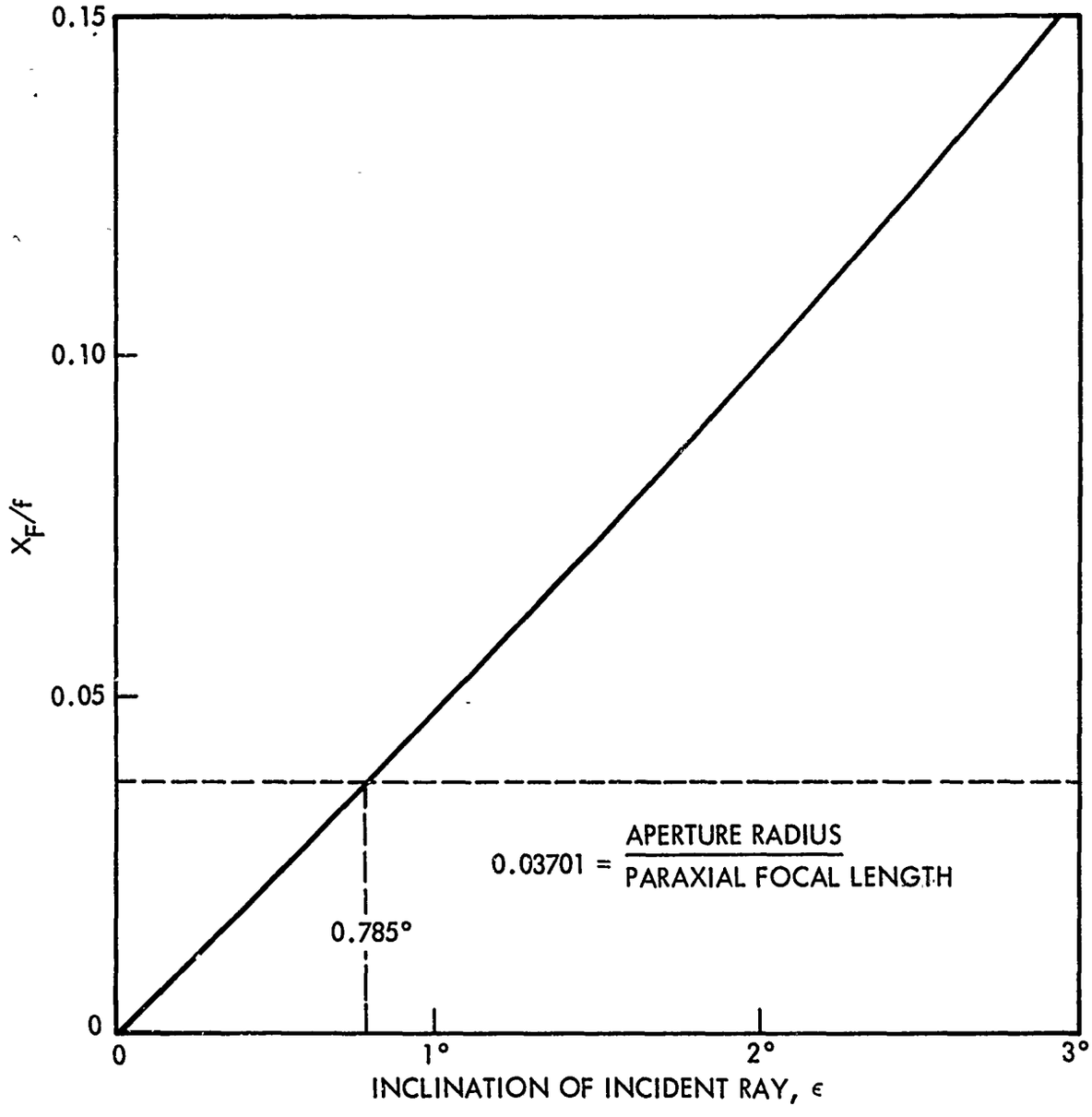

Figure 18 Point-Source Image Deviation From Optical Axis in Paraxial Focal Plane; Dependence on Hypothetic Incidence Angle ϵ ; Zone Angle: θ = 60 deg

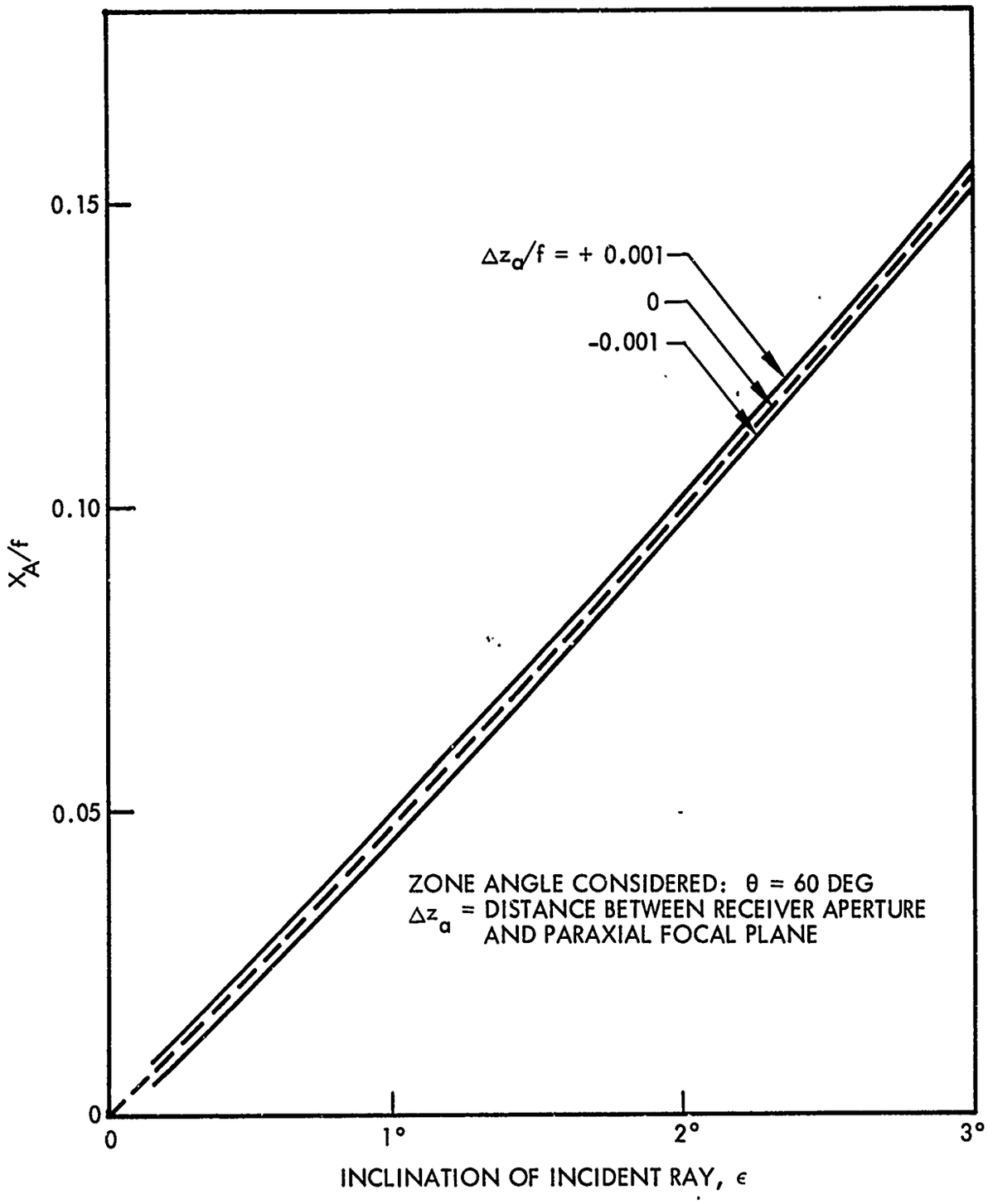

Figure 19 Point-Source Image Deviation From Optical Axis in Displaced Receiver Aperture Plane; Dependence on Hypothetic Incidence Angle ϵ ; Zone Angle: θ = 60 deg

increase in inclination angle. With respect to aperture plane inclination errors, it is evident that they produce images reduced or enlarged in size. Summarizing the statements, one concludes that dislocation and inclination errors of the receiver aperture plane relative to the paraxial focal point and the optical axis, respectively, are equivalent to an inclination angle change, and, consequently, have an effect upon the sun disk's actual image similar to that of a mirror misalignment error, i.e., of an error in pointing the reflector's optical axis toward the solar disk's center.

Appendix II

IMAGE FORMATION BY A PARABOLOIDAL MIRROR SEGMENT – MISALIGNMENT ERRORS

1. GENERAL INFORMATION

A particular form of a paraboloidal solar radiation reflector is one that is composed of segmental areas or petals. This design permits furling the mirror for installation on a satellite launching vehicle during the boost and injection-into-orbit phases. The satellite-borne reflector is unfurled after the orbit is achieved, and its optical axis is oriented towards the apparent solar disk's center. To perform the furling and unfurling process, the mirror petals are mounted, usually, on a hub around the reflector's optical axis. The hole at the mirror's central portion, of course, produces an effect similar to that of obscuration, and, therefore, the hub diameter has to be determined carefully in order to avoid too large radiation losses. A reflector of this type, obviously, can not be expected to show the performance of a perfect paraboloid in a terrestrial environment.

The misalignment errors of a perfect reflector (tilt of the optical axis relative to the line-of-sight to the solar disk's center, as well as dislocation of the radiation receiver aperture with respect to the paraxial focal point and inclination with respect to the optical axis) are errors which probably will be encountered continuously in space, but this problem, to some extent, has already been treated in Appendix I. For this reason, a perfectly aligned segment of an ideal reflector is taken as a reference for the theoretical performance analysis of an imperfect petal.[10] If convenient, in some instances, the effect of mirror misalignments will be incorporated.

Misalignment errors of individual petals may be classified as:

- Tilt of the optical axis of the actual petal relative to that of the reference segment at the theoretical vertex
- Hub displacement along the optical axis and perpendicular to it
- Petal inclination error at hub or any other point on the contour of the reference segment

The analyses performed are, in general, based on the specific considerations of Appendix I. However, before these analyses are presented, it is desirable to describe briefly the overall image of a circular source if this is produced by a perfectly aligned

---

10. Perfect alignment of an ideal reflector, described by a paraboloid of revolution, and of every one of its segments is understood in the sense that the optical axis coincides with the line-of-sight to the sun disk's center, and that the receiver aperture plane is identical with the paraxial focal plane.

and perfectly shaped paraboloidal mirror segment. The extension of the petal may be described by $\theta_h \leqq \theta \leqq \theta_m$, $-\phi_s \leqq \phi \leqq \phi_s$, where θ_h and θ_m denote the zone angles at the hub and the rim, respectively, and $2\phi_s$ is the angular subtense of the petal with respect to the optical axis. The image of a light cone, incident at a specific point (ϕ, θ), again is an ellipse in the paraxial focal plane (or in any plane inclined, relative to the reflected cone's symmetry axis, by an angle other than $\pi/2$). The size of the overall image obtained by superimposition of all possible ellipses is determined by the edges of the sectorial area of incidence, i.e., by $\phi = \pm\phi_s$, $\theta = \theta_h$, and $\theta_s = \theta_m$. Thus, the image, essentially has sectorial shape, but without sharp corners. It is to be noted that the image area always contains the paraxial focal point. Although not of primary concern for understanding the content of this appendix, the statement on the image shape may be useful if one wishes to determine, by theoretical considerations, the intensity distribution and/or the zonal energy content in images of the sun produced by single segmental areas of the mirror or by multiple petal arrangements.

2. TILT OF THE OPTICAL AXIS OF THE ACTUAL PETAL RELATIVE TO THAT OF THE REFERENCE SEGMENT AT THE THEORETICAL VERTEX

If, for a perfectly aligned paraboloid of revolution, a reference system, (x, y, z),[11] as shown in Appendix I, Fig. 5, has been chosen, then, in general, the description of an arbitrary segment can be referred to a system, (ξ, η, ζ), which is rotated about the z-axis by an angle ϕ_o. (ϕ_o may define the location of the petal's symmetry axis such that the angular width is given by $\phi_o - \phi_s \leqq \phi \leqq \phi_o + \phi_s$, where ϕ_s is the half angular subtense as seen from the optical axis.) As long as the reflector, including each of its segments, is perfectly aligned with respect to a point source at infinity (parallel beam of light) or with respect to the principal ray (light-cone symmetry axis) of a circular source, every (meridional) plane containing the z-axis may be chosen to characterize, in the most convenient way, specific features. From this fact, it follows that the rotation by the angle ϕ_o is unimportant as long as single petals are to be analyzed. For this reason, in the following analyses of single petals, the (ξ, ζ)-plane is taken as a specific meridional plane, i.e., as tangential plane. (The combined effects of more than one petal are not taken into consideration at this moment.)

The misalignment of the petal can now be described as resulting in one of the following:

- A rotation about the η-axis by an angle ϵ_η
- A rotation about the ξ-axis by an angle ϵ_ξ
- Combined rotations by angles ϵ_η and ϵ_ξ

---

11. The coordinate system, (x, y, z), with origin at the paraboloidal vertex is here used for greater convenience.

a. Rotation About the η-Axis

This case refers to an elevation of the ζ-axis, and, obviously, constitutes the simplest to be considered. In principle, it is handled in Appendix I.

The transformation matrix is

$$\left.\begin{aligned} \begin{bmatrix} \xi' \\ \zeta' \end{bmatrix} &= \begin{bmatrix} \cos \epsilon_\eta & -\sin \epsilon_\eta \\ \sin \epsilon_\eta & \cos \epsilon_\eta \end{bmatrix} \begin{bmatrix} \xi \\ \zeta \end{bmatrix} \\ \eta' &= \eta \end{aligned}\right\} \quad (1)$$

The specific incident ray from a bundle of parallel rays, at an arbitrary point of the well-aligned reference segment, may be defined by the two planes

$$\xi = \xi_i = R_i \cos \phi_i$$

$$\eta = \eta_i = R_i \sin \phi_i$$

which take, in the new system, the form

$$\xi' \cos \epsilon_\eta + \zeta' \sin \epsilon_\eta = \xi_i$$

$$\eta' = \eta_i$$

Since the actual petal as a part of the paraboloidal reflector is described by

$$\xi'^2 + \eta'^2 = 4f\zeta'$$

one may calculate the coordinates $(\xi_i', \eta_i', \zeta_i')$ of the incidence point on the actual petal, and proceed according to Appendix I, subsection 2b. After the direction cosines of the actually reflected ray are found, the equations of this ray may be expressed by the original coordinate system, (ξ, η, ζ), to determine its intersection point with the paraxial focal point, $\zeta = f$. The deviation of this point from the theoretical paraxial focus is denoted as misalignment error, and has the same meaning as a geometrical optical aberration.

Rays lying in the specific meridional plane of the reference system turn into tangential rays in the primed system with an incidence angle ϵ_η. The extreme image point deviations, encountered along the parallel to the ξ-axis in the paraxial focal plane, are determined by the zone angles $\theta = \theta_h$ and $\theta = \theta_m$, where θ_h and θ_m refer to the hub and the rim of the paraboloidal segments respectively. Sagittal rays, in the usual sense, do not exist in the primed system because of the limited angular

extensions of the petal. However, for rays lying in planes perpendicular to the specific meridional planes, the image points may be determined by applying the considerations developed in Appendix I, subsection 3a. The point source image will be a straight line.

With respect to a circular source, a single incident light cone produces an elliptically shaped image whose area, of course, is larger than that encountered from the reference segment. Because of the misalignment error, the ellipse center may appreciably deviate from the paraxial focus. The longitudinal ellipse axis lies in the direction of ξ.

b. Rotation About the ξ-Axis

Here, the transformation matrix is

$$\left.\begin{aligned} \begin{bmatrix} \eta' \\ \zeta' \end{bmatrix} &= \begin{bmatrix} \cos \epsilon_\xi & \sin \epsilon_\xi \\ -\sin \epsilon_\xi & \cos \epsilon_\xi \end{bmatrix} \begin{bmatrix} \eta \\ \zeta \end{bmatrix} \\ \xi' &= \xi \end{aligned}\right\} \qquad (2)$$

The two planes defining the incident ray,

$$\xi = \xi_i = R_i \cos \phi_i$$

$$\eta = \eta_i = R_i \sin \phi_i$$

take, in the primed system, the form

$$\xi' = \xi_i$$

$$\eta' \cos \epsilon_\xi - \zeta' \sin \epsilon_\xi = \eta_i$$

The further analysis is practically identical with that of Appendix I, subsection 3a. Its results are quite similar, except that rays lying in the specific meridional plane of the reference system turn into sagittal rays of the primed system with an incidence angle ϵ_ξ, and tangential rays, in the usual sense, do not exist in the primed system.

With respect to the circular source, one obtains, from a single cone of incidence, an elliptical image with longitudinal axis in the direction of η. Again, the area of the image ellipse is larger than that obtained from the reference segment, and the ellipse center shows a misalignment error.

c. Combined Rotations

The term "combined rotations" is here understood in the Eulerian sense; i.e., first a rotation about the η-axis by the angle ϵ_η is performed, followed by a second rotation about the ξ'-axis by the angle ϵ_ξ, such that the transformation matrix becomes

$$\begin{bmatrix} \xi'' \\ \eta'' \\ \zeta'' \end{bmatrix} = \begin{bmatrix} \cos\epsilon_\eta & 0 & -\sin\epsilon_\eta \\ \sin\epsilon_\eta \sin\epsilon_\xi & \cos\epsilon_\xi & \cos\epsilon_\eta \sin\epsilon_\xi \\ \sin\epsilon_\eta \cos\epsilon_\xi & -\sin\epsilon_\xi & \cos\epsilon_\eta \cos\epsilon_\xi \end{bmatrix} \begin{bmatrix} \xi \\ \eta \\ \zeta \end{bmatrix} \tag{3}$$

The same incidence ray as used above, Eqs. (2.1 and 2.2), is defined in the double-primed system, by the two planes

$$\xi'' \cos\epsilon_\eta + \eta'' \sin\epsilon_\eta \sin\epsilon_\xi + \zeta'' \sin\epsilon_\eta \cos\epsilon_\xi = \xi_i$$

and

$$\eta'' \cos\epsilon_\xi - \zeta'' \sin\epsilon_\xi = \eta_i$$

These equations may be written in the form

$$\begin{bmatrix} \eta'' \\ \zeta'' \end{bmatrix} = \frac{1}{k_0} \begin{bmatrix} -k_1 \xi'' + k_2 \\ -k_3 \xi'' + k_4 \end{bmatrix}$$

where

$$\begin{aligned} k_0 &= \sin\epsilon_\eta \\ k_1 &= \cos\epsilon_\eta \sin\epsilon_\xi \\ k_2 &= \xi_i \sin\epsilon_\xi + \eta_i \sin\epsilon_\eta \cos\epsilon_\xi \\ k_3 &= \cos\epsilon_\eta \cos\epsilon_\xi \\ k_4 &= \xi_i \cos\epsilon_\xi - \eta_i \sin\epsilon_\eta \sin\epsilon_\xi \end{aligned}$$

Introduction into the equation of the paraboloid,

$$\xi''^2 + \eta''^2 = 4f\zeta''$$

results in the coordinates of the incidence point on the actual petal

$$\left.\begin{aligned} \xi_i'' &= \frac{k_1 k_2 - 2f k_0 k_3}{k_0^2 + k_1^2}\left[1 \pm \sqrt{1 - \frac{\left(k_0^2 + k_1^2\right)\left(k_2^2 - 4f k_0 k_4\right)}{\left(k_1 k_2 - 2f k_0 k_3\right)^2}}\right] \\ \eta_i'' &= \frac{1}{k_0}\left(-k_1 \xi_i'' + k_2\right) \\ \zeta_i'' &= \frac{1}{k_0}\left(-k_3 \xi_i'' + k_4\right) \end{aligned}\right\} \quad (4)$$

Expressing the equations for the incident ray in terms of $(\xi'' - \xi_i'')$, $(\eta'' - \eta_i'')$, $(\zeta'' - \zeta_i'')$, one obtains the direction cosines

$$\cos \alpha_i'' = -\sin \epsilon_\eta$$

$$\cos \beta_i'' = \cos \epsilon_\eta \sin \epsilon_\xi$$

$$\cos \gamma_i'' = \cos \epsilon_\eta \cos \epsilon_\xi$$

One has, furthermore, the direction cosines of the normal to the actual petal at $(\xi_i'', \eta_i'', \zeta'')$:

$$\cos \alpha_n'' = \frac{\xi_i''}{\sqrt{\xi_i''^2 + \eta_i''^2 + 4f^2}}$$

$$\cos \beta_n'' = \frac{\eta_i''}{\sqrt{\xi_i''^2 + \eta_i''^2 + 4f^2}}$$

$$\cos \gamma_n'' = -\frac{2f}{\sqrt{\xi_i''^2 + \eta_i''^2 + 4f^2}}$$

Hence, the direction cosines and the equations of the reflected ray can be determined according to the procedure described in Appendix I, subsection 2b. Finally, the equations for the reflected ray may be transformed into the original coordinate system and intercepted by the theoretical paraxial focal plane $\zeta = f$.

Although misalignment errors can be calculated, the application of the terms "tangential and sagittal rays" as referred to the double-primed system is no longer useful.

With respect to the circular source, a single cone of light incidence produces an elliptically shaped image whose longitudinal axis may be along the ξ-axis or along the η-axis, depending on the magnitude of the rotation angles ϵ_η and ϵ_ξ with respect to each other. The ellipse center is characterized by coordinates (ξ_e, η_e). The ellipse area is probably larger than that obtained from the nondistorted petal and also larger than those of the cases 1 and 2 in this section.

3. HUB DISPLACEMENT

Hub displacements can be characterized as dislocations of the hub center along and perpendicular to the optical axis of the reference segment. Their effects are expected to be quite similar to those encountered by a displaced receiver aperture plane. The theoretical paraboloid, in this case, may be given by

$$\xi^2 + \eta^2 = 4f(\zeta + f)$$

i.e., it may be referred to a coordinate system with origin at the paraxial focus. The most general hub displacement is described by the translation

$$\begin{bmatrix} \xi' \\ \eta' \\ \zeta' \end{bmatrix} = \begin{bmatrix} 1 & 0 & 0 \\ 0 & 1 & 0 \\ 0 & 0 & 1 \end{bmatrix} \begin{bmatrix} \xi - \Delta\xi_h \\ \eta - \Delta\eta_h \\ \zeta - \Delta\zeta_h \end{bmatrix} \tag{5}$$

This means that one has $\Delta\xi_h = \Delta\eta_h = 0$ for displacements along the optical axis, and $\Delta\zeta_h = 0$ for dislocations perpendicular to the optical axis.

It can easily be shown that, for a perfectly aligned, paraboloidal reference segment, the misalignment errors of a single ray of incidence due to a hub displacement of the actual petal along the optical axis are given by

$$\left.\begin{aligned} \xi_F &= \Delta\zeta_h \tan\theta_i \cos\phi_i \\ \eta_F &= \Delta\zeta_h \tan\theta_i \sin\phi_i \\ \zeta_F &= 0 \end{aligned}\right\} \tag{6}$$

where

$$\xi_i' = \xi_i = R_i \cos \phi_i = R_i' \cos \phi_i'$$
$$\eta_i' = \eta_i = R_i \sin \phi_i = R_i' \sin \phi_i' \text{ , i.e., } R_i = R_i' , \phi_i = \phi_i' ,$$
$$\zeta_i' = \zeta_i - \Delta\zeta_h = -R_i \operatorname{cotan} \theta_i - \Delta\zeta_h ,$$

are the coordinates of the incidence point, and

θ_i = zone angle of the reference segment

The image of a single light cone from a circular source, perfectly aligned with regard to its symmetry axis, again is an ellipse in the paraxial focal plane of the reference segment.

Of course, the situation is changed to some extent if the point source at infinity or the circular source is in off-axis position. As an example, the situation is considered where this off-axis position is defined, in the specific meridional plane, by an inclination error ϵ_i with respect to the optical axis (Fig. II-1) and where $\phi_i = 0$ is assumed for further simplification. The determination of the misalignment error is not complicated, but somewhat lengthy. It results in

$$\xi_F = -R_i' \frac{\sin \epsilon_i}{\sin \theta_i \cos (\theta_i' + \epsilon_i)} + \Delta\xi_h \tan (\theta_i' + \epsilon_i)$$

$$\eta_F = 0$$

$$\zeta_F = 0$$

where

R_i' = zone radius for a single ray incident at the actual petal

θ_i' = actual zone angle, i.e., the angle between the radius vector from the actual focal to the actual incidence point and the optical axis

Equations (6) correspond exactly to those that will be obtained from the dislocation of the receiver aperture plane along the optical axis of a perfectly aligned paraboloidal reflector. In Appendix I, this aperture plane dislocation was denoted by Δz_a. To get equivalent expressions for both cases, the term $\Delta\zeta_h$ in Eqs. (6) is to be replaced by $-\Delta z_a$.

From Fig. 20, it is seen that the misalignment error ξ_F described above can be interpreted as composed of a misalignment error

$$\xi_F' = -R_i' \frac{\sin \epsilon_i}{\sin \theta_i' \cos (\theta_i' + \epsilon_i)}$$

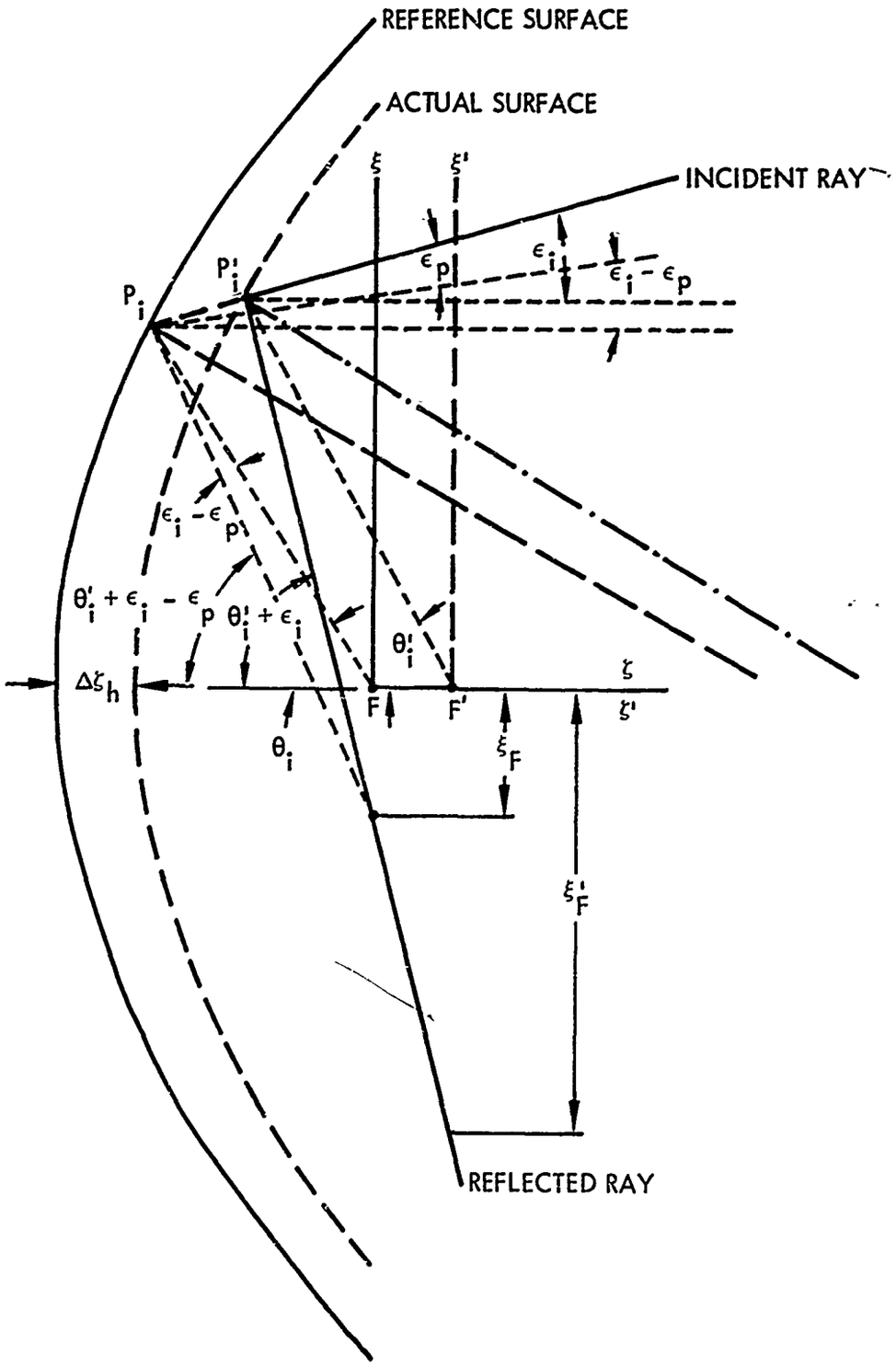

Figure 20 Simplified Configuration Encountered in Evaluating Petal Misalignments; Hub Displacement

and of the value

$$\Delta\xi'_F = \Delta\zeta_h \tan(\theta'_i + \epsilon_i)$$

The term ξ'_F represents the misalignment error which would be encountered in the actual focal plane; $\Delta\xi'_F$ is a correction quantity resulting from the hub displacement along the optical axis. Furthermore, if P'_i is the actual incidence point and P_i is the fictitious point of incidence on the reference surface, it is seen that ξ_F may also be interpreted as resulting from a fictitious incidence angle, $\bar{\epsilon}_i = \epsilon_i - \epsilon_p$, where ϵ_p is a correction quantity to be introduced for compensating the angle between the actual surface normal at P'_i and the fictitious surface normal at P_i; i.e., one can describe the misalignment error by

$$\xi_F = -R_i \frac{\sin \bar{\epsilon}_i}{\sin \theta_i \cos(\theta_i + \bar{\epsilon}_i)} = \xi'_F + \Delta\zeta_h \tan(\theta'_i + \epsilon_i)$$

Comparing this formula with Eq. (22) of Appendix I proves the anticipated similarity of the effects of a displaced hub with those of a dislocated receiver aperture plane, and shows that displacement errors of that kind are indeed equivalent to inclination angle changes.

Although, for the dislocation of the hub perpendicular to the optical axis, the analysis may be more difficult to perform than for the simple cases treated, there is no reason at all to suspect that the resulting misalignment error will not be similar to that of a receiver aperture center displaced perpendicularly to the optical axis. Therefore, all the conclusions drawn are equally applicable for both hub center and receiver aperture plane dislocations.

4. PETAL INCLINATION ERROR AT THE HUB

As in case B, the reference segment and the actual are described by Eq. (10), i.e., by the respective paraboloids

$$\xi^2 + \eta^2 = 4f(\zeta + f)$$

and

$$\xi'^2 + \eta'^2 = 4f(\zeta' + f)$$

where the coordinate system origins are located at the theoretical and actual focal points. For simplification, only the meridional plane specified by the ξ- and ζ-axes is considered. The inclination error at the hub is denoted by ϵ_h and the center of rotation at the hub by the coordinates $(\xi_h, 0, \zeta_h)$. The actual optical axis makes the same angle ϵ_h with the theoretical optical axis as does the actual with the

theoretical normal at the hub. Then, the rotation of the reference segment into the actual petal is defined by the transformation

$$\begin{bmatrix} \xi' - \xi'_f \\ \eta' \\ \zeta' - \zeta'_f \end{bmatrix} = \begin{bmatrix} \cos \epsilon_h & 0 & -\sin \epsilon_h \\ 0 & 1 & 0 \\ \sin \epsilon_h & 0 & \cos \epsilon_h \end{bmatrix} \begin{bmatrix} \xi \\ \eta \\ \zeta \end{bmatrix} \tag{7}$$

where the coordinates $(\xi'_f, 0, \zeta'_f)$ determine the theoretical focus in the (ξ', η', ζ')-system. Similarly, one has

$$\begin{bmatrix} \xi - \xi_{\bar{f}} \\ \eta \\ \zeta - \zeta_{\bar{f}} \end{bmatrix} = \begin{bmatrix} \cos \epsilon_h & 0 & \sin \epsilon_h \\ 0 & 1 & 0 \\ -\sin \epsilon_h & 0 & \cos \epsilon_h \end{bmatrix} \begin{bmatrix} \xi' \\ \eta' \\ \zeta' \end{bmatrix} \tag{8}$$

where $(\xi_{\bar{f}}, 0, \zeta_{\bar{f}})$ denote the coordinates of the actual focal point in the (ξ, η, ζ) system. Of course, the specific focal point displacements (ξ'_f, ζ'_f) and $(\xi_{\bar{f}}, \zeta_{\bar{f}})$ are uniquely determined by ϵ_h and the specific center of rotation (ξ_h, ζ_h), and vice versa. This implies that an arbitrary focal point dislocation defines a unique point of rotation on the paraboloidal surface, and that, for this reason, Eqs. (7) and (8) can be considered the expression for a more general transformation; i.e., they may be referred to an arbitrary center of rotation on the reflector surface. If one assumes $\xi_{\bar{f}}, \zeta_{\bar{f}}$ and ϵ_h as given, one obtains the center of rotation

$$\xi_h = 2f \frac{\sin \theta_h}{1 + \cos \theta_h}$$

$$\zeta_h = 2f \frac{\cos \theta_h}{1 + \cos \theta_h}$$

$$\theta_h = \epsilon_h/2 + \tan^{-1} \frac{\zeta_{\bar{f}}}{\xi_{\bar{f}}}$$

where usually θ_h is the zone angle of the rotation center.

For further simplification, it may now be assumed that the incident ray is determined by an arbitrary point $P^*(\xi^*, 0, \zeta^*)$ in the (ξ, η, ζ) system and an inclination angle ϵ_i relative to the theoretical optical axis[12]:

$$(\xi - \xi^*) \cos \epsilon_i - (\zeta - \zeta^*) \sin \epsilon_i = 0$$

$$\eta = 0$$

take, in the transformed system, the form

$$\xi' \cos (\epsilon_i - \epsilon_h) - \zeta' \sin (\epsilon_i - \epsilon_h) = (\xi^* - \xi_{\bar{f}}) \cos \epsilon_i - (\zeta^* - \zeta_{\bar{f}}) \sin \epsilon_i$$

$$\eta' = 0$$

and are to be used, in connection with the paraboloidal equation

$$\xi'^2 + \eta'^2 = 4f(\zeta' + f)$$

to determine the coordinates $(\bar{\xi}'_i, 0, \bar{\zeta}'_i)$ of the incidence point $\bar{P}_i$ on the actual surface. Hence, in the following, these coordinates can be supposed to be known, and the incidence ray can be expressed by

$$(\xi' - \bar{\xi}'_i) \cos (\epsilon_i - \epsilon_h) - (\zeta' - \bar{\zeta}'_i) \sin (\epsilon_i - \epsilon_h) = 0$$

$$\eta' = 0$$

The situation encountered is illustrated in Fig. 21. The actual surface normal is defined by

$$(\xi' - \bar{\xi}'_i) \cos \theta'_i/2 + (\zeta' - \bar{\zeta}'_i) \sin \theta'_i/2 = 0$$

$$\eta' = 0$$

where θ'_i is the zone angle to the actual incidence point in the primed system. It is easily seen (and analytically derived) that the incidence angle is

$$\alpha_i = \theta'_i/2 + \epsilon_i - \epsilon_h$$

---

12. This includes the specific case, $\epsilon_i = 0$, of the perfectly aligned reference segment.

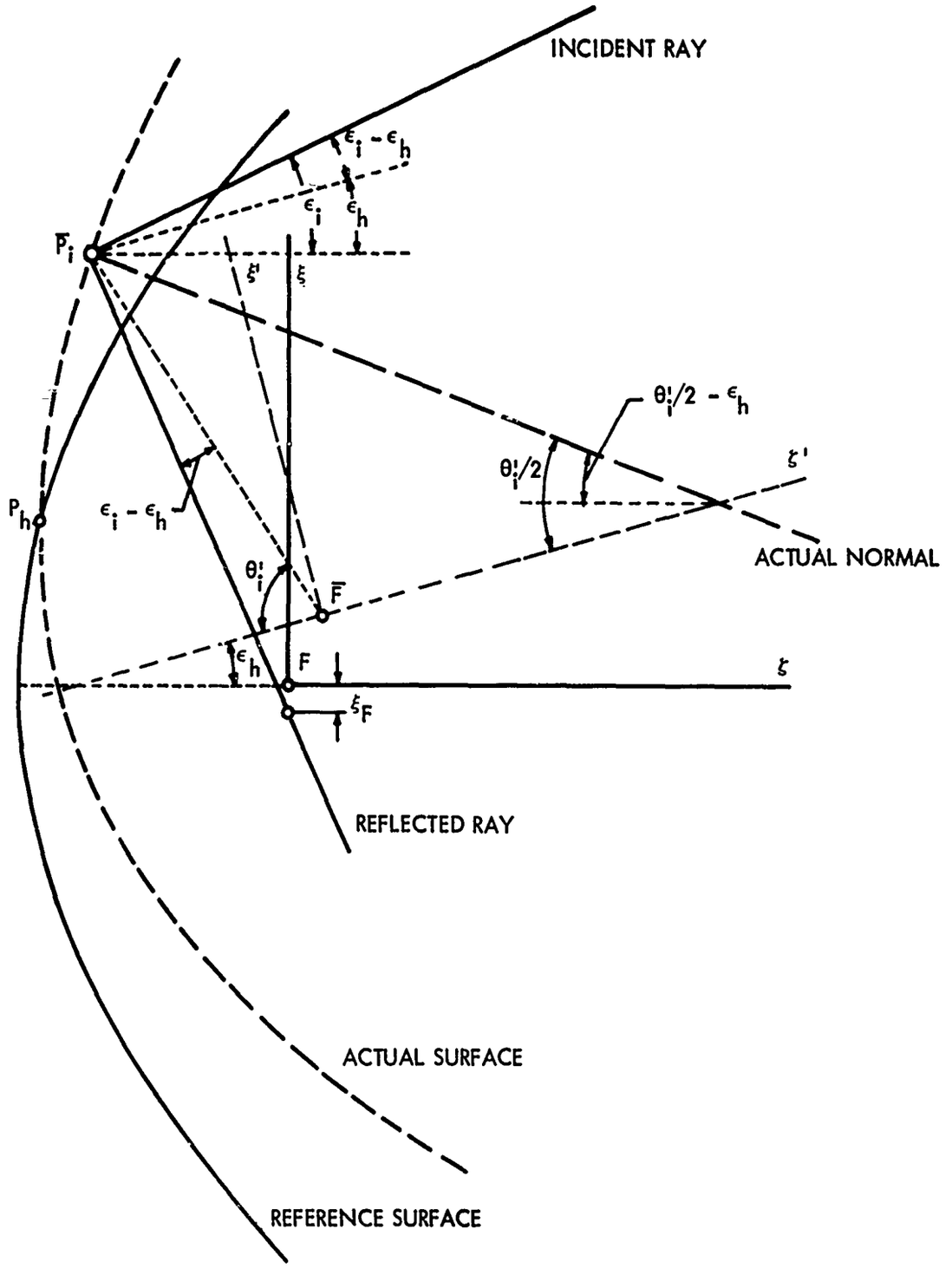

Figure 21 Simplified Configuration Encountered in Evaluating Petal Misalignments; Petal Inclination at Hub

Hence, the reflected ray is determined by

$$(\zeta' - \bar{\xi}_i') \cos (\theta_i' + \epsilon_i - \epsilon_h) + (\zeta' - \bar{\zeta}_i') \sin (\theta_i' + \epsilon_i - \epsilon_h) = 0$$

$$\eta' = 0$$

By using the transformation Eq. (14.1), i.e.,

$$\xi' - \bar{\xi}_i' = (\xi - \bar{\xi}_i) \cos \epsilon_h - (\zeta - \bar{\zeta}_i) \sin \epsilon_h$$

$$\zeta - \bar{\zeta}_i' = (\xi - \bar{\xi}_i) \sin \epsilon_h + (\zeta - \bar{\zeta}_i) \cos \epsilon_h$$

the equations of the reflected ray become

$$(\xi - \bar{\xi}_i) \cos (\theta_i' + \epsilon_i - 2\epsilon_h) + (\zeta - \bar{\zeta}_i) \sin (\theta_i' + \epsilon_i - 2\epsilon_h) = 0$$

$$\eta = 0$$

It follows that the misalignment error, defined by the intersect of the reflected ray with the theoretical paraxial focal plane, is determined by

$$\left.\begin{aligned} \xi_F &= \bar{\xi}_i + \bar{\zeta}_i \tan (\theta_i' + \epsilon_i - 2\epsilon_h) \\ \eta_F &= 0 \\ \zeta_F &= 0 \end{aligned}\right\} \quad (9)$$

where $(\bar{\xi}_i, \bar{\zeta}_i)$ are the coordinates of the actual incidence point in the reference system, and may be expressed by

$$\bar{\xi}_i = \xi_{\bar{f}} + \bar{\xi}_i' \frac{\sin (\theta_i' + \epsilon_h)}{\sin \theta_i'}$$

$$\bar{\zeta}_i = \zeta_{\bar{f}} + (\bar{\xi}_i - \xi_{\bar{f}}) \operatorname{cotan} (\theta_i' + \epsilon_h)$$

It is to be noted that, in the final form, Eq. (9), for the misalignment error, the surface inclination error ϵ_h appears with twice its amount. Major difficulties are not expected in treating more general cases, although the analysis will be lengthy.

Since focal point dislocations have proved to be equivalent to fictitious surface inclination errors, the determination of the misalignment error of a single paraboloidal petal can always be obtained from applying the general derivations of Appendix I, provided that the particular angular errors are properly defined and accumulated into one total error ϵ.

Appendix III

IMAGE FORMATION BY A PARABOLOIDAL MIRROR SEGMENT – DEFORMATION ERRORS

1. CLASSIFICATION OF ERRORS

The errors of single segments considered here are denoted as deformation errors because, in contrast to the petal misalignments of Appendix II, they are produced by a change of the paraboloidal contour. The errors of this type belong essentially to two categories: macrodeformations and microdeformations.

2. MACRODEFORMATIONS

Large-scale mechanical deformations are those which are produced by the following:

- Improper surface shape due to the manufacturing process
- Bending under gravitational load
- Time-dependent thermal stress in orbit

They affect the contour of the mirror segment as a whole in a continuous manner and can be characterized by the appearance of displacements, as well as inclinations of the tangential plane to the actual petal relative to the reference segment. They are different from the dislocations and inclinations caused by mechanical petal misalignments insofar as the actual surfaces are to be described by analytic equations which contain higher (and lower) than second-order terms in the coordinates ξ and η perpendicular to the optical axis, and perhaps also higher than first-order terms in the coordinate ζ along the optical axis, if this axis can be defined at all. Moreover, the surface describing a single, discrete petal is not necessarily a surface of revolution. Of course, a paraxial focal point, in the Gaussian sense, can be defined very well, but this focus probably can not be expected to represent the locus of all rays incident parallel to the optical axis and reflected from the mirror surface.

For the analysis of the deformation errors, one may envision essentially two methods:

Method 1. Taking the contour of the real petal and, by application of the rules of conventional geometrical optics, comparing its effect upon the image formation with that of the conjugated paraboloidal reference segment. This method, certainly, will result in a detailed and complete insight into the mechanism of image formation by a deformed petal, and will define the contribution of the deformation to the overall error.

Method 2. Replacing the real contour by a paraboloid which best fits it in the least-squares sense and comparing this paraboloid of approximation with the reference surface. Most probably, the approximate paraboloid will be misaligned with respect to the reference petal and, therefore, can be handled by adequately using the derivations of Appendix II. Of course, application of this method will reveal only coarse knowledge of the image-formation mechanism and of the contribution of the deformation to the over-all error.

For both methods, the knowledge of real petal contours or even of families of possible surface contours is a prerequisite for the performance of the error analysis. Of course, the image produced is, in size and shape, basically due to conventional optical aberrations.

3. MICRODEFORMATIONS

Small-scale deformation effects may be due to:

- Waviness, in a general sense
- Sharp surface inflections (especially at the petal edges) and other discontinuities
- All surface elements which scatter radiation in random directions

The deformations of this kind, which sometimes may tend toward the microscopic, affect the contour of the reflector segment locally rather than as a whole. Although the small-scale deformations may also be characterized as local displacements and inclinations of the tangential planes to the actual petal with respect to the reference segment, the treatment gets complicated insofar as there may be hundreds or even thousands of irregular and random, single and complex deformations of this type. Nevertheless, the actual surface as a whole may be describable by an analytic equation which contains even more higher-order terms than that for the surface affected by large-scale deformations; it may also be possible that the actual surface has to be described by Fourier, or other series, expansions. These descriptions, of course, must always be considered as approximations never revealing the true contour in detail. Then, however, there is no reason not to proceed with a second step of approximation by replacing the contour obtained by a paraboloid best fitted in the least-squares sense. As noted in section B, the analysis performed on this basis yields average inclination errors; the average displacement errors occurring simultaneously may again be replaced by fictitious inclinations. Therefore, the study has primarily to consider the problem of obtaining enough detailed information in order to determine the form of the higher-order, approximate surface by both theory and/or experimentation.

Radiation scattering surface elements, distributed at random, such as mark-off (show-through) and the like, probably can not be handled on the basis of theoretical analysis. Sharp surface inflections, certainly, will not be as numerous as the random small-scale deformations. However, they will be caused by the petal design and the unfolding process, and one would need more specific knowledge about them to perform a successful analysis.

Waviness may be thought of as a series of local deviations from the reference segment, involving displacements along, and inclinations relative to, the theoretical normals. This waviness may be due to the manufacturing process (faulty tool masters, locally inducing thermal stress effects during evaporation, etc.) and, in orbit, to the locally varying thermal stress caused by the absorption of solar radiation in the surface protecting layer (silicon monoxide). The particular wavelets may be distributed regularly, irregularly, or even at random over the total area of the disturbed reflector segment. They can certainly be described, however, by continuous equations of second or higher order (spheres, ellipsoids, paraboloids, catenoids, sinusoidal surfaces, and the like), and, therefore, can be considered to be linear in character. Discontinuities between adjacent wavelets or between a particular wavelet and a surrounding undisturbed field element are not very likely. Hence, Fourier or other series expansions are to be applied to describe the disturbed surface as a whole. These expansions are necessary because, besides their distribution, the wavelets may be characterized by equal or different wavelengths (full length of the "periodicity" interval) and by equal or varying maximum displacements (amplitude); of course, the maximum inclination at the ends of the full or half interval of definition is a function of wavelength and amplitude.

The effect of a single wavelet upon the image formation can be regarded as that of a small optical element superimposed on the reference segment and characterized by its size, optical axis, and paraxial focal point, i.e., as a secondary small-scale reflector with properties which differ from those of the reference petal. In order to determine this effect, it may be sufficient to consider only the errors caused by the extreme values of displacement and inclination. If referred to the contour of the reference segment, the maximum displacement (along the common surface normal) is encountered at a point where the tangential plane inclination angle of the actual surface equals that of the reference petal. That is, this displacement can be regarded as equivalent to a focal point dislocation, and, therefore, is replaceable by a fictitious inclination error, as pointed out earlier. The fictitious inclination error, of course, will be larger at the petal rim than at its hub. However, since the maximum displacements encountered in practice will be very small quantities, the fictitious inclination error due to waviness may almost always be negligible. The maximum inclination error, on the other hand, is encountered at the intersection of the wavy with the reference surface; i.e., the maximum inclination error can be considered equivalent to a (local) petal misalignment, and, therefore, can be treated in the manner outlined in Appendix II. This treatment results in an error because of the inclination between the actual and theoretical normals accompanied by a fictitious inclination error due to a focal point dislocation. Because of the small values for the maximum inclination angles practically expected from wavy surfaces, the fictitious error may be negligible.

To provide a better insight, the relationship between maximum inclination and maximum displacement is established for a sinusoidal surface of regularly distributed wavelets.[13] Along a meridional cross-section through the reference petal, the

13. It can be shown that, assuming equal amplitudes and interval lengths, the sinusoidal surface has a larger inclination angle at the interval ends than the paraboloidal or catenoidal surfaces.

sinusoidally disturbed surface may be defined by the continuous wave

$$\Delta r_n = \Delta r_{no} \sin 2\pi \frac{n\Delta s}{s_o} \tag{1}$$

where

Δr_{no} = amplitude (maximum displacement of peak or trough from zero line)

s_o = meridional arc of the reference petal between hub and rim

n = number of periods (wavelets) per petal arc s_o

Δs = the (variable) arc between the petal hub and a specific point on the reference meridian

The value for s_o is easily determined as

$$s_o = f\left(\frac{\sin \theta_m/2}{\cos^2 \theta_m/2} + \sin h^{-1} \tan \theta_m/2 - \frac{\sin \theta_h/2}{\cos^2 \theta_h/2} - \sin h^{-1} \tan \theta_h/2\right) \tag{2}$$

The wavelength, of course, is

$$\Delta s_o = s_o/n$$

By differentiation with respect to Δs, one has

$$\tan \epsilon_w = 2\pi \frac{n}{s_o} \Delta r_{no} \cos 2\pi \frac{n\Delta s}{s_o} \tag{3}$$

Hence,

$$\epsilon_{wmax} = \tan^{-1}\left(2\pi \frac{n}{s_o} \Delta r_{no}\right) \tag{4}$$

Taking Δr_{no} as a parameter, this relation is illustrated in Fig. 22.

If one assumes an incident ray in the specified meridional plane of the petal, one may use the results of Appendix II, Eq. (9), to describe formally the deviation of the image point from the paraxial focus:

$$\left.\begin{aligned} \xi_F &= \bar{\xi}_i + \bar{\xi}_i \tan(\theta_i' + \epsilon_i - 2\epsilon_w - \bar{\epsilon}_w) \\ \eta_F &= 0 \\ \zeta_F &= 0 \end{aligned}\right\} \tag{5}$$

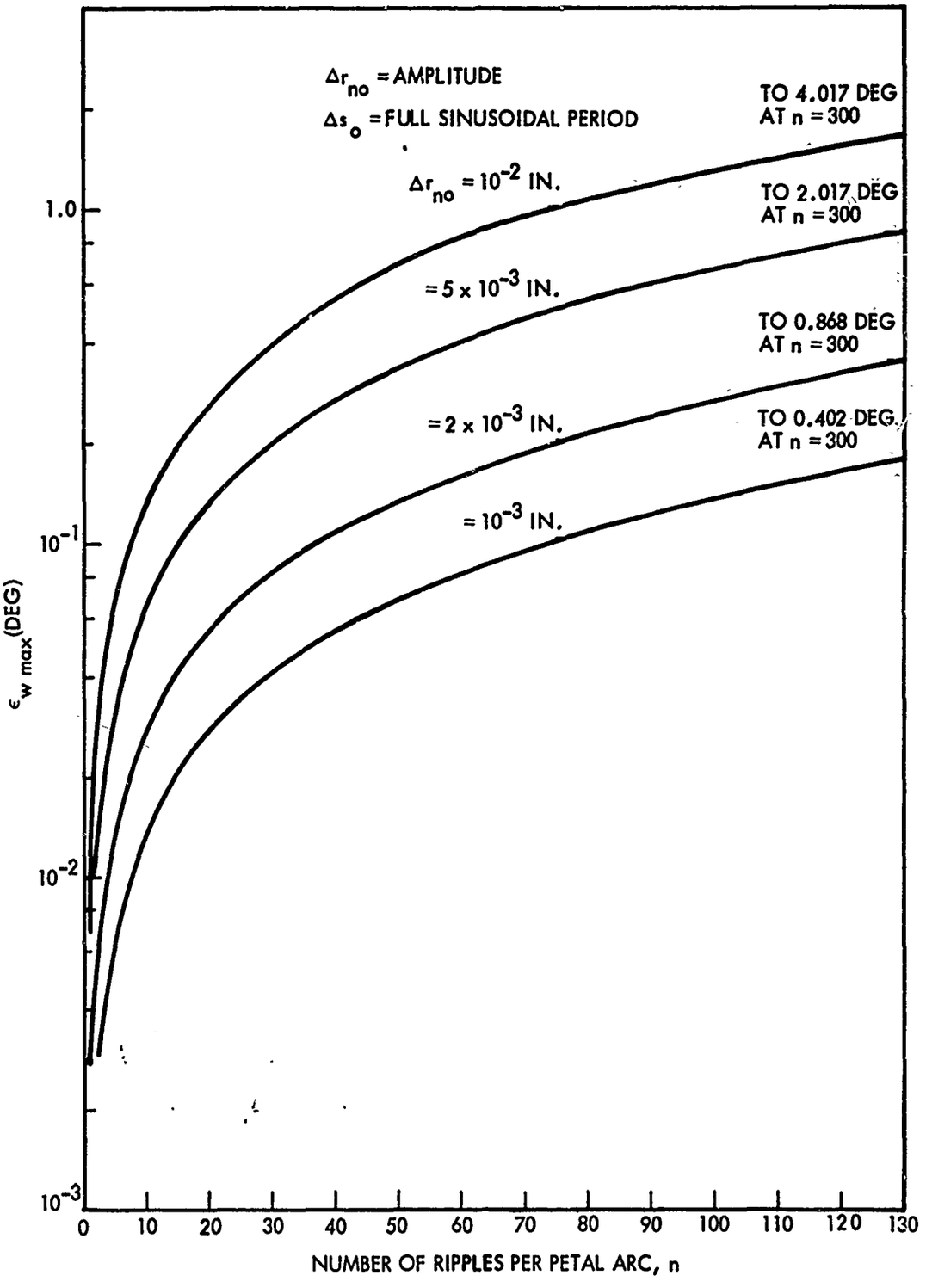

Figure 22 Maximum Inclination Error of a Wavy Petal Surface,

$$\epsilon_{W_{max}} = \pm \tan^{-1} 2\pi (\Delta r_{no}/\Delta s_o)$$

Of course, the evaluation of Eq. (5) becomes complicated since the normal inclination error ϵ_w, the fictitious error $\bar{\epsilon}_w$ representing the displacement effect, and the actual zone angle θ_i' are functions of the real incidence point $(\xi_i, \bar{\zeta}_i)$; the coordinates $(\bar{\xi}_i, \bar{\zeta}_i)$, in turn are dependent on the three parameters defining the incidence ray, i.e., on ϵ_i and the coordinates of a fixed point in the meridional plane. The evaluation gets even more complicated if points outside the meridional plane are considered and/or if the incident ray is defined by inclinations relative to the optical axis of the reference segment and to the meridional plane specified.

In summary, then, the treatment of every case of interest can be performed by applying appropriately the method of analytical ray tracing derived, on a general basis, in Appendix I, if the actual surface of a petal (or a petal assembly) is describable in detail (or approximated in the least-squares sense) by functions with at least first derivatives. For this reason, the conclusions drawn there have a much wider validity, and they are applicable to any well-defined total angle of inclination.

If every particular angle of inclination encountered is positively measured in the direction of a rotation of the ζ-axis into the ξ-axis and η-axis, respectively, properly defining the total angle of inclination is understood in the sense of a summation over the half-angular subtense of the solar disk; the mirror misalignment error; and the appropriate components of the fictitious inclination error, standing for the receiver aperature dislocation (measured, like any other displacement, positive according to the orientation of the coordinate axes ξ , η , ζ), the petal misalignment errors, and the macrodeformation and microdeformation errors.

The total angle of inclination may be given by an expression like

$$\epsilon = \epsilon_s + \epsilon_i + \epsilon_a - 2\epsilon_h - \bar{\epsilon}_h - 2\epsilon_d - \bar{\epsilon}_d - 2\epsilon_w - \bar{\epsilon}_w \qquad (6)$$

where

ϵ_s = half-angular subtense of apparent solar disk
ϵ_i = off-axis position of sun center
ϵ_a = fictitious inclination standing for receiver aperture dislocation
ϵ_h = constant petal inclination due to misalignment
$\bar{\epsilon}_h$ = fictitious inclination due to misalignment standing for focal point displacement
ϵ_d = locally variable petal inclination due to macrodeformation
$\bar{\epsilon}_d$ = coordinated fictitious inclination
ϵ_w = locally variable petal inclination due to waviness
$\bar{\epsilon}_w$ = correlated fictitious inclination

The locally variable errors can be replaced by constant values if the actual surface is best fitted in the least-squares sense (fixed regression curve).

It is therefore quite reasonable to refer to the total error in order to establish specifications for the admissible errors due to petal misalignment and deformation.

REFERENCES

1. J. H. Saxton and D. E. Kline, "Optical Characteristics and Physical Properties of Filled-Epoxy Mirrors," Journal, Optical Society of America, Vol. 50, No. 11, Nov 1960, pp. 1103–1111
2. A. P. Bradford, W. W. Erbe, and G. Hass, "Two-Step Method for Producing Replica Mirrors with Epoxy Resins," Journal, Optical Society of America, Vol. 49, No. 10, Oct 1959, pp. 990–991
3. G. Hass, "Filmed Surfaces for Reflecting Optics," Journal, Optical Society of America, Vol. 45, No. 11, Nov 1955, pp. 945–952
4. A. P. Bradford and Georg Hass, "Increasing the Far-UV Reflectance of Silicon-Oxide–Protected Aluminum Mirrors by UV Irradiation," Journal, Optical Society of America, Vol. 53, No. 9, Sep 1963, pp. 1096–1100
5. J. B. Sidgwick, Amateur Astronomers' Handbook, Faber and Faber, Ltd., 1955, pp. 188–190

BIBLIOGRAPHY

G. Abetti, The Sun, translated by J. B. Sidgwick, London, Faber and Faber, 1955

C. W. Allen, Astrophysical Quantities, University of London, The Athlone Press, 1955

W. A. Baum and J. D. Strong, "Basic Optical Considerations in the Choice of a Design for a Solar Furnace," J. Solar Energy Sci. and Eng'g., Vol. 2, No. 3/4, Jul/Oct 1958, pp. 37–48

H. E. Bennett and J. O. Portens, "Relation Between Surface Roughness and Specular Reflectance at Normal Incidence," J. Opt. Soc. Am., Vol. 51, No. 2 Feb 1961, pp. 123–129

H. E. Bennett, J. M. Bennett, and E. J. Ashley, "Infrared Reflectance of Evaporated Aluminum Films," J. Opt. Soc. Am., Vol. 52, No. 11, Nov 1962, pp. 1245–1250

H. E. Bennett, M. Silver, and E. J. Ashley, "Infrared Reflectance of Aluminum Evaporated in Ultra-High Vacuum," J. Opt. Soc. Am., Vol. 53, No. 9, Sept 1963, pp. 1089–1095

R. W. Bliss, "Notes on Performance Design of Parabolic Solar Furnaces," J. Solar Energy Sci. and Eng'g., Vol. 1, No. 1, Jan 1957, pp. 22–29

-----, "Designing Solar Furnaces for Specific Performance," J. Solar Energy Sci. and Eng'g., Vol. 1, No. 2, Apr 1957, pp. 55–62

M. H. Cobble, "Theoretical Concentrations for Solar Furnaces," J. Solar Energy Sci. and Eng'g., Vol. 5, No. 2, Apr 1961, pp. 61–72

R. E. De La Rue, Jr., E. Loh, J. L. Brenner, and N. K. Hiester, "Flux Distribution Near the Focal Plane," J. Solar Energy Sci. and Eng'g., Vol. 1, No. 2, Apr 1957, pp. 94–98

J. Farber and B. I. Davis, "Analysis of Large Aperture Parabolic Mirrors for Solar Furnaces," J. Opt. Soc. Am., Vol. 47, No. 3, Mar 1957, pp. 216–220

G. Hass and J. E. Waylonis, "Optical Constants and Reflectance and Transmittance of Evaporated Aluminum in the Visible and Ultraviolet," J. Opt. Soc. Am., Vol. 51, No. 7, Jul 1961, pp. 719–722

N. Hukuo and H. Mii, "Design Problems of a Solar Furnace," J. Solar Energy Sci. and Eng'g., Vol. 1, No. 2, Apr 1957, pp. 108–114

P. D. Jose, "The Flux Through the Focal Spot of a Solar Furnace," J. Solar Energy Sci. and Eng'g., Vol. 1, No. 4, Oct 1957, pp. 19–22

G. P. Kuiper, ed., The Sun, Vol. I of The Solar System, Chicago, Illinois, University of Chicago Press, 1953

R. P. Madden, L. R. Canfield, and G. Hass, "On the Vacuum-Ultraviolet Reflectance of Evaporated Aluminum Before and During Oxidation," J. Opt. Soc. Am., Vol. 53, No. 5, May 1963, pp. 620–625

D. H. McClelland and C. W. Stephens, Solar-Thermal Energy Sources, Vol. II of Energy Conversion Systems Reference Handbook, WADD-TR-60-699, Vol. II, Sept 1960 (EOS-Rep. 390-Final)

A. W. Simon, "Calculation of the Concentration of Energy of Points Outside the Focal Spot of a Parabolic Condenser," J. Solar Energy Sci. and Eng'g., Vol. 2, No. 2, Apr 1958, pp. 22–24

-----, "Calculation of the Concentration of the Solar Radiation Through the Focal Spot of a Parabolic Mirror," J. Solar Energy Sci. and Eng'g., Vol. 2, No. 2, Apr 1958, pp. 25–29

-----, "The Loss of Energy by Absorption and Reflection in the Heliostat and Parabolic Condenser of a Solar Furnace," J. Solar Energy Sci. and Eng'g., Vol. 2, No. 2, Apr 1958, pp. 30–33

-----, "Calculation of the Concentration of Energy at Points Outside the Focal Spot of a Parabolic Condenser," J. Solar Energy Sci. and Eng'g., Vol. 3, No. 4, Dec 1959, pp. 67–69